

UNCLASSIFIED

AD NUMBER
AD865323
NEW LIMITATION CHANGE
TO Approved for public release, distribution unlimited
FROM Distribution authorized to U.S. Gov't. agencies and their contractors; Administrative/Operational Use; Dec 1969. Other requests shall be referred to Air Force Materials Lab., Attn: MAMC, Wright-Patterson AFB, OH 45433.
AUTHORITY
AFML ltr, 29 Mar 1972

THIS PAGE IS UNCLASSIFIED

AD 865323

AFML-TR-69-84
PART III. VOLUME II

**STABILITY CHARACTERIZATION OF
REFRACTORY MATERIALS UNDER HIGH
VELOCITY ATMOSPHERIC FLIGHT
CONDITIONS**

**PART III. VOLUME II: EXPERIMENTAL RESULTS OF HIGH
VELOCITY COLD GAS/HOT WALL TEST**

ROGER PERKINS

Lockheed Missile/Space Company

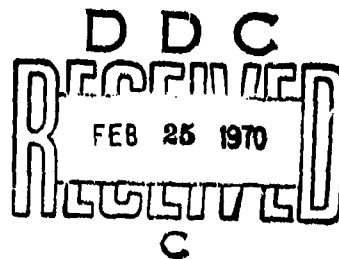
LARRY KAUFMAN

HARVEY NESOR

- ManLabs, Inc.

TECHNICAL REPORT AFML-TR-69-84, PART III, VOLUME II

DECEMBER 1969



This document is subject to special export controls and each transmittal to foreign governments or foreign nationals may be made only with prior approval of the Air Force Materials Laboratory (MAMC), Wright-Patterson Air Force Base, Ohio 45433.

Reproduced by the
CLEARINGHOUSE USE
for Federal Scientific and Technical
Information Springfield, Va. 22151

**AIR FORCE MATERIALS LABORATORY
AIR FORCE SYSTEMS COMMAND
WRIGHT-PATTERSON AIR FORCE BASE, OHIO**

AFML-TR-69-84
PART III. VOLUME II

**STABILITY CHARACTERIZATION OF
REFRACTORY MATERIALS UNDER HIGH
VELOCITY ATMOSPHERIC FLIGHT
CONDITIONS**

**PART III. VOLUME II: EXPERIMENTAL RESULTS OF HIGH
VELOCITY COLD GAS/HOT WALL TEST**

*ROGER PERKINS
LARRY KAUFMAN
HARVEY NESOR*

This document is subject to special export controls and each transmittal to foreign governments or foreign nationals may be made only with prior approval of the Air Force Materials Laboratory (MAMC), Wright-Patterson Air Force Base, Ohio 45433.

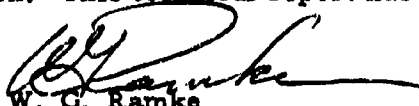
FOREWORD

This report was prepared by ManLabs, Inc. with the assistance of Lockheed Missile/Space Co., Palo Alto, California (Roger Perkins, Project Leader). This contract was initiated under Project 7312, "Metal Surface Deterioration and Protection", Task 731201, "Metal Surface Protection", and Project 7350, "Refractory Inorganic Non-metallic Materials", Task Nos. 735001, "Refractory Inorganic Non-metallic Materials: Nongraphitic", and 735002, "Refractory Inorganic Nonmetallic Materials: Graphitic", under AF33(615)-3859 and was administered by the Metals and Ceramics Divisions of the Air Force Materials Laboratory, Air Force Systems Command, with J. D. Latva, J. Krochmal and N. M. Geyer acting as project engineers.

This report covers the period from April 1966 to July 1969.

ManLabs personnel participating in this study included L. Kaufman, H. Nesor, H. Bernstein, E. Peters, J. R. Baron, G. Stepakoff, R. Pober, R. Hopper, R. Yeaton, S. Wallerstein, E. Sybicki, J. Davis, K. Meaney, K. Rose, J. Dudley, E. Offner, A. Macey, A. Silverman and A. Constantino.

The manuscript of this report was released by the authors in September 1969 for publication. This technical report has been reviewed and is approved.



W. G. Ramke
Chief, Ceramics and Graphite Branch
Metals and Ceramics Division
Air Force Materials Laboratory

The following reports will be issued under this contract.

Part/Volume

I-I	Summary of Results
II-I	Facilities and Techniques Employed for Characterization of Candidate Materials
II-II	Facilities and Techniques Employed for Cold Gas/Hot Wall Tests
II-III	Facilities and Techniques Employed for Hot Gas/Cold Wall Tests
III-I	Experimental Results of Low Velocity Cold Gas/Hot Wall Tests
III-II	Experimental Results of High Velocity Cold Gas/Hot Wall Tests
III-III	Experimental Results of High Velocity Hot Gas/Cold Wall Tests
IV-I	Theoretical Correlation of Material Performance with Stream Conditions
IV-II	Calculation of the General Surface Reaction Problem

ABSTRACT

The oxidation of refractory borides, graphites and JT composites, silicon carbide, hypereutectic metal carbide-graphite composites, refractory metals, coated refractory metals, metal-oxide composites, and siliconized graphite in air over a wide range of conditions was studied over the spectrum of conditions encountered during reentry or high velocity atmospheric flight, as well as those employed in conventional furnace tests. Elucidation of the relationship between hot gas/cold wall (HG/CW) and cold gas/hot wall (CG/HW) surface effects in terms of heat and mass transfer rates at high temperatures was a principal goal.

High velocity CG/HW exposures at air velocities ranging from below 10 ft/sec to 250 ft/sec have been performed at temperatures between 2500° and 4000°F for seventeen candidate materials. Materials which form condensed oxide scales exhibited no definite dependence on air flow rate. Significant temperature gradients (200°-1000°F) develop across thin oxide scales formed during oxidation (scale thicknesses ranged between 0.010 and 0.060 inch) due to the insulating oxide scale on the surface. The practical implications of this finding are quite substantial since if thin layers of these solid oxides can result in such large gradients (and if the gradients exist under free flight conditions), the temperature level experienced by the substrate is substantially below that of the HG/CW surface. Thus, the predicted strength and load carrying capacity of the substrate would be much higher than for the case where gradients are ignored. The high velocity CG/HW oxidation behavior of materials forming condensed oxidation products is comparable with the behavior in furnace tests for equal surface temperatures. Thus, the rate of oxidation is limited by the minimum temperature in the condensed oxide layer.

High velocity CG/HW testing of flat faced, hemispherical type and conical samples of graphite, showed a sixfold increase in recession rate between 1 and 250 ft/sec at 2850°F due to variations of the oxygen pressure at the surface. A temperature dependence for the rate of oxidation was observed at all flow rates in the temperature range of 2000° to 4000°F. The apparent activation energy is estimated to be 4200 cal/mole. Recession rates at 250 ft/sec were comparable with recession rates observed in Mach 0.3 HG/CW arc plasma tests. Rates exhibited by conical samples were found to be twice those observed for flat faced cylinders. Linear recession rates of all graphites correlate directly with density.

Coating failure temperatures and low temperature degradation behavior of several materials were established.

The emittance of fourteen of the candidate materials was measured under oxidizing conditions between 2500° and 4000°F. Extensive data for graphite are presented covering these conditions. A marked decrease in emittance with increased temperature was observed. Data for WSi_2/W were obtained over a range of temperature. Values are reported for borides, boride composites, glassy carbon, siliconized RVC, KT-SiC, graphite composites, Sn-Al coated tantalum and Hf-Ta-Mo.

This abstract is subject to special export controls, and each transmittal to foreign governments or foreign governments or foreign nationals may be made only with prior approval of the Air Force Materials Laboratory (MAMC), Wright-Patterson Air Force Base, Ohio 45433.

TABLE OF CONTENTS

Section		Page
I	INTRODUCTION AND SUMMARY	1
A.	Introduction	1
B.	Summary	2
II	MEASUREMENT OF TEMPERATURE GRADIENTS THROUGH SAMPLES DURING HIGH VELOCITY COLD GAS/HOT WALL TESTS	6
A.	Temperature Gradients through Candidate Materials Forming Volatile Oxides	6
1.	Graphite	6
2.	KT-SiC (E-14)	7
3.	Si/RVC (B-8)	8
B.	Measurements of Temperature Gradients through Candidate Materials Forming Oxide Scales	8
1.	ZrB ₂ (A-3) and HfB _{2.1} (A-2)	9
2.	Hf-20Ta-2Mo (I-23)	10
3.	JTA (D-13)	11
4.	SiO ₂ + 60 w/o W(H-23)	13
5.	ZrC + C (C-12)	14
III	RESULTS OF HIGH VELOCITY COLD GAS/HOT WALL OXIDATION TESTS ON CANDIDATE MATERIALS	15
A.	Test Results for HfB _{2.1} (A-2)	15
B.	Test Results for ZrB ₂ (A-3)	15
C.	Test Results for HfB ₂ + SiC (A-4) and ZrB ₂ + SiC (A-8)	17
D.	The Oxidation of RVA (B-5), Speer 710, ATJS, PT0178(B-9) Graphites and Glassy Carbon (B-11)	17
E.	Oxidation of Siliconized RVC Graphite Si/RVC (B-8)	31
F.	Oxidation of Hypereutectic Carbides HfC+C(C-11) and ZrC+C(C-12)	31
1.	ZrC+C(C-12)	31
2.	HfC+C(C-11)	32
G.	Oxidation of KT-SiC(E-14)	32
H.	Oxidation of Graphite Composites JT0992(F-15) and JT0981(F-16)	33

TABLE OF CONTENTS (CONT)

Section		Page
	1. JT0992 (F-15)	34
	2. JT0981 (F-16)	35
I.	Oxidation of WSi ₂ /W (G-18)	35
J.	Oxidation of Sn-Al/Ta-10W (G-19)	37
K.	Oxidation of SiO ₂ +60 w/o W (H-23) Composite . .	37
L.	Test Results for Hf-20Ta-2Mo (I-23)	38
M.	Summary of High Velocity CG/HW Results	39
IV	MEASUREMENT OF EMITTANCE AT 0.65μ FOR CANDI- DATE MATERIALS UNDER OXIDIZING CONDITIONS IN HIGH VELOCITY AIR FLOWS	41
REFERENCES	44

LIST OF ILLUSTRATIONS

Figure		Page
1	Schematic Representation of the MOTEL (Minimum Oxide Temperature Limit Criterion)	3
2	Temperature Relationship in Graphite Test Cylinders .	46
3	Temperature Gradients and Emittance of SiC in Static Air	47
4	Effect of Flow on Temperature Gradients in SiC Cylinders	48
5	Temperature Drop through Cb_2O_5 Scale on Cb-1Zr. . .	49
6	Temperature Drop through ZrO_2 Scale on ZrB_2	50
7	Macrograph of $\text{ZrB}_2(\text{A-3})$ -18 (Lockheed 45-1) and $\text{ZrB}_2(\text{A-3})$ -13 (L46-1) after High Velocity CG/HW Exposure	51
8	Section through $\text{ZrB}_2(\text{A-3})$ -13 (L46-1) after 30 Minute Exposure at 50 ft/sec in Air	51
9	Section through $\text{ZrB}_2(\text{A-3})$ -18(L45-1) after 60 Minute Exposure at 50 ft/sec in Air	52
10	Oxide-Matrix Interface of $\text{ZrB}_2(\text{A-3})$ -18(L45-1) Showing Adherent Oxide	52
11	Section through $\text{HfB}_{2.1}(\text{A-2})$ -13(L38-1) after 60 Minute Exposure at 50 ft/sec in CG/HW Test	53
12	Oxide-Matrix Interface of $\text{HfB}_{2.1}(\text{A-2})$ -13 (L38-1) Showing Adherent Oxide	53
13	Section through $\text{HfB}_{2.1}(\text{A-2})$ -15 (L39-2) after 60 Minute Exposure at 50 ft/sec in CG/HW Test.	54
14	Oxide-Matrix Interface of $\text{HfB}_{2.1}(\text{A-2})$ -15 (L39-2) Showing Adherent Oxide	54
15	Section through Hf-19Ta-2Mo (I-23) (L44-1) after 30 Minutes at 1-10 ft/sec in CG/HW Test	55
16	Oxide-Subscale-Matrix Zones in Hf-19Ta-2Mo (I-23) (L44-1)	55
17	Section through Hf-19Ta-2Mo(I-23) (L44-2) after 60 Minutes at 1-10 ft/sec in CG/HW Test	56

LIST OF ILLUSTRATIONS (CONT)

Figure		Page
18	Oxide-Subscale-Matrix Zones in Hf-19Ta-2Mo (I-23) (L44-2)	56
19	Oxide-Subscale-Matrix Interface of Hf-19Ta-2Mo (I-23) (L76-1) after 60 Minute Exposure at 50 ft/sec	57
20	Oxide-Subscale-Matrix Interface of Hf-19Ta-2Mo (I-23) (L77-1) after 60 Minute Exposure at 50 ft/sec in CG/HW Test	57
21	Section through Hf-19Ta-2Mo (I-23) (L77-2) after 60 Minutes at 50 ft/sec in CG/HW Test	58
22	Oxide-Subscale-Matrix Zones in Hf-19Ta-2Mo (I-23) (L77-2)	58
23	Temperature Gradients in Oxide Scales on Graphites and Carbides	59
24	JTA(D-13)-L5, Surface Temperature 3821°F, Air Flow Rate 10 ft/sec	60
25	JTA(D-13)-L4, Surface Temperature 3921°F, Air Flow Rate 10 ft/sec	60
26	SiO ₂ -60%W (H-23-L1), after 15 Min. at 3150°F in Air at 50 ft/sec (X8)	61
27	SiO ₂ -60w/oW(H-23)-L1, Surface Temperature 3150°F, Air Flow Rate 50 ft/sec	62
28	Effect of Air Flow Rate on Oxidation of HfB ₂ (A-2) Near 3300°F	63
29	Effect of Air Flow Rate on Oxidation of ZrB ₂ (A-3) Near 3400°F	64
30	Post Exposure Photomicrographs of HfB ₂ + SiC (A-4) after Exposure in Air at Flow Rates up to 150 ft/sec Near 3000°F	65
31	Post Exposure Photomicrographs of ZrB ₂ + SiC (A-8) after Exposure in Air at Flow Rates up to 150 ft/sec	65
32	Surface Recession Curves for Four Grades of Graphite in Flowing Air at 2850°F	66

LIST OF ILLUSTRATIONS (CONT)

Figure		Page
33	Surface Recession Curves, Speer 710 at 50 fps	67
34	Surface Recession Curves, Speer 710 at 150 fps	68
35	Surface Recession Curves, RVA at 50 and 150 fps	69
36	Effect of Temperature and Gas Velocity on the Surface Recession of Two Grades of Graphite	70
37	Effect of Velocity on the Surface Recession of RVA Graphite Flat Face Cylinders	71
38	Changes in Specimen Configuration during the Oxidation of Graphite	72
39	Effect of Specimen Configuration on the Surface Recession of Graphite	73
40	Effect of Specimen Configuration on the Surface Recession of Graphite in CG/HW Tests	74
41	Effect of Specimen Shape on Temperature Dependence of Oxidation Rates for Graphite	75
42	Measurement of Surface Recession on Conical Samples . .	76
43	Section through RVA(B-5)(L-6)(65-1) after 6 Minutes at 50 ft/sec in CG/HW Tests at 3250°F	77
44	Section through RVA(B-5)(L-16)(108-3) after 1.5 Minutes at 50 ft/sec in CG/HW Tests at 3850°F	77
45	Effect of Temperature and Velocity on the Surface Reces- sion of Graphite	78
46	Arrhenius Plot of Surface Recession Data for Graphite in High-Velocity Air	79
47	Effect of Velocity on the Surface Recession Rate of Graphite	80
48	Summary of Graphite Oxidation Data; Subsonic Flow, 2500°- 6500°F, 1 Atmosphere	81
49	Effect of Structure and Density on the Oxidation of Graphite	82

LIST OF ILLUSTRATIONS (CONT)

Figure		Page
50	PT0178(B-9)-L14, Surface Temperature 3050°F, Air Flow Rate 150 ft/sec, Exposure Time 2 Minutes, Initial Configuration 30° Cone, 321 Mil Recession, One Inch Scale	83
51	PT0178(B-9)-L14, Hot Surface At Top	83
52	Glassy Carbon (B-11)-2000-3, Surface Temperature 3550°F, Air Flow Rate 50 ft/sec	84
53	Glassy Carbon (B-11)-2000-3, Hot Surface at Left	84
54	Si-RVC(B-8)-(L-6) Survived 60 Minutes at 150 ft/sec and 2900°F; (L-7) Coating Failed after 15 Minutes at 10 ft/sec and 3100°F; (L-8) Coating Failed after 60 Minutes at 10 ft/sec and 3000°F	85
55	Si-RVC(B-8)-L-7 High Velocity Cold Gas/Hot Wall Test at 3100°F and Air Flow Rate of 10 ft/sec	85
56	Surface Recession Behavior of HfC + C(C-11) and ZrC + C(C-12) in CG/HW Flow Studies	86
57	Effect of Carbon Content on Surface Appearance of Oxidized HfC + C Samples	87
58	ZrC + C(C-12)-L8, Surface Temperature 3800°F, Air Flow Rate 50 ft/sec	88
59	ZrC + C(C-12)-L8, Hot Surface	88
60	HfC + C(C-11)-L4, Surface Temperature 3600°F, Air Flow Rate 50 ft/sec	89
61	HfC + C(C-11)-L4, Hot Surface	89
62	KT-SiC(E-14)-L4, Surface Temperature 3660°F, Air Flow Rate 150 ft/sec	90
63	KT-SiC(E-14)-1, Surface Temperature 3450°F, Air Flow Rate 50 ft/sec	90
64	Surface Recession Behavior of JT0981(F-16) and JT0992 (F-15) in CG/HW Flow Studies	91
65	Effect of Velocity on the Oxidation Behavior of JT0992 and JT0981 Graphites	92

LIST OF ILLUSTRATIONS (CONT)

Figure		Page
66	Degradation of JT0992(F-15) and JT0981(F-16) Graphites at Low Temperatures	93
67	Active-Passive Transition in the Oxidation of JT0992 (F-15) Graphite	94
68	JT0992(F-15)-L11, Surface Temperature 3400°F, Air Flow Rate 50 ft/sec	95
69	JT0992(F-15)-L4, Surface Temperature 2000°F, Air Flow Rate 50 ft/sec	95
70	JT0981(F-16)-L7, Surface Temperature 3200°F, Air Flow Rate 150 ft/sec	96
71	JT0981(F-16)-L10, Surface Temperature 2800°F, Air Flow Rate 50 ft/sec	96
72	WSi ₂ /W(G-18)-40-1, Surface Temperature 3500°F, Air Flow Rate 150 ft/sec	97
73	WSi ₂ /W(G-18)-40-1, Hot Surface at Top Showing WSi ₂ Layer, Over W ₅ Si ₃ Layer Coating Tungsten Matrix at Bottom	97
74	Growth of W ₅ Si ₃ Zone on WSi ₂ /W(G-18) as a Function of Flow Rate and Pressure Compared with the Results of Bartlett and Gage (13) for W ₅ Si ₃ and Perkins and Packer for Mo ₅ Si ₃ (14)	98
75	Sn-Al/Ta-10W(G-19)-41-2, Surface Temperature 3000°F, Air Flow Rate 150 ft/sec	99
76	Sn-Al/Ta-10W(G-19)-37-1, Surface Temperature 3300°F, Air Flow Rate 50 ft/sec	99
77	Active-Passive Transition in the Oxidation of SiO ₂ -60W (H-23)	100
78	Surface Recession Behavior of SiO ₂ -60W in CG/HW Flow Studies	101
79	SiO ₂ -60w/oW(H-23)-L5, Surface Temperature 2500°F, Air Flow Rate 50 ft/sec	102
80	SiO ₂ -60w/oW(H-23)-L5, Hot Surface at Top showing Zone Depleted of Tungsten	102

LIST OF ILLUSTRATIONS (CONT)

Figure		Page
81	Effect of Temperature on the Emittance of Graphite . .	103
82	Emittance of $WSi_2/W(G-18)$ in Flowing Air as a Function of Temperature	104

LIST OF TABLES

Table		Page
1	List of Candidate Materials	105
2	Results of Temperature Gradient Measurements in High Velocity Cold Gas/Hot Wall Tests	106
3	Results of High Velocity Cold Gas/Hot Wall Tests on HfB_2 , 1 (A-2)	107
4	Results of High Velocity Cold Gas/Hot Wall Tests on ZrB_2 (A-3)	108
5	Results of High Velocity Cold Gas/Hot Wall Tests on $\text{HfB}_2 + \text{SiC}$ (A-4)	109
6	Results of High Velocity Cold Gas/Hot Wall Tests on $\text{ZrB}_2 + \text{SiC}$ (A-8)	110
7	Summary of High Velocity Cold Gas/Hot Wall Tests of Graphites	111
8	Results of High Velocity Cold Gas/Hot Wall Tests on PT0178(B-9) and Glassy Carbon (B-11)	113
9	Results of High Velocity Cold Gas/Hot Wall Tests on Si/RVC (B-8) (4 Mil Coating)	114
10	Results of High Velocity Cold Gas/Hot Wall Tests on Arc Cast $\text{HfC}+\text{C}$ (C-11) and $\text{ZrC}+\text{C}$ (C-12)	115
11	Results of High Velocity Cold Gas/Hot Wall Tests on KT-SiC (E-14)	116
12	Results of High Velocity Cold Gas/Hot Wall Tests on JT0981(F-16) and JT0992 (F-15)	117
13	Results of High Velocity Cold Gas/Hot Wall Tests on WSi_2/W (G-18)	121
14	Results of High Velocity Cold Gas/Hot Wall Tests on Sn-Al / Ta-10W (G-19)	122
15	Results of High Velocity Cold Gas/Hot Wall Tests on $\text{SiO}_2 + 60 \text{ w/o W}$ (H-23) for 30 Minute Exposures at a Flow Rate of 50 ft/sec	123
16	Results of High Velocity Cold Gas/Hot Wall Tests on Hf-20Ta-2Mo (I-23)	124
17	Average Values of Normal Spectral Emittance under Oxidizing Conditions	125

I. INTRODUCTION AND SUMMARY

A. Introduction

The response of refractory materials to high temperature oxidizing conditions imposed by furnace heating has been observed to differ markedly from the behavior in arc plasma "reentry simulators." The former tests are normally performed for long times at fixed temperatures and slow gas flows, the latter under high velocity gas-flow conditions where energy flux rather than the temperature is defined. Consequently, philosophy, observables and techniques used in the "material centered" regime and the "environment centered, reentry simulation" area differ so significantly as to render correlation of material responses at high and low speeds, impossible in many cases. Consequently, expeditious utilization of the background information available in either area for optimum matching of existing material systems with specific missions or synthesis of advanced material systems to meet future requirements is sharply curtailed.

In order to reduce this gap, an integrated study of the response of refractory materials to oxidation in air over a wide range of time, gas velocity, temperature and pressure has been designed and implemented. This interdisciplinary study spans the heat flux and boundary layer-shear spectrum of conditions encountered during high-velocity atmospheric flight, covering conditions employed in conventional materials-centered investigations. Significant efforts have been directed toward elucidating the relationship between hot gas/cold wall (HG/CW) and cold gas/hot wall (CG/HW) surface effects at high temperatures, so that full utilization of both types of experimental data can be made.

The principal goal is coupling of the material-centered and environment-centered philosophies to gain a better insight into systems behavior under high-speed atmospheric flight conditions. This function has been provided by an interdisciplinary panel representing the component philosophies. The coupling framework consists of an intimate mixture of theoretical and experimental studies designed to overlap temperature/energy and pressure/velocity conditions, thus providing a means for the evaluation of test techniques and the performance of materials systems over a wide range of conditions. In addition, it provides a base for translating reentry systems requirements such as velocity, altitude, configuration and lifetime into requisite material properties as vaporization rates, oxidation kinetics and density. The correlation of heat flux, stagnation enthalpy, Mach No., stagnation pressure and specimen geometry with surface temperature through the utilization of thermodynamic, thermal and radiation properties of the material and environmental systems used in this study was of prime importance in defining the conditions for overlap between materials-centered and environment-centered tests. Progress along the above mentioned lines necessitated evaluation of refractory material systems which exhibit varying gradations of stability above 2700°F. Emphasis has been placed on candidates for 3400° to 6000°F exploitation. Thus,

borides, carbides, boride-graphite composites (JTA), JT composites, carbide-graphite composites, pyrolytic and bulk graphite, PT graphite, coated refractory metals/alloys, oxide-metal composites, oxidation-resistant refractory metal alloys and iridium-coated graphites were considered (see Table 1). A range of test facilities and techniques including oxygen pickup measurements, cold sample/hot gas, and hot sample/cold gas devices at various air flow velocities, as well as different arc plasma facilities capable of covering a wide range of conditions were employed. Stagnation pressures covered the range between 0.001 and 10 atmospheres. The range of heat flux and stagnation enthalpy employed produced surface temperatures between 2000° and 6500°F.

This report describes the results obtained for the High Velocity Cold Gas/Hot Wall tests performed at Lockheed Missile/Space Company under the direction of Roger Perkins. Other reports in this series characterize the candidate materials (1)*, describe facilities and techniques employed in the cold gas/hot wall tests (2), provide the results of low velocity CG/HW (3) and HG/CW (4) tests, and correlate the performance of the candidate materials with stream conditions (5).

B. Summary

Evaluation of refractory materials oxidation under high velocity (10-250 ft/sec) CG/HW conditions shows that significant temperature gradients develop across thin oxide scales formed during oxidation (scale thicknesses ranged between 0.010 and 0.060 inch). The gradient is due to the insulating oxide scale on the surface. With the present induction heating technique, the substrate is heated directly by coupling with the electromagnetic field (2). The nonconducting oxide scale does not couple with the field and is heated indirectly by conduction from the heated substrate. The surface is cooled by radiation and convection leading to an inverse gradient in which the temperature at the metal/oxide interface is higher than that at the oxide/air interface. As the oxide thickens with time, the resistance to heat transfer is increased. If the substrate temperature is held constant, surface temperature will decrease. If the surface temperature is held constant, the substrate temperature must be increased to overcome the added resistance to heat flow.

The importance of this aspect of materials behavior depends upon the rate-controlling factor in oxidation. Since surface temperature is measured and controlled in most tests, oxidation data will be accurate only if surface temperature is controlling. If the substrate or interface temperature is rate controlling, the measured rate of oxidation will be too high or too low, depending on the method of heating used in conducting the tests. If the substrate is heated by induction or direct resistance, it will be hotter than the surface. If the surface is heated by radiation, the substrate may be cooler or at the same temperature, depending on heat losses to supporting devices or structures. In most gas torch or plasma tests, the substrate will be cooler than the surface. Only in furnace tests

* Underscored numbers in parentheses indicate References given at the end of this report.

where the sample is brought to a uniform temperature throughout, will the surface and substrate be at the same temperature. In the current testing program temperature gradients ranging between 200° and 1000°F were found to exist through 100 mil oxide walls on the surfaces of candidate materials during oxidation between 3000° and 4000° F in air flowing at 10-250 ft/sec.

Results for boride-base materials indicate substantially lower recession rates in the HG/CW arc plasma tests (4) than in the CG/HW furnace tests (3). Thus $\text{HfB}_{2.1}$ (A-2) and ZrB_2 (A-3) exhibit an order of magnitude difference at surface temperatures near 4000°F. The results of the "in-depth" temperature measurements during arc plasma tests indicate that these differences are principally due to temperature gradients through the oxide where temperature gradients of 1500°F are observed through 100 mil wall thickness of boride plus oxide (4). Similar results were obtained for Hf-20Ta-2Mo (I-23). The gradients exist for long periods of time in agreement with deductions based on post-mortem metallography. Figure 1 shown below offers a schematic representation of the behavior of oxide forming refractory materials in the CG/HW and HG/CW tests.

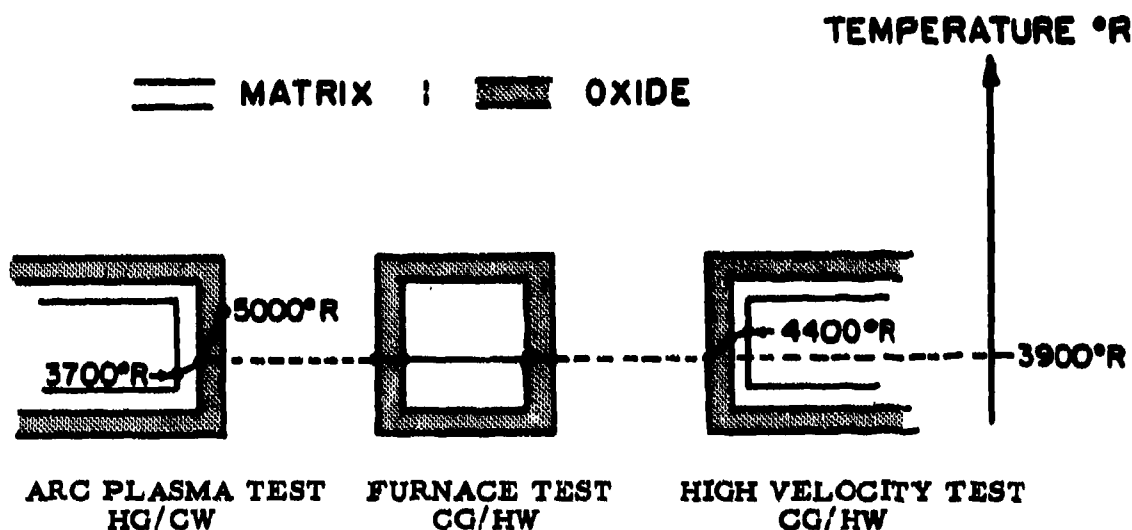


Figure 1. Schematic Representation of the MOTEL (Minimum Oxide Temperature Limit) Criterion.

The central figure represents the oxide and matrix of a solid oxide forming material (i. e., $\text{HfB}_{2.1}$ (A-2), ZrB_2 (A-3) or Hf-20Ta-2Mo (I-23) in a CG/HW furnace test at 3900°F). The temperature distribution across the oxide and matrix zones is assumed constant. In the figure at the right, representing a high velocity CG/HW sample (inductively heated), the temperature is lowest at the CG/HW surface. Conversely, in the

figure at the left representing a HG/CW arc plasma test sample, the temperature is highest at the HG/CW surface. Thus, if the observed recession is limited by the minimum temperature in the oxide (where diffusion rates of oxygen and components of the substrate would be slowest) the present HG/CW and high velocity CG/HW results could be brought into line with the CG/HW furnace results where temperature gradients are largely absent.

The practical implications of this finding are quite substantial since if thin layers of these solid oxides can result in such large gradients (and if the gradients exist under free flight conditions), the temperature level experienced by the substrate is substantially below that of the HG/CW surface. Thus, the predicted strength and load carrying capacity of the substrate would be much higher than for the case where gradients are ignored.

High velocity CG/HW exposures at velocities ranging from below 10 ft/sec to 250 ft/sec have been performed for seventeen of the candidate materials (see Table 1). Materials which form condensed oxide scales exhibited no definite dependence on air flow rate. Graphites which form volatile oxidation products exclusively, exhibited a strong dependence of oxidation rate on air velocity. The high velocity CG/HW oxidation behavior of materials forming condensed oxidation products is comparable with the behavior in furnace tests for equal surface temperatures. Thus the rate of oxidation is limited by the minimum temperature in the condensed oxide layer, which in the CG/HW samples, is at the surface.

High velocity CG/HW testing of flat faced, hemispherical type and conical samples of graphite, showed a sixfold increase in recession rate between 1 and 250 ft/sec at 2850°F. This is due to variations of the oxygen pressure at the surface (5). Recession rates observed in CG/HW tests at 250 ft/sec were comparable with recession rates observed in Mach 0.3 HG/CW arc plasma tests (4). Recession rates exhibited by conical samples were found to be twice those observed for flat faced cylinders.

High velocity CG/HW tests of PT0178(B-9) and Glassy Carbon (B-11) showed recession rates increased significantly with air flow. Linear recession rates of all graphites correlate directly with density. The recession rate of all graphites was found to increase with temperature according to the classic Arrhenius relationship. The apparent activation energy in the range of 2000°-4000°F was 4200 cal/mole. A higher activation energy (14,000-20,000 cal/mole) was indicated in the range 4000°-6000°F based on results of arc plasma studies. This may be the result of a change in oxidation products from CO+CO₂ to CO rich.

Coating failure temperatures for $\text{WSi}_2/\text{W}(\text{G}-18)$ and $\text{Sn-Al}/\text{Ta}-10\text{W}(\text{G}-19)$ were 3650°F and 3200°F in the high velocity CG/HW tests. The former value is higher than in furnace tests (3) and represents a better evaluation of the temperature limit of $\text{WSi}_2/\text{W}(\text{G}-18)$ in the absence of reactions with ZrO_2 .

The failure temperature for $\text{Si}/\text{RVC}(\text{B}-8)$ at 3000°F agrees with the results of CG/HW furnace tests (3). Low temperature degradation of $\text{JTA}(\text{D}-13)$, $\text{JT0992}(\text{F}-15)$, $\text{JT0981}(\text{F}-16)$ and $\text{SiO}_2+60\text{w/oW}(\text{H}-23)$ observed in the furnace tests was also noted. The temperature gradients observed to exist through a 200 mil wall of $\text{SiO}_2+60\text{w/oW}(\text{H}-23)$ were so large that the internal temperature exceeded 4000°F while the surface was only 3150°F . This led to internal melting. The usefulness of this composite is limited since protective behavior is not observed below the fusion range for silica (2700°F - 3000°F). However, SiO_2 softens and becomes viscous above this range leading to a loss of strength.

The emittance of fourteen of the candidate materials was measured under oxidizing conditions between 2500° and 4000°F . Extensive data for graphite are presented covering these conditions for the first time. In addition, data for $\text{WSi}_2/\text{W}(\text{G}-18)$ are presented covering a range of temperature. Moreover, values are reported for borides, boride composites, glassy carbon, siliconized RVC, KT-SiC , graphite, composites, Sn-Al coated tantalum and Hf-Ta-Mo .

II. MEASUREMENT OF TEMPERATURE GRADIENTS THROUGH SAMPLES DURING HIGH VELOCITY COLD GAS/HOT WALL TESTS

Evaluation of refractory materials oxidation under high velocity CG/HW conditions performed along the lines described earlier (2) showed that significant temperature gradients can be developed across thin oxide scales formed on the surface of metals or intermetallic compounds during oxidation (scale thicknesses ranged between 0.010 and 0.060 inch). The gradient results from the formation of an insulating oxide scale on the surface. With induction heating, the metallic substrate is heated directly by coupling with the electromagnetic field. The nonconducting oxide scale, however, does not couple with the field and is heated indirectly by conduction from the heated substrate. The surface is cooled by radiation and convection. This leads to an inverse gradient in which the temperature at the metal/oxide interface is higher than that at the oxide/air interface. As the oxide thickens with time, the resistance to heat transfer is increased. If the substrate temperature is held constant, surface temperature will decrease. If the surface temperature is held constant, the substrate temperature must be increased to overcome the added resistance to heat flow. The importance of this aspect of materials behavior depends upon the rate-controlling factor in the oxidation process. Since the surface temperature is measured and controlled in most tests of materials, oxidation data will be accurate only if surface temperature controls the reaction rate. If the substrate or interface temperature is rate controlling, however, the measured rate of oxidation will be too high or too low, depending on the method of heating used in conducting the tests. If the substrate is heated by induction or direct resistance, it will be hotter than the surface. If the surface is heated by radiation, the substrate may be cooler or at the same temperature, depending on heat losses to supporting devices or structures. In most gas torch or plasma tests, the substrate will be cooler than the surface. Only in furnace tests where the sample is brought to a uniform temperature throughout, will the surface and substrate be at the same temperature.

Subsequent portions of this section provide data concerning some of the candidate materials listed in Table 1. Temperature gradients were measured through samples of graphite, KT-SiC(E-14), and Si-RVC(B-8) which form volatile oxides, and ZrB₂(A-3), HfB₂(A-3), Hf-20Ta-2Mo(I-23), JTA(D-13), SiO₂+60W/oW(H-23) and ZrC+C(C-12) where solid oxides form during exposure.

A. Temperature Gradients Through Candidate Materials Forming Volatile Oxides

1. Graphite

Tests were conducted with graphite cylinders 0.5-inch diameter by 1.5-inch long with a hemispherical leading edge. The temperature at the stagnation point and at the root of a blackbody hole drilled axially in from the base of the sample was measured simultaneously with micro-optical pyrometers (0.65μ). In static tests, the distance between the root of the blackbody hole and the stagnation point was varied to determine the temperature gradient, if any, through the wall. As shown in Figure 2, little if any gradient existed with a wall thickness of 0.1 inch. The apparent surface temperature

was lower than the hole temperature due to emittance effects. Normal spectral emittance was estimated to range between 0.7 and 0.8 over the temperature range of 2400 to 3000°F. This is in reasonable agreement with published data on the emittance of graphite. When the wall thickness was increased to 0.3 or 0.4 inch, a noticeable temperature gradient was observed. The surface temperature was 100 to 200°F lower for a given hole temperature compared with 0.1-inch wall specimens. The gradient was larger at the higher temperature where the rate of heat loss by radiation becomes pronounced. Flowing air past the specimen at 150 fps had a pronounced cooling effect on the surface in the low temperature range where heat loss by conduction was large compared with the loss by radiation. Surface temperature decreased an additional 300°F in the range 2200 to 2600°F. At high temperature, an additional 100°F drop was observed.

2. KT-SiC(E-14)

Studies using graphite as a model were complicated by high rates of surface recession (1-2 mils/sec). It was difficult to establish equilibrium conditions due to rapidly changing geometry. Silicon carbide was selected for more refined studies since surface recession rates are low and the sample geometry is stable. Cylinders of KT-SiC(E-14) 0.5-inch diameter by 1-inch long were used. A blackbody hole, 0.125-inch diameter by 0.6-inch deep, was drilled in each sample. Three sensing devices were used to measure temperatures: (1) a micro-optical pyrometer (0.65μ) sighted on the top surface (stagnation point), (2) a two-color Milletron pyrometer sighted at the same point, and (3) a micro-optical pyrometer (0.65μ) sighted on the base of the blackbody hole. With this arrangement, true and apparent temperature of the surface could be measured. These data yield a reasonably good estimate of emittance. Results of several repetitive tests in static air are plotted in Figure 3.

The Milletron (two-color pyrometer) and optical-blackbody hole readings (2) are in excellent agreement from 2200 to 3000°F. These data indicate that true surface temperature was recorded by the Milletron and no significant temperature gradient exists through the 0.4-inch thick wall of the sample. The apparent surface temperatures when plotted against the hole temperature indicate that the emittance is between 0.65 and 0.70. These results are in good agreement with published data on KT-SiC.

Sightings with the Milletron were made on both the top and side wall during static and flowing (50-142 fps) tests. Results are summarized in Figure 4. Under static conditions, the sidewall and blackbody hole temperatures were in good agreement. Top temperature was low compared with the sidewall. This was found to be due to a crack in the sample. With flowing gas, sidewall temperature dropped 50 to 100°F. Separation of the flow due to use of a flat face specimen results in little cooling of the sides. The top, however, was cooled significantly by the impinging air. The top (stagnation) temperature dropped by 300 to 400°F below the static values. This is comparable to the effect observed with graphite specimens.

Results of these tests showed that blackbody holes are a poor choice for use in measurement and control of test temperature in cold

gas flow tests. It was decided to measure and control the top (stagnation) surface temperature with the Milletron two-color pyrometer. Calibration was checked weekly to assure accurate data. The top and blackbody hole temperatures were measured with micro-optical pyrometers and recorded for use in calculating emittance and temperature gradient data.

3. Si/RVC(B-8)

The results obtained for Si/RVC(B-8) are shown in Table 2. Sample Si/RVC(B-8)-L1 was tested at 3600° F (surface control) in air at 50 ft/sec. Sample temperature was very difficult to control and wide fluctuations occurred. It appeared that some type of coupling transition existed with poor coupling below this temperature and excellent coupling above. It was necessary to steadily increase power input with time to hold the surface at 3600° F. At 6.5 minutes, maximum power was drawn. At 7.2 minutes a hole burned through the side wall and the test was terminated. Surface temperature measurements indicated a normal spectral emittance for this material of 0.47 - 0.42 at 3600° F. A temperature gradient of 200° F after 3 minutes and 400° F after 7 minutes was measured through the top wall. The rapid increase with time indicates that most of this gradient exists through the outer oxide scale. The low emittance results (0.47-0.42) do not appear reliable.

B. Measurements of Temperature Gradients Through Candidate Materials Forming Oxide Scales

Two methods were developed for measuring the temperature gradients through oxide scales on the surface of induction heated samples. In the first method, the metal/oxide interface temperature was measured by a Pt/Pt-Rh therm couple while the surface temperature was measured with an optical pyrometer. This method is limited to temperatures of about 3000° F and was used to study gradients in a Cb_2O_5 scale formed on Cb-12Zr alloy. A thermocouple well was drilled down the center of a 0.3 x 0.3 x 0.75 inch sample to within 0.060 inch of the surface. The sample was supported vertically within an induction coil using the thermocouple insulating sleeve (alumina) as a stinger. The thermocouple bead was bare and made direct contact with the metal at the base of the drilled hole. Helium gas was passed up the alumina support rod to shield the internal surfaces and contact area from oxidation. Surface temperature was measured with a micro-optical pyrometer using a previously established normal spectral emittance of 0.59 to convert from brightness to true temperature. Samples were heated for 30 to 60 minutes holding either the surface (T_S) or metal (T_M) temperature constant and measuring the corresponding temperature at the uncontrolled site (surface or metal) at 5-minute intervals. The results are shown in Figure 5.

Initially, the indicated temperatures for the top surface and the substrate were within ± 10 ° F of each other. With the metal temperature held constant at 2200° F, surface temperature decreased gradually with time of holding. After 1 hour, the surface was at 2100° F while the substrate was still at 2200° F. In experiments where the surface temperature was held constant at 2200° F, the metal temperature increased with time of holding. After 50 minutes, the metal substrate was 150° -200° F hotter than the surface. The time rate of change in temperature for both cases is shown in Figure 5.

In the second method used to study this effect, the substrate or interface temperature was measured with a micro-optical pyrometer while the true surface temperature was measured with a two-color pyrometer. This approach was used for tests above 3000° F where contact thermocouples could not be used. A 0.25 inch diameter hole was core drilled along the center line of a 0.5 inch diameter by one inch long cylindrical sample to within about 150 mils of the top surface. The specimens were supported on alumina, zirconia, or water-cooled copper tubular stingers having a 0.125 inch inside diameter. Helium was passed slowly up the tube to prevent oxidation of the substrate and to clear out smoke or vapors. A calibrated front surface mirror was positioned to sight up the tube for optical measurement of substrate temperature. Brightness readings were converted to true temperature using previously established emittance corrections.

1. ZrB₂(A-3) and HfB_{2.1}(A-2)

This method was used to study the temperature gradients through ZrO₂ scales formed on ZrB₂ samples heated to 3400° F in air flowing at 50 ft/sec.² The behavior was identical to that observed in tests of the Cb-1Zr alloy. As shown in Figure 6, the surface temperature decreased with time as the substrate was held constant at 3400° F. After 1 hour, the surface was 220° F cooler than the induction-heated core. The gradient here is more than double that observed in tests with Cb-1Zr alloy at 2200° F. Similarly, as shown in Figure 6, the metal (boride) temperature increased rapidly in tests where the surface was held constant at 3400° F. After 20 minutes, the substrate was 250° F hotter than the surface. This is about 3 times the gradient observed with Cb-1Zr at 2200° F. Figures 7-10 show post exposure photographs of samples ZrB₂(A-3)-13(L45-1) and ZrB₂(A-3)-18(L46-1) after CG/HW exposures at 50 ft/sec air flow. In both cases, the oxide thickness is about 15 mils and the boride wall thickness is 100 mils.

Two tests with HfB_{2.1}(A-2) revealed a behavior like that observed with ZrB₂(A-3). At 3400° F, where the recession rate is low, steady state surface temperatures could be maintained. At higher temperatures where the recession rate is rapid, scale growth resulted in a continuous temperature drop. This behavior is summarized below:

Time (min)	<u>Surface Temperature (°F)</u>	
	<u>Slow Recession</u>	<u>Fast Recession</u>
	Run 38-1 HfB _{2.1} (A-2)-13	Run 39-2 HfB _{2.1} (A-2)-15
0	3400	3600
5	3400	----
10	3400	3520
15	3400	3400
20	3400	3420
25	3400	3420
30	3400	3350
40	3400	3300
50	3400	3250
60	3400	3190

In the fast recession rate tests, full power input was maintained and the indicated temperature is the maximum attainable at a flow rate of 50 ft/sec. Assuming the substrate to be at 3600° F or even higher, a temperature gradient of over 400° F through the oxide scale is indicated. Figures 11-14 show photomicrographs of HfB_2 (A-2)-13(L38-1) and HfB_2 (A-2)-15(L39-2) after exposure. The latter sample cracked after cooling. Metallographic examination showed that the HfB_2 (A-2) material contained porous bands. Sample HfB_2 (A-2)-15 also exhibited several shallow cracks which might have led to failure.

2. Hf-20Ta-2Mo(I-23)

Temperature gradients were measured in 0.5 inch diameter by 1 inch long cylinders of Hf-20Ta-2Mo(I-23) alloy. Five samples were machined to form closed end cylinders with a minimum wall thickness at the top of 0.12 to 0.15 inch. In the first test (44-1), the sample was supported on a 0.25-inch OD x 0.10 inch ID ZrO_2 tube and was purged internally with helium to prevent oxidation. The top surface temperature was measured and held constant at 3400° F using the Milletron two-color pyrometer. A micro-optical pyrometer (0.65 μ) was sighted up the tube to measure substrate temperature. The alignment was poor, however, and no useful readings could be obtained. The test was terminated at 30 minutes when full power was required to maintain the surface at 3350° F in air flowing at 1 to 10 fps. The sample had a light grey adherent scale on the top surface and a thick white scale on the side walls. It cracked on cooling and broke into two pieces. Figures 15 and 16 show post exposure photographs of this sample.

In a second test (44-2), the sample was supported on an Al_2O_3 tube having a 0.22 inch ID hole. This permitted better sighting with the micro-optical pyrometer and good measurements of substrate temperature were obtained. An emittance value of 0.55 was assumed for calculation of substrate temperature. Figures 17 and 18 show photographs of this sample after testing. The following three tests were conducted maintaining the metallic substrate at constant temperature. In tests (44-1 and 44-2) the samples reacted and fused with the ZrO_2 and Al_2O_3 support tubes. It is necessary to support the samples on nonreactive materials, and previous experience has shown that water-cooled copper is very good for this purpose. A new support stinger was designed and built from hard drawn 0.25 inch OD copper tube. The outside surface and specimen support were water cooled. The inside was open and was connected to a gas purge system and a front surface mirror for temperature measurement. With this device, internal temperature could be measured while using a helium purge to prevent oxidation of the sample from the inside. The outside diameter of the completed stinger was 0.5 inch. This matches the specimen diameter and minimizes disturbance of the air stream. All subsequent tests were conducted using this support.

In run 44-2, the surface temperature initially was about 45° F higher than the substrate temperature. Normally, the surface should be cooler because of air flow effects. This may be due to an error in the assumed value of emittance. The internal surface was purged with helium

and did not develop an oxide scale. If the actual value of emittance was less than 0.55; the substrate temperature would be higher than the calculated value of 3355°F. It also is possible that at the low flow rate used, very little cooling of the surface occurs. The surface temperature held constant for about 20 minutes and then began to decrease slowly with time. At the end of 60 minutes, the surface temperature was 3220°F with the substrate still at 3350°F. This behavior is very similar to that found for Cb-1Zr and the borides.

The last three runs in this series (76-1, 77-1 and 77-2) were conducted in air flowing at 50 fps using substrate temperature control. In each case, the initial surface temperature was 320° to 400°F lower than the substrate temperature with wall thickness of 0.11 to 0.15 inch, illustrating the significant effect of air flow on cooling of the surface. Metal temperature below the oxide scale is assumed to be close to that reported for the substrate measurement. Again, an emittance value of 0.55 was assumed to calculate true temperature. Actual values may be somewhat higher due to the use of an internal helium purge to minimize oxidation. In all tests, top surface temperature decreased with time. After 60 minutes, the surface temperature was 400° to 500°F lower than the substrate temperature. Figures 19-22 show post exposure photomicrographs of these samples.

3. JTA(D-13)

Hemispherical-capped one half inch diameter by one inch long samples were core drilled with a 0.25-inch diameter hole to within 175/225 mils of the top surface (wall thickness). Substrate and surface temperatures were measured simultaneously, and tests were made using both substrate and surface temperature control. The results are summarized in Figure 23 and Table 2.

In the first test, JTA(D-13)-L2, substrate control at 3400°F was used with air flowing at 50 ft/sec. A sharp temperature gradient existed over the top surface and it was not possible to measure brightness temperature for calculation of emittance. The indicated true surface temperature was 350°F lower than the substrate control temperature, indicating the existence of a severe gradient through the wall.

In all subsequent tests, specimens were machined to a flat face configuration in order to obtain a uniform top surface temperature. The second test, JTA(D-13)-L1, was a repeat of the first test using a flat face specimen. Good optical readings were obtained and the normal spectral emittance was calculated to be 0.69 at a surface temperature of about 3000°F. As in the first test, a steep temperature gradient of over 400°F through the wall was indicated. The top surface temperature remained fairly steady with a drop of only 50°F after 1 hr. exposure. Examination of the specimen revealed a thin oxide scale with very little recession. Total recession appeared to be greater than that obtained with the hemispherical cap specimen.

Furnace data on JTA(D-13) indicates surface recessions of 80 to 180 mils after 1 hour at 3400°F. The low recession with substrate

control at 3400°F suggests that surface (oxide scale) temperature may be the rate-governing factor. This possibility was explored further by conducting tests in slowly moving air (~10 ft/sec) at 3820°F using both substrate and surface control. The low flow rate was used to minimize the temperature gradient through the wall thickness. As shown in Table 2, this was achieved in that the initial values of true surface and substrate temperature with a 180-mil thick wall were in perfect agreement based on an assumed emittance correction of 0.6 for the substrate.

In the test with a substrate control, JTA(D-13)-L5, the surface temperature decreased from an initial value of 3821°F to 2901°F after 1 hour while the substrate remained constant at 3820°F. The time rate of change in surface temperature is shown in Figure 23. Most of the drop (700°F) occurred in the first 5 minutes of test. The initial thin oxide layers show a strong insulating effect. Surface temperature drops until the rate of heat loss by radiation and convection is balanced by the heat transfer outward through the scale. As the scale grows in thickness, the temperature gradient increases, and at the end of 1 hour the indicated drop is 920°F. Figure 24 shows a post exposure photomicrograph of this sample.

On cooling, the oxide scale spalled off the top surface. Total surface recession measured by reduction in wall thickness was 33 mils. Furnace oxidation data for JTA at 3800°F indicates a recession of over 200 mils in 1 hour(3). The very low recession in the CG/HW test clearly indicates that substrate temperature is not rate governing. From Figure 23, the average temperature of the surface for 55 minutes of the test was about 3000°F. Furnace data for JTA at 3000°F indicate a conversion depth of 4 to 7 mils in 1 hour. This is in reasonably good agreement with the measured value of 15 mils for this test, lending further support to the conclusion that oxide scale temperature and not substrate temperature governs the rate of surface recession of JTA(D-13) in CG/HW tests.

Test JTA(D-13)-L4 was conducted at a constant surface temperature of 3820°F in slowly moving air (<10 ft/sec). The power input had to be increased steadily to maintain the top surface temperature at 3820°F. After 6 minutes, full power was drawn from the RF-generator and the surface temperature began to fall off. The substrate temperature at this time was 4563°F (using an emittance correction of 0.6). A 740°F temperature gradient through the scale was developed in 6 minutes. This is the same gradient found in tests using substrate control at 3820°F. In this case, however, the heat losses from the surface are constant and the substrate temperature is increased to maintain the needed rate of heat flow through the scale. The time rate of change in temperature drop through the scale is shown in Figure 23. The test was terminated at 7.5 minutes, when it was no longer possible to maintain a constant surface temperature. A post exposure photograph of JTA(D-13)-L4 is shown in Figure 25.

The surface of the sample bubbled continuously during the test and a thick layer of white oxide was deposited on the water-cooled copper support rod. It is assumed that SiO was given off as a vapor and the condensate is SiO₂ and Si formed by the disproportionation of SiO on cooling

$(2 \text{ SiO}_{(g)} \rightarrow \text{Si}_{(s)} + \text{SiO}_{2(s)})$. The surface oxide was adherent and many large crystals were observed on the inside wall of the sample (helium shielded). These have the appearance of Si or SiC and were formed by sweating of a liquid phase formed in the material.

Sample JTA(D-13)-L3 suffered a thermal stress failure. After 1 minute at 3820°F, a 1/16-in.-thick wafer slice literally exploded off the top surface. A loud snap was heard and the piece shot up out of the test area several feet into the air and landed on the floor next to the operator. The test was terminated at this point.

Good temperature readings for emittance calculations were obtained in tests with the flat face cylinders. At 3820°F, emittance was found to increase with time from an initial value of 0.5-0.55 to a final value of 0.7-0.75 after 10 minutes. Little change was observed on continued holding to 1 hour.

4. $\text{SiO}_2 + 60 \text{ w/o W(H-23)}$

The results obtained for $\text{SiO}_2 + 60 \text{ w/o W(H-23)}$ are shown in Table 2. Sample $\text{SiO}_2 + 60 \text{ w/o W(H-23)}$ -L1 was tested at 3150°F (surface control) in air flowing at 50 ft/sec. The sample was difficult to heat with the RF-generator due to poor coupling and 3150°F was the maximum temperature reached at full power output. Better coupling and higher temperatures could be realized by using the 10,000-cycle motor generator set power supply. Temperature held very steady for 25 minutes. The specimen tipped on its support when the helium flow to the inside wall was increased to clear the sight tube and the test was terminated.

A temperature gradient of over 1000°F was observed through the 200-mil-thick top wall. The substrate temperature was 4154°F, with the surface at 3150°F in less than 1 minute at temperature. The gradient was constant for 7 minutes and appeared to be through the entire section, not just through the outer oxide scale. This restricted testing of the material to temperatures below 3100°F.

This test also revealed one other important aspect of the behavior of $\text{SiO}_2 + 60\text{W}$. At temperatures below the fusion range for silica (2700-3000°F), the surface is not healed and the tungsten phase is rapidly oxidized. Accelerated attack and rapid failure will occur at low temperatures. The material is resistant to oxidation only when the silica phase is liquid and completely covers the outer surface with a thick viscous coating. A deep crack existing in the specimen was healed over most of its length. The growth of tungsten oxide from below the surface occurred at one point in the cracked region. This formed during cooling and may be the result of localized tungsten segregation. One aspect of behavior that further limits the usefulness of $\text{SiO}_2 + \text{W}$ composites is related to the softening of SiO_2 . Good oxidation behavior is exhibited only above 2800°F. However, SiO_2 softens and becomes a viscous liquid above this temperature. Thus, as shown in Figures 26 and 27, Test $\text{SiO}_2 + 60\text{w/o W(H-23)}$ -L1 exhibited a surface temperature

of 3150°F and an internal temperature above 4000°F. This led to viscous flow. Consequently, the structural utility of the material will be very limited at temperatures where the best resistance to oxidation is exhibited. Emittance of the material was found to be 0.80 and was steady with time.

5. ZrC+C(C-12)

The results obtained for ZrC+C(C-12) are shown in Table 2 and in Figure 23. Sample ZrC+C(C-12)-L1 was tested at 3600°F (surface control) in air at 50 ft/sec. No problems in heating were encountered and a very low power input was required to hold the surface at 3600°F. The temperature gradient through the wall (154 mil thick) increased from 110°F at less than 1 minute to 788°F after 15 minutes. The time rate of change is shown graphically in Figure 23. The temperature gradient is similar to that found for JTA(D-13) and appears to be due to the growth of a thick ZrO₂ scale on the surface. The test was terminated at 15 minutes due to the very high internal temperature (4388°F) and apparent rapid surface recession. The surface was covered with a thick adherent oxide scale and no evidence of vaporization from the surface was found. The amount of oxidation appeared to be heavier near the base (cooled) of the sample than near the top (hot).

The top surface had a faceted appearance at high temperature, and brightness temperature readings were very difficult to obtain. The readings were very low and yielded a calculated normal spectral emittance of 0.10. The reason for this behavior is that the large primary graphite flakes found in the material oxidize preferentially and leave large voids and cracks in the heavy ZrO₂ scale which forms (see Figures 57-59).

III. RESULTS OF HIGH VELOCITY COLD GAS/HOT WALL OXIDATION TESTS ON CANDIDATE MATERIALS

The results of more than three hundred tests of candidate materials listed in Table 1 are presented below. The conditions under which these tests were performed at atmospheric pressure cover surface temperatures between 2000°F and 4000°F at flow rates which were less than ten ft/sec as a lower limit and up to 250 ft/sec as an upper limit. The candidate materials which were characterized under these conditions included $\text{HfB}_{2.1}$ (A-2), ZrB_2 (A-3), HfB_2+SiC (A-4), ZrB_2+SiC (A-8); RVA(B-5), Speer 710, ATJS, Si/RVC(B-8) and PT0178(B-9) graphites, Glassy Carbon(B-11), $\text{HfC}+\text{C}$ (C-11), $\text{ZrC}+\text{C}$ (C-12), KT-SiC(E-14), JT0992(F-15), JT0981(F-16), WSi_2/W (G-18), Sn-Al/Ta-10W (G-19), $\text{SiO}_2+60\text{w}/\text{oW}$ (H-23) and Hf-20Ta-2Mo (I-23).

A. Test Results for $\text{HfB}_{2.1}$ (A-2)

The results for $\text{HfB}_{2.1}$ (A-2) are summarized in Table 3. Figures 11 and 12 show typical post exposure photomicrographs of sectioned samples. As indicated earlier in Section II-B-1, substantial temperature gradients through the oxide which forms on this material are indicated. Moreover, at temperatures where thick oxides form (due to rapid oxidation), constant surface temperatures could not be maintained. No problems were encountered in runs at 3000°-3400°F. Temperatures could be held constant in all cases. The maximum temperature attainable at high velocity was 3240°F. All samples had a uniform light cream colored oxide scale on the top surface. Initial values for emittance ranged from 0.46 to 0.71 with an average of 0.55. The emittance tended to decrease with holding time. Final values (after 30 minutes) ranged from 0.18 to 0.57 with an average of 0.41. The average is 0.49 if three suspicious low values (0.18, 0.27, 0.37) are discounted. The surface appearance of HfB_2 after testing indicates a sensitivity to air flow. For a given temperature, samples from high air flow tests appeared to have a thicker scale. Subsequent measurements, however, did not support this observation. Heavy deposits of a white powder condensed on the cooled support rod indicating that a volatile oxidation product had been formed. Smoking of all samples was evident during testing.

Figure 28 shows the conversion depths observed after 30 minute exposure of $\text{HfB}_{2.1}$ (A-2) near 3300°F as a function of air flow. Comparison of these results with those obtained in furnace tests at flow rates of 1 ft/sec (3) indicates no definite effect of velocity. Moreover, these results support the MOTEL Criterion presented in Section I.

B. Test Results for ZrB_2 (A-3)

The behavior of ZrB_2 (A-3) is specified in Table 4. Figures 7-10 show typical post exposure photomicrographs, while the extent to which temperature gradients exist through oxide films on ZrB_2 and the effects of air flow rate on oxidation under high velocity CG/HW conditions are illustrated in Figures 6 and 29.

None of the ZrB_2 samples could be run at constant temperature in the CG/HW tests. In all runs at $3300^\circ\text{--}3500^\circ\text{F}$, the surface temperature began to fall off after the first two minutes. As the oxide scale grew in thickness, the surface temperature dropped. This behavior has been observed in all tests and is the result of rapid scaling and a large temperature drop through the scale. The emittance for ZrB_2 ranged from 0.47 to 0.76 with an average of 0.60 initial and 0.42 to 1.00 with an average of 0.69 final. The averages are in the range previously established for this material at $\lambda = 0.65\mu$. Viscous flow of the oxide was evident above 3400°F .

Comparison of the present results with the observations made in furnace tests at flow rates of 1 ft/sec indicate no definite effect of flow rate. In addition, the current results are in general agreement with the furnace tests thus supporting the MOTEL Criterion presented in Section I.

The results clearly indicate that the recession rates of ZrB_2 and HfB_2 are governed by surface (oxide scale) temperatures rather than substrate (interface) temperatures. This behavior suggests that transport through the oxide scale (ZrO_2 or HfO_2) governs the oxidation behavior of these materials. Minimum scale temperature controls the rate. Surface control of temperature should be used in CG/HW oxidation testing of these materials. This conclusion is based on the comparison of the current results obtained by induction heating (where the substrate temperature is higher than the surface temperature) and the results of furnace tests (3) (in which the substrate and surface temperatures are equal) shown below:

Material	Temperature		Time (min)	CG/HW Measured Recession	
	Substrate	Surface		High Velocity	Furnace
	°F	°F		(mils)	(mils)
ZrB ₂ (A-3-18)	3400 (constant)	3400→3180	60	12	
		3400	60		40-80
		3225	60		17-40
ZrB ₂ (A-3-13)	3400→3680 (3575 Avg)	3400	24	14	
		3400	30		20-40
		3575	30		35-70
ZrB ₂ (A-3-6)	>3400 (variable)	3400→3000	30	18	
		3400	30		20-40
		3300	30		12-26

Material	Temperature		Time (min)	CG/HW Measured Recession	
	Substrate	Surface		High Velocity	Furnace
	$^{\circ}\text{F}$	$^{\circ}\text{F}$		(mils)	(mils)
$\text{HfB}_{2.1}$ (A-2-15)	>3600 (variable)	3600→3190	60	18	
		(3400 Avg)			
		3600	60		34-74
		3400	60		18-40
$\text{HfB}_{2.1}$ (A-2-13)	>3600 (variable)	3400	30	4	
		(constant)			
		3600	30		17-37
		3400	30		9-20

C. Test Results for HfB_2+SiC (A-4) and ZrB_2+SiC (A-8)

Testing of HfB_2+SiC (A-4) presented no unusual problems or behavior during test. Glassy viscous (semiliquid) oxide films formed on all samples. The surfaces bubbled and blistered throughout the tests at 2900°-3300°F. Test temperatures were limited to the lower end of this range at high gas velocity due to coupling and power supply limitations. Temperatures held steady with time. Emittance values ranged from 0.87 to 1.00 with an average of 0.94. The values probably are not valid due to the nonuniformity (blistering) of the surface. This condition precluded accurate measurement of brightness temperature. Many of the samples had spotty areas of a green colored oxide scale (matte finish). Large areas of green scale formed on the side walls at temperatures above 3000°F. The cause of this condition could not be determined.

The behavior of ZrB_2+SiC (A-8) was quite similar to that of HfB_2+SiC (A-4), except that the patchy green oxide did not form on this material. Samples were covered with a smooth black glass at low temperatures (2675°F). At 2800°F and above, a patchy white oxide formed. The samples were more difficult to heat than HfB_2+SiC (A-4) and could not be run at temperatures much above 3000°F. Emittance values ranged from 0.83 to 0.98 with an average of 0.92. Blistering of the surface again precluded accurate measurement of brightness temperature. Figures 30 and 31 show post exposure photomicrographs of HfB_2+SiC (A-4) and ZrB_2+SiC (A-8). Metallographic observations after sectioning showed very little depletion of silicon carbide and small conversion depths which are in general agreement with the results obtained in furnace tests (3). Consequently, there does not appear to be any pronounced effect of air flow rate on the oxidation of these materials.

D. The Oxidation of RVA(B-5), Speer 710, ATJS, PT0178(B-9)
Graphites and Glassy Carbon (B-11)

More than two hundred samples of graphite and carbon have been tested in a study of the effect of temperature, gas velocity, specimen

configuration, and grade of material on oxidation behavior. The following grades of material were studied:

1. RVA(B5-L1 through B5-L22)
Density - 1.79 ± 0.02 gm/cc
Carbon - 99.2%
2. Speer Carbon Grade 710 (extruded rod)
Density - 1.65-1.75 gm/cc
Average Porosity - 18%
Ash Content - 2% max.
3. ATJS (National Carbon Co.)
Density - 1.82 gm/cc
Porosity - 9% average
Carbon - 99.5 + %
4. PT0178(B-9) (Union Carbide Corp.)
Density - 1.29 gm/cc
Carbon - 99.6%
5. Glassy Carbon - Grade 2000 (Lockheed Missile & Space Co.)
Density - 1.45 gm/cc
Porosity - nil
Carbon - 99.5 + %

All materials except the glassy carbon were solid cylinders 0.5 inch diameter by 1.0 to 1.5 inch long. The glassy carbon samples were hollow cylinders with one end closed (crucible-type) of a nominal 0.5 inch diameter by 0.7 inch long. Wall thickness at the sides and top was 0.122 inch.

The samples were mounted vertically on a water cooled copper stinger and were heated by induction using a 475 KC-23 KVA Lepel power supply (2). Ambient air was drawn past the heated specimens at 50 to 250 fps. Temperature of the top surface exposed to the gas flow was measured with a Milletron two-color pyrometer and a microoptical pyrometer (0.65μ wavelength). The two-color temperature was held constant during the test. The normal test procedure consisted of (1) setting the proper air flow, (2) heating the sample to test temperature within 15 seconds, (3) holding temperature and flow constant for various time increments, and (4) simultaneously cutting off power and air flow to terminate the test. The total time at the test temperature was recorded as the testing time. The change in length from the top stagnation point to the water cooled base as determined from micrometer measurements before and after test was taken as the total surface recession. The materials, conditions, and results of all tests are listed in Tables 7 and 8 and the significant results are summarized in Figures 32 through 53.

Oxidation rate curves for the four high density grades of graphite at 2850°F and 50 fps are presented in Figure 32. RVA and

ATJS are shown to have the same rate of oxidation. The latter is a leading grade of material for reentry applications. The Speer 710 graphite has a 10% higher rate of recession, most likely due to its lower density and purity. The most significant finding, however, is that glassy carbon oxidized at 1/3 the rate of RVA and ATJS under identical test conditions. This material has a low density (1.45 gm/cc) but has no porosity. It is a noncrystalline (glassy) material that appears to be quite different from the graphitic forms of carbon.

The effect of variations in temperature and gas velocity on the rate of surface recession was studied for Speer 710, RVA and glassy carbon. Oxidation rate curves are shown in Figures 33-35 and the effect of these variables on recession rates is summarized in Figure 36. Many of the rate curves for the flat-faced specimens exhibited a nonlinear rate behavior in which the rate tended to increase with time of exposure (Figures 33 and 35). As will be shown later, this results from a shape change. The flat faced specimens burn to a conical tip which effectively alters the flow conditions and increases the rate of recession. With the exception of some edge rounding, the top surface remained fairly flat for the first three minutes. The rate curve appeared to be linear during this initial period and the slope of the best fit straight line for the first 3 to 4 minutes was taken as the surface recession rate. In subsequent tests single runs were made with a three minute exposure and the recession rate was taken as 1/3 of the total measured recession. As will be shown later, however, even these values are not representative of the true recession behavior.

Figure 36 shows that the oxidation behavior for each of three different materials was different. The surface recession rate for RVA did not increase with temperature from 2850° to 3250°F at flow rates of 50 or 150 fps. This behavior agrees with results of furnace tests on RVA graphite above 2800°F (3). The oxidation rate, however, increased by 56% (from 36 to 56 mil/min) when the air flow rate was increased from 50 to 150 fps. In furnace tests at low flow rates (< 10 fps), the recession rate above 2800°F was in the range of 8 to 14 mil/min. The effect of air velocity on recession rate of flat faced cylinders of RVA is summarized in Figure 37. The significant increase in rate with increased velocity demonstrates that surface recession is governed by the gas phase in these tests. As will be discussed later, increasing the velocity raises the partial pressure of oxygen near the surface and thereby increases the rate of reaction.

Unlike RVA, the surface recession rate of Speer 710 was sensitive to variations in both temperature and flow rate. The rate increased by about 30% with an increase in temperature from 2650° to 3050°F. At a flow rate of 50 fps, the rate became insensitive to temperature above 3000°F and the behavior was like that of RVA (Figure 36). The surface recession rate was 20% higher than that of RVA in this temperature range. Like RVA, the surface recession of Speer 710 also increased with flow rate. At high flow rates (150 fps), it appears that sensitivity of rate to temperature for Speer 710 extended to higher temperatures.

The glassy carbon materials exhibited still a third type of behavior in this initial series of tests. As shown in Figure 36, a very strong dependence of recession rate on temperature was found. Below 3000°F, this material oxidized at a much slower rate than the graphites. However, above 3000°F, glassy carbon burned at much higher rate than the other materials. At 2850°F, the rate increased by 23 mil/min on raising the flow rate to 150 fps. This differential is the same as that found for RVA (21 mil/min) and Speer 710 (22 mil/min).

Two different grades of glassy carbon were evaluated in these tests. The oxidation behavior of both grades should be similar. The grade 3000 material is produced by the same process but is cured at a higher temperature to enhance resistance to thermal shock. No problems with thermal shock were encountered in the tests conducted with either grade of glassy carbon. As shown in Table 7 the calculated values of normal spectral emittance for glassy carbon at 2850°-3250°F was 0.54-0.55. This is significantly lower than the values of 0.75 to 0.80 obtained for RVA and Speer 710 graphites in this temperature range.

The differences in oxidation behavior observed for these three materials indicated a need for a more detailed study of factors controlling recession rates in CG/HW tests before proceeding with the test program. Shape changes during testing and nonlinearity of rate curves were of particular concern. The marked effect of gas velocity on rates indicated that slight variation in shape could be an important factor. Shape influences the flow patterns and the nature of gas phase boundary layer at the surface. To check the effect of sample configuration on surface recession, tests were conducted on flat-faced, hemispherical-capped (0.25 inch radius) and conical tipped (30° included angle) cylinders of Speer 710 graphite. The starting configurations and shape changes with time of exposure at 2850°F in air at 50 fps are shown in Figure 38. Corresponding rate curves are given in Figures 39 and 40.

As shown in Figure 38, the nose configuration of both the flat-faced and hemispherical capped specimens changed during testing. The edges of the flat-faced cylinder were rounded at 3 minutes and the top surface became hemispherical at about 6 minutes. After 9 minutes the sample was approaching a conical shape. The hemispherical-capped sample developed a well formed conical shape at 9 minutes. On the other hand, the nose configuration of the 30° cone specimen was not altered significantly during testing. As shown in Figure 38, the very tip became rounded (about 0.06 inch radius) but the 30° conical nose was stable to 9 minutes. This appears to be a limiting configuration that the other samples are tending to approach.

The rate curves (Figures 39 and 40) support the conclusion that a 30° cone is the limiting stable configuration in CG/HW tests. The surface recession rate curves for the conical samples were perfectly linear out to 9 minutes. This is the normal behavior that would be expected for the oxidation of graphite. It indicates a stability of temperature and gas phase compositions at all points on the surface during testing. The rate curves for the hemispherical and flat-faced samples were not linear and tended to increase in slope with time. The initial slopes indicated approximately half the rate exhibited by the conical sample. After 9 minutes, however, the instantaneous linear rate (tangent slope) for the hemispherical sample was the same as the rate for the conical sample. As shown in Figure 38, the hemispherical sample at this point was approaching the limiting conical configuration and the nose radius was approaching 60 mils.

Since the total recession after 3 minutes had been used to calculate linear rates in the study of temperature and velocity effects, the shape factors were studied for short exposure times. As shown in Figure 88, the recession rate curve for the flat-faced cylinders is non-linear from the very start. The slope of the curve increased steadily with time. Even the slight shape change during the first 3 minutes results in significant rate variations. Rates obtained as calculated by (1) linear extrapolation to zero, or (2) tangent to rate curve at various times are summarized below:

<u>Time</u> <u>(min)</u>	<u>Recession Rate (Mil/Min)</u> <u>at 3650°F and 50 ft/sec</u>	
	<u>Linear</u>	<u>Tangent</u>
1	42	42
2	45	48
3	48	52
4	50	60
5	53	86

Any rate from 42 to 86 mil/min can be obtained depending on length of test and method of rate calculation. The results clearly show that constant rates of surface recession of graphite cannot be obtained using flat-faced samples in these CG/HW flow tests.

The rate curve for the 30° cone tipped sample, on the other hand was linear over the entire range. This confirmed results of previous tests (Figure 39) and clearly demonstrated the suitability of the conical shape for the CG/HW tests. Since shape and surface recession rates are constant with time, meaningful data can be obtained.

With all other configurations, shape changes during the test and a wide range of rate values can be obtained for any set of test conditions depending on length of test, temperature, flow rate, and method of calculation. The inconsistency of data in these cases leads to results that have limited utility and which, in some cases, may prove to be misleading. This is illustrated by Figure 41 which compares the effect of temperature on the surface recession of conical and flat-faced samples. The conical sample has twice the surface recession rate and about the same temperature dependency of rate as the flat sample to 3600°F. However, above 3600°F, the rate for the flat sample remains constant with increasing temperature while that for the conical sample shows a marked increase. As indicated below, these differences are due to changes in the gas phase, particularly in the concentration of oxygen (oxygen partial pressure) with increasing temperature. Oxygen pressure is higher and less variable for the conical samples. It is recommended that 30° cone tipped samples be used exclusively in all future CG/HW tests of graphites. A specimen length of 1-1/2 to 2 inches is required for preparing these samples.

Two problems have been encountered in the use of conical tipped samples. The first is related to temperature distributions and the measurement of temperature in samples heated by induction. The tip portion does not couple with the inductive field as well as the bulk portion. Thus, temperature at the tip will be lower than that of the bulk sample. This condition is aggravated by the air flow which tends to cool the tip still more. It has not been possible to obtain an exact measurement of tip temperature. The surfaces are inclined to the line of sight at a steep angle and readings cannot be made with the micro-optical pyrometer. The two-color pyrometer has a field of view that includes the entire top surface. Although readings are not influenced by the viewing angle, they do not represent actual tip temperature. Instead, an average temperature based on the intensity of radiation from the entire conical surface is indicated. The exact difference between the indicated temperature and actual tip temperature could not be determined. Visual observations indicate that the gradient is less pronounced at temperatures above 3000°F. In all cases, however, the tip temperature is less than the indicated and reported values.

The second problem with respect to the use of conical tipped samples is related to the measurement of surface recession. At low temperatures and high flow rates, the tip cools to a point where its rate of recession is equal to or less than that of the conical surface. Under these conditions, the actual tip recession is governed by the rate of side wall recession as shown in Figure 42. If the side wall recedes 1 mil (measured normal to the surface) the tip will recede by 3.86 mil if the 30° cone geometry remains unchanged. Under these conditions, the tip will retain a sharp point (dashed lines in Figure 42). The actual recession rate is about 1/4 of the apparent total tip recession. Recession is measured normal to the surface and in this case, it is the recession of the conical surface that controls the tip recession.

A test that approached this condition is shown in Figure 42B. This sample of Speer 710 was exposed for 3 minutes at 2650°F to air flowing at 150 fps. After testing, a thin spire 10-20 mil in diameter extended almost 0.25 inch upward from the tip. A short length of the spire is still evident in the photograph. It is obvious that the tip recession in this case was controlled by recession of the conical surfaces and not by burning of the tip. Measured tip recession after removing the spire was 259 mils. Had the sidewalls retained a perfect 30° shape to the very tip, the tip recession would appear to be 3.86 times the actual recession normal to the surface (Figure 42). Actual surface recession, therefore, would be 67 mils or a rate of 22 mils/min. However, as shown in Figure 42, the upper part of this sample conforms to a 45° cone. Geometrical considerations in this case show that the tip will recede 2.61 mils when recession normal to the surface is 1 mil. The actual recession rate for this sample, therefore, is 99 mils or 33 mil/min.

At higher temperatures, the rate of tip recession exceeds the rate of recession normal to the cone surface and a rounded nose is formed on the sample. This condition is illustrated in Figure 42C (3 minutes, 2850°F, 50 fps). The tip now has a well defined radius (about 60 mils) and even a 90° angle cannot be used to approximate the surface. The recession on the tip is normal to the surface at all points and the total change in length along the vertical axis is a direct measure of surface recession. Surface recession for this sample is 240 mils or 80 mil/min. If this were not the case, the tip would form a sharp point with a well defined conical surface. Figures 43 and 44 show post-exposure sections through samples RVA(B-5)(L-6)(65-1) and RVA(B-5)(L-16)(108-3). The former was a flat face cylinder while the latter was a 30° cone prior to exposure. Reference to Table 7 shows that the former sample experienced a recession of 227 mils while the latter had a recession of 264 mils.

Using Speer 710 and RVA grades of graphite, a detailed study was made of the effect of temperature and gas velocity on surface recession in CG/HW tests. The 30° cone tipped samples were used and test conditions were limited to those in which a spherical tip of uniform and constant radius was generated (Figure 42C). Under these conditions, the total change in length along the vertical axis is a measure of the surface recession. The results of studies from 2550° to 4050°F in air at 50 to 250 fps are given in Table 7 and Figures 45-48.

The data indicate a relatively low but definite sensitivity of recession rate to temperature up to 3650°F. The rates tend to reach a plateau at about this temperature. Above 3700°F, the rates increase with temperature, and tend to approach a second plateau at 3950°F. A significant velocity effect is indicated with rates almost doubling on a five-fold increase in air velocity.

An Arrhenius plot (log rate vs. $1/T - ^\circ K$) of the data was made to aid in interpretation of the results. As shown in Figure 46, an Arrhenius relationship ($K = Ae^{-E/RT}$) can be used to describe the data in the low temperature region at each of the three flow rates. The slope or apparent activation energy (E) is calculated to be 4220 cal/mole. All

the data can be represented by straight lines on an Arrhenius plot to 3750°F. Above 3750°F, an increase in slope is indicated for the 50 fps data. The higher velocity data, however, appear to be linear to 3950°F. It is possible that a plateau (temperature insensitive region) exists from 3350° to 3750°F with a second temperature region of higher slope above 3750°F at all flow rates. Although the data suggest this, they are not adequate to justify plotting the high velocity results in this manner. One straight line gives the most reasonable fit. Many additional test points are needed to establish the exact shape and slope of the curves.

Most of the data in Figures 45 and 46 are from tests of Speer 710 graphite ($\rho = 1.65$ to 1.75 gm/cc). The behavior of RVA graphite ($\rho = 1.79$ gm/cc) was checked at each flow rate. As shown, the surface recession behavior of RVA was the same as that of Speer 710. No significant differences were noted. This indicates that the slight differences in density, structure and purity of these two grades did not materially affect the oxidation behavior. The data generated from tests of Speer 710 can be used to describe the behavior of RVA.

The value of activation energy for the oxidation of graphite found in this study is in excellent agreement with results of other investigators. Gulbransen, Andrew and Brassart (6) found a sharp transition in activation energy for the oxidation of graphite at 725°C (1337°F). Values for E of 39,000 cal/mole were observed from 400° to 725°C (752°-1337°F) and of 3600 cal/mole from 725° to 1500°C (1337°-2732°F). Okada and Ikegawa (7) observed a similar transition at about 800°C (1472°F). Their data show a high activation energy region from 700° to 800°C (1292°-1472°F) and a low activation energy region from 800° to 2000°C (1472°-3632°F). According to the authors, the latter consists of two low slope regions (about 3000 cal/mole activation energy each) separated by a transition region of moderate slope from 1200° to 1400°C (2192°-2552°F). Considering scatter in test data, the entire region could be represented by one straight line having a slope of about 5000 cal/mole. Results of the present study indicate an activation energy of 4220 cal/mole from 2550°F (1371°C) to 3750°F (2066°C).

Gulbransen, Andrew and Brassart (6) also found that the rate of oxidation was dependent on oxygen pressure to the 0.32 power. That is, for any given temperature, rate increased with oxygen pressure. At each pressure, however, the data fitted an Arrhenius plot with the slope at 3600 cal/mole. The following empirical equation was derived to describe the oxidation behavior:

$$\dot{m} = 1.86 \times 10^{-6} P_{O_2}^{0.32} e^{\frac{-3600}{RT}} \text{ gm/cm}^2\text{sec} \quad (1)$$

For graphite of a density of 1.8 gm/cm^3 , this converts to:

$$\dot{S} = 2.44 \times 10^{-2} P_{O_2}^{0.32} e^{\frac{-3600}{RT}} \text{ mil/min} \quad (2)$$

where T is in °Kelvin and P is in Torr.

As shown in Figure 47, the CG/HW test data show a velocity dependency of rate. This behavior was analyzed by plotting log rate vs. log velocity for normalized 2950°F data at 50, 150 and 250 fps from Figure 46 and single point 2650°F data for tests at 25, 50, 75 and 100 fps. Both curves are parallel with a slope (velocity dependency) of 0.38. This is numerically similar to the pressure dependence data of Gulbransen, et al. (6). The equivalency of the power dependency of rate on oxygen pressure and gas velocity is considered to be a significant factor and not a mere coincidence. Total gas pressure at the surface does not increase with increased velocity in subsonic CG/HW tests. Even at 250 fps, total pressure at the surface is still one atmosphere. This was proven experimentally by means of pressure probes and can also be shown analytically. In fact, with the 30° cone in a 1.5 inch diameter tube, total pressure may decrease slightly on the conical surfaces due to velocity increases in the flow constricted region of the tube. The effect of velocity on oxidation rates, therefore, must be due to changes in composition of the boundary layer or localized atmosphere near the surface.

At the start of oxidation, oxygen is consumed rapidly. The atmosphere near the surface is depleted in oxygen and enriched in CO, CO₂ and N₂. This causes a significant drop in oxygen partial pressure and a drastic reduction in the rate of reaction at the surface. Transport of oxygen into the atmosphere surrounding the sample and removal of reaction products tends to increase the oxygen partial pressure with a resultant increase in the rate of reaction. Eventually, a balance will be approached between the inward transport of oxygen, the outward transport of CO, CO₂ and N₂ and the reaction rate at the surface. Oxygen partial pressure will tend to stabilize at some value considerably below that of normal air. For example, in studies of the oxidation of tungsten wires at 2590°C (4690°F) in slowly moving air at 5 Torr pressure, the oxygen content of the air in a 1 cubic foot volume stabilized at 2.4 volume percent (normal 21 volume percent) after four minutes (8). Oxygen partial pressure decreased to 0.36 Torr (original 3.15 Torr).

The effect of gas velocity or flow is to increase the oxygen partial pressure by increasing transport of oxygen to the atmosphere surrounding the sample and/or sweeping away of reaction products and inert gases. It is reasonable to expect a linear relationship between oxygen partial pressure and velocity over some finite range of gas velocities. Doubling the mass flow rate doubles the amount of oxygen brought into the system. Hence, it is not surprising that the power dependencies of rate on oxygen pressure and gas velocity in subsonic flow are similar. There will, however, be an upper limit on gas velocity where this relationship will not hold and further increases in velocity will not increase oxygen partial pressure or rate of oxidation. This will be the velocity at which the oxygen partial pressure (concentration) at the surface approaches that of normal air. In the oxidation of tungsten at 5 Torr pressure, this condition was achieved at a velocity of about Mach 1. Further increases in oxygen pressure now can only be achieved by an increase in total pressure. This of course will occur during hypersonic

flight or reentry. The incremental pressure increase, however, will be proportional to the square of the velocity and the 0.3-0.4 power dependence of rate on velocity probably will not be found.

The foregoing discussion relates to the so-called diffusion or transport controlled regime of the oxidation of graphite. Many investigators, including Gulbransen, Andrew and Brassart (6) point out that the rate of oxidation in the region of low sensitivity of rate to temperature (low activation energy) is controlled by transport diffusion of oxygen to the surface. It is common to have this region referred to as one in which the rate is not sensitive to temperature. Even the current test data (Figures 36 and 45) show a broad temperature range for flat-faced samples in which the rate of surface recession did not increase with temperature but did increase with flow rate. A similar behavior was found for tungsten in air at low pressure (8). Here, in fact, rates actually were observed to decrease with increased temperature. The truth, however, is that the rate of C-O₂ reaction in all cases is increasing with temperature. But as the reaction rate increases, the partial pressure of oxygen will decrease unless the rate of oxygen transport to the surface is also increased. Under a given set of flow conditions, this does not happen. Thus, the so-called diffusion regime in which little change of rate with temperature is observed is characterized by a decreasing partial pressure of oxygen with increasing temperature. In a low activation energy process such as this (3000-5000 cal/mole) the slight increase in reaction rate at the surface due to a temperature increase is easily offset by a decrease in oxygen partial pressure.

The correct picture for the oxidation of graphite above 800°C (1472°F) is one of continually increasing rate with both temperature and oxygen pressure according to the Arrhenius relationship:

$$\dot{m} = kP^z e^{-E/RT} \quad (3)$$

From 800°C to 2065°C (1472°C-3750°F) $z = 0.32-0.38$ and $E = 3600-4220$ based on results of Gulbransen's work (6) and this study on Speer 710 and RVA graphites. Although the activation energies observed in the present study are comparable to those reported by Gulbransen et al., (6), the rates are much higher in the present investigation. Thus, for $P_{O_2} = 150$ torr, at $T = 1700^\circ K$, Eq. (2) yields a rate of about 0.04 mils/minute. The present study indicates 60 mils/minute at 250 fps.

The tendency for the data to show a plateau at 3750°F suggests that even in tests to 250 fps, oxygen partial pressure may not be holding constant at high temperatures where the surface reaction rates are rapid. This fact also is indicated by results of HG/CW tests on graphites at velocities of 300 to 500 fps. A summary of all the oxidation data for graphites in both HG/CW and CG/HW tests is presented in Figure 48. The HG/CW data are from tests with the Model 500 arc at Avco using flat-faced specimens (4). Tests were conducted at 1 atm. pressure with gas velocities at 300 or 500 fps.

At 3950°F, the rate for conical samples at 300 fps would be about 200 mils/min. This is double the rate for the flat-faced specimens in HG/CW tests at this temperature and flow rate. As shown in Figures 39, 40 and 41, conical samples oxidize at twice the rate of flat-faced specimens at all temperatures to 3650°F. Thus, the data for HG/CW and CG/HW tests are consistent and in near perfect agreement at 3950°F when the shape factor is taken into account. However, above 3950°F, The HG/CW data show a steady increase of rate with temperature that is greater than that observed in CG/HW tests at lower temperatures. The rate data are linear on an Arrhenius plot, giving a slope (activation energy) of 14,000 cal/mole. This is more than three times the value found in CG/HW tests below 3950°F. The data for three different grades of graphite (RVA(B-5), AXF-POCO(B-10) and Pyrolytic Graphite (B-6) (A-Plane) all fit the same curve. The results indicate that minor variations in purity, density, porosity and general structure have little effect on oxidation rates. However, large differences in density do have a pronounced effect on the oxidation rate of graphite as illustrated by the results obtained for PT0178(B-9) and Glassy Carbon (B-11). The results obtained for these materials are shown in Table 8 and Figure 49.

Samples of PT0178(B-9) (1.29 gms/cc) were machined to a 30° conical tip so that results are directly comparable to those from tests on the higher density RVA (1.79 gm/cc) and Speer 710 (1.73 gm/cc) materials. The data are reasonably represented by a straight line on an Arrhenius plot that parallels the base line data for RVA and Speer 710 at 50 ft/sec. The activation energy (slope) is 4220 cal/mole. The recession rates for PT0178 are significantly higher than those for the higher density materials. Assuming that the mass loss rate (\dot{m}) is the same for all materials, the surface recession rate (\dot{S}) for PT0178 was corrected by a simple ratio of densities. As shown in Figure 49, the density corrected rate data are in excellent agreement with data for RVA and Speer 710. The studies were extended to higher flow rates (150 ft/sec) and a similar behavior was found. Four test points (Table 8) were in excellent agreement with data on RVA and Speer 710 under the same conditions when corrected for density differences. It is concluded that the oxidation behavior and mass loss rates (\dot{m}) for these different grades of graphite are identical from 2750° at 3450°F in subsonic flow environments. The surface recession rates (\dot{S}) differ by virtue of differences in density only. Figures 50 and 51 show post exposure photomicrographs of PT0178(B-9)-L4.

Five samples of LMSC Grade 2000 glassy carbon flat face cylinders were tested in air at 50 ft/sec to determine behavior at temperatures above 3150°F. The results along with 3 previous data points (contained in Table 7) are shown in Figure 49. At temperatures below 3250°F, a strong temperature dependency of rate is indicated. The slope of the best fit straight line indicates an activation energy of 40,500 cal/mol. Above 3250°F, a definite change in slope is indicated and the data can be reasonably represented by a line of slope 4220.

The data on glassy carbon were corrected for both shape and density. The rates were doubled to convert flat face data to conical tip data and then were divided by 1.23 to correct for the density. As shown in Figure 49 the corrected data are in almost perfect agreement with the RVA base line data from 3250° to 3550°F. Figures 52 and 53 show post exposure photomicrographs of Test Glassy Carbon (B-11)-2000-3 at 3550°F.

At higher temperatures, a major structural change does not appear to influence the oxidation of carbon. Graphite and glassy carbon have widely different structures but show the same mass rate loss (\dot{m}) above 3250°F. The transition to a high slope region with glassy carbon below 3250°F may be similar to the transition observed for normal graphites below 1500°F. At low temperatures, CO₂ is the principal reaction product and the activation energy is in the range of 39,000-40,000 cal. Above 1472°F, both CO and CO₂ form and the activation energy is low, 3500-5000 cal. It may be that glassy carbon undergoes this same transition in behavior but at a much higher temperature (3250°F). This is not unreasonable in view of the nature of the bonds and structure of glassy carbon compared with normal graphite. The two materials appear to have identical behavior over a shifted temperature range. In temperature-pressure regions where the same rate laws are followed, glassy carbon will recede faster than RVA or equivalent graphites due to its lower density. It is interesting to speculate whether the shift in behavior to a high activation energy (14,000-20,000 cal) observed at about 4000°F for high density graphites will be similarly shifted to still higher temperatures for glassy carbon. If this is the case, glassy carbon should exhibit lower recession rates than other graphites above 4000°F.

Films of arc plasma tests of 2000 grade glassy carbon in the Avco Model 500 (4) arc suggested that surface melting occurred on one sample tested at the highest level of heat flux in air at one atmosphere pressure. The carbon phase diagram shows the triple point of graphite to be 100 atm, and 4020°K (3747°C, 6777°F) (9). Tests with glassy carbon at a pressure of 110 atm showed that melting occurs the same as with graphite (10). After solidification, the material was found to have the hexagonal structure of graphite. The unmelted material remained as glassy carbon, even after heating very close to the melting point.

Samples of glassy carbon (2000 grade) were heated in an arc furnace under helium at a pressure of 1 atm to determine if this material can be melted at pressures below the triple point (100 atm) for normal graphite. In the first series of tests, a water cooled tungsten electrode was used to establish the arc. The surface of glassy carbon was readily melted. However, metallographic examination revealed that melting resulted from the formation of a W/WC eutectic on the surface by transfer of tungsten from the electrode. A zone of very fine grained equiaxed graphite crystals was formed beneath the eutectic layer. The zone graded off into the glassy carbon matrix. No trace of W or WC was found in this region and the general appearance suggested that melting of the glassy carbon had occurred in this region. A second series of tests was conducted using a water cooled graphite (Speer 710) electrode to prevent surface melting by contaminants. A thin layer of pyrolytic

graphite was deposited on the surface. Below this layer, a zone of very fine grain equiaxed crystals of graphite similar to that found in tests with the tungsten arc was found. Again, this layer had the appearance of a molten zone. Melting in this case, however, was found to be the result of formation of a carbon-titanium carbide eutectic. Contamination by titanium occurred from melting on a water-cooled copper hearth previously used for melting titanium alloys. Electron probe studies showed that only trace amounts of the metallic impurities were needed to cause localized surface melting and graphitization. The metallic elements appear to diffuse rapidly into the glassy carbon structure.

Tests were conducted in a clean system using direct resistance heating of glassy carbon rods. The rods were heated to temperatures at which large amounts of carbon vapor were evolved. No evidence of localized melting or graphitization was found. At one atmosphere (helium) the glassy carbon structure was retained right to the vaporization temperature. Extensive fine porosity was developed in a uniform pattern from surface to center of the rods. This condition appeared to be caused by a condensation of vacancies during heating. Extensive plastic deformation of the rods also occurred at high temperature.

It is concluded that glassy carbon does not melt at low pressure. The apparent surface melting observed in plasma tests with the Model 500 arc most likely was the result of surface contamination with an element that caused eutectic melting. It is believed that tungsten contamination from the stinger may have caused this behavior.

The linearity of the HG/CW data shown in Figure 48 (4) with respect to temperature on an Arrhenius plot and the high value of activation energy indicate that the gas velocity in these tests (300-500 fps) was sufficiently high to maintain a constant partial pressure of oxygen near the surface at temperatures from 4000° to 6000°F. The results tend to confirm the indications from CG/HW tests that the temperature sensitivity of rate (activation energy) is higher above 3750°F. This suggests that a change in the surface reaction occurs at or near this temperature.

Gulbransen, et al. (6) found a sharp decrease in activation energy above 725°C (1337°F). This coincides with a change in reaction products. Below 800°C (1472°F), CO₂ is the principal reaction product. At 800°C (1472°F), the ratio of CO₂ to CO was found to be 115 to 1 (6). Above 800°C both CO and CO₂ are formed. With increasing temperature, the rate of CO formation increases while that of CO₂ formation decreases. Hence, the ratio of CO₂ to CO decreases with increasing temperature. At 1400°C (2552°F), the ratio was found to be 0.73 to 1 (6). A change in activation energy will occur with a process shift of this type. A low apparent activation energy often characterizes a duplex process where the rate of formation of one product (CO₂) decreases with temperature while the rate of a second product (CO) increases. The total rate of oxidation is the sum of the two and will show a low apparent temperature dependency. At still higher temperatures, the formation of CO will be predominant and an increased temperature sensitivity (activation energy) may be observed. This may very well be the case for oxidation above 4000°F where plasma arc tests indicate an activation energy of 14,000 cal/mole.

Opinion is divided on whether the oxidation of graphite is controlled by diffusion processes in the gas phase or by phase boundary processes at the surface. Those favoring the first view cite flow sensitivity and temperature insensitivity of rates at high temperature to support this theory. The foregoing discussion, however, tends to support the second point of view (Phase Boundary Control). A detailed theoretical treatment of the subject which also supports this point of view has been given by Ong (11). It is postulated that the rate of oxidation at a constant partial pressure of oxygen is governed by surface reactions and hence by temperature up to at least 6000°F. Three regimes are indicated: (1) a low temperature region where CO₂ is the primary product and the activation energy is high (40,000 cal/mole), (2) a moderate temperature region in which both CO and CO₂ are formed and the activation energy is low (3000-5000 cal/mole), and (3) a high temperature region in which CO is the primary product and the activation energy is intermediate (10,000-15,000 cal/mole). In the second region, rates at any temperature will vary with oxygen pressure to the 0.3-0.4 power. The extent of each region and the transition from one region to the next will depend on oxygen partial pressure (and perhaps total pressure).

The data in Figure 48 show that pyrolytic graphite in an A-plane orientation oxidizes the same as other grades of polycrystalline high density graphite. This supports the findings of Gulbransen, Andrew and Brassart (12) who demonstrated that pyrolytic graphite had the same activation energy and pressure dependence for oxidation as spectrographic carbon in the 800°-1500°C range. In the C-orientation, however, pyrolytic graphite has a significantly lower rate of oxidation at all temperatures and a slightly higher activation energy (20,000 cal/mole) compared with the A-direction behavior. Since transport should be the same in these tests, the differences in behavior must be due to changes in chemical reactions at the surface. This lends further support to arguments that the oxidation of graphite is a phase boundary controlled process.

The behavior of graphite is strikingly similar to that found for the oxidation of tungsten at temperatures and pressures where volatile oxides are formed. The so-called transport or diffusion controlled oxidation regime of graphite results from a decrease in oxygen partial pressure at the surface with increased temperature. It is a characteristic of a given system and not of the oxidation behavior of the material. Increasing gas velocity increases the oxygen partial pressure at the surface, thereby "restoring" the temperature dependency of rate. The contribution of boundary layer theory to rate prediction should be one of clearly defining surface temperatures and oxygen partial pressures. However, unless accurate data on activation energies and pressure dependencies are available, reliable predictions of recession rates cannot be made. With a more accurate determination of activation energies and pressure dependencies, equations can be derived to accurately predict the surface recession over a broad range of temperatures and pressures.

E. Oxidation of Siliconized RVC Graphite Si/RVC (B-8)

The results of tests with siliconized RVC graphite are summarized in Table 9. The samples were exposed to temperatures of 2900°, 3000° and 3100°F for 60 minutes at velocities of < 10, 50 and 150 ft/sec. After test, the top surface was examined for signs of coating failure. As shown in Figures 54 and 55, failures were not observed in 1 hour at 2900°F. At 3000°F, one out of three samples had random failures on the top surface and all samples had sidewall failures where the temperature was somewhat higher. Complete failure was observed in 15 minutes at a temperature of 3100°F. The temperature for a 1 hour life in subsonic flow appears to be about 3000°F. This is in good agreement with a value of 3060°F established by furnace tests (3).

In the subsonic flow tests, the one sample that failed at 3000°F was tested at the highest velocity (150 ft/sec). There may be a slight reduction in coating performance with increased gas velocity. However, test results are by no means conclusive. All samples were observed to form blisters above 2900°F, indicating the existence of a low viscosity oxide film (fluid silica). No significant differences in appearance were noted at the various temperatures and gas velocities.

F. Oxidation of Hypereutectic Carbides HfC+C(C-11) and ZrC+C(C-12)

The test data for CG/HW tests of hypereutectic carbides are given in Table 10 and results are summarized in Figures 56 and 57.

Temperature and velocity appear to have little effect on the surface recession behavior of hypereutectic carbides. As shown in Figure 56, rates were not consistently increased as temperature increased from 3400° to 3600°F and flow rate increased from 10 to 150 ft/sec. Most of the variation appears to be scatter in test results. As shown below, the surface recession data at 3400°F at all flow rates are in good agreement with results of furnace tests in slowly moving air. The relative insensitivity of rate to temperature also is in agreement with results found in furnace tests (3).

<u>Surface Recession in 30 Min.</u>					
<u>Material</u>	<u>Temperature</u> (°F)	<u>Furnace Test</u> < 10 ft/sec (mil)	<u>CG/HW Tests</u>		
			<u>10 ft/sec</u> (mil)	<u>50 ft/sec</u> (mil)	<u>150 ft/sec</u> (mil)
HfC+C(C-11)	3400	30-50	43	55	53
ZrC+C(C-12)	3400	50-80	53	79	61

1. ZrC+C(C-12)

Samples were exposed at 3400°, 3600° and 3800°F to air at < 10, 50 and 150 ft/sec. Brightness temperatures were difficult to measure due to extreme color variations on the surface. This is reflected in the low values of emittance calculated from tests data (Tables 2 and 10).

Values ranged from 0.05 to 0.18 and are not considered valid measurements. All samples had a crazed surface appearance with acicular particles, presumably graphite, protruding out through the scale. Typical structures are similar to those for HfC+C as shown in Figure 57A. The oxide scale developed over most of the surface was cream colored. Around the protrusions, the scale had rust or brown color. No other significant features were observed during testing. Tests were terminated short of 30 minutes when it was not possible to hold surface temperatures constant due to excessive temperature gradients in the oxide scales. Figures 58 and 59 show typical post exposure photomicrographs of ZrC+C(C-12)

2. HfC+C(C-11)

The behavior and sample appearance of this material was very similar to that of ZrC+C. In four samples, however, a very marked difference in appearance was observed. These samples developed a smooth oxide surface of a uniform cream color. As shown in Figure 57B, the acicular protrusions were absent. All four samples were from the same billet, #1422A (see Table 8 of Reference 1). This billet had the highest density (9.32 gm/cc) and the lowest carbon content (13.60%) of all the HfC+C billets. The sample shown in Figure 57A is from billet #1416B, with a carbon content of 14.25% and a density of 9.1 gm/cc. The marked difference in behavior is most likely due to the variation in carbon content. It is possible in this case to assess the contribution, if any, that excess carbon and acicular particles in the scale make to oxidation behavior. Although results are not conclusive, the low carbon material appears to have a lower recession rate than the high carbon material at equivalent temperatures (Table 10). Variations in flow rate, however, preclude a clear analysis of behavior. Accelerated attack at low temperatures is indicated by the bulge at the base of the low carbon sample (Figure 57B). Figures 60 and 61 show typical post exposure photographs of HfC+C(C-11).

G. Oxidation of KT-SiC(E-14)

Four samples of KT-SiC were tested in high velocity air using top surface temperature control. The first test (59-1) was conducted in air at 50 fps with the top surface at 3960°F. A thick puffy oxide scale developed immediately and the top surface appeared to cool due to a separation and/or an insulating effect. Surface temperature could not be maintained; at 1.9 minutes it had dropped to 3560°F at full power. The substrate temperature probably was well above 4000°F. The top surface was heavily eroded and dished, and the side wall also was heavily attacked. The remaining tests were run at lower temperatures. Heavy attack of the side wall was also noted in tests at 3660°F (in 2 minutes) and 3450°F (in 27 minutes). Since the side wall tends to run at least 50° to 150°F hotter than the top surface, very rapid oxidation of this material appears to occur above 3500°F. This is in reasonably good agreement with results of furnace tests and HC/CW tests. At a test temperature of 3360°F, the top surface was only lightly attacked and side wall erosion was moderate in 30 minutes. One of the four samples tested had a thermal shock failure (Run 67-1).

The tested samples were cross-sectioned and the surface recession was measured. The results of the two 30 minute tests are shown below along with corresponding data from furnace tests (3). Post exposure photomicrographs of these tests are shown in Figures 62 and 63.

Sample No.	Surface Temperature °F	Time min	CG/HW Measured Depth of Conversion	
			High Velocity mils	Furnace mils
E-14-L4	3360	30	NIL	
(67-1)	3350	30		1-3
E-14-L1	3450	27	15	
(59-2)	3450	30		6-13

The results are in reasonable good agreement and indicate that the recession of KT-SiC is governed by surface temperature and these rates are not significantly influenced by velocity in the subsonic range.

H. Oxidation of Graphite Composites JT0992(F-15) and JT0981 (F-16)

The oxidation behavior of graphites modified with HfC-SiC-C (JT0992)(F-15) and ZrC-SiC-C(JT0981)(F-16) was evaluated in CG/HW tests and the data are presented in Table 12 and Figures 64-71. The surface recession behavior is summarized in Figure 64. The data have been normalized to 30 minute exposure using a parabolic rate law to extrapolate short run data.

As shown in Figure 64, JT0992 samples have less total surface recession in 30 minutes than JT0981 at all temperatures from 2800° to 3800°F. A dependency of rate on gas velocity is indicated for both materials at the higher temperatures. The effect is very pronounced for JT0981. The results of these tests are compared with furnace test data below. Significantly higher rates are indicated for the high velocity CG/HW tests for both materials at 3000° and 3500°F. JT0992 also was found to have significantly higher rates in Mach 0.3 plasma arc tests (4). Both materials appear to oxidize at higher rates in high velocity air.

Material	Temperature (°F)	Surface Recession in 30 Minutes	
		Furnace Test (mil)	CG/HW Test (mil)
JT0981	3000	2-4	13-16
	3500	20-40	>30
JT0992	3000	1-2	2
	3500	15-30	30-40

Detailed comments on the oxidation behavior of each of these materials follows.

1. JT0992 (F-15)

No difficulties were encountered in testing this material at temperatures to 3400°F in air at velocities of 50 and 150 ft/sec. Top surface control of temperature was used in all tests. A steady increase in power was required throughout the test to hold the surface temperature constant. Above 3400°F, full power was required to hold temperature after the first few minutes and it was necessary to stop short of 30 minutes exposure due to the inability to maintain the desired temperature.

All samples developed a thick oxide scale, light grey to white in color, on the top surface and upper sidewalls. At 3400°-3800°F, the scale was duplex in nature. One phase was a clear glassy silica or silicate that was continuous over the surface and appeared to have been liquid during the test. The second phase was a milky grey-white oxide with a rough texture. This most likely is a hafnium-rich oxide or silicate. The oxide tended to spall on cooling and the recession of the underlying substrate appeared to be minimal. No significant effect of velocity was indicated from surface appearance after testing.

Accelerated oxidation at low temperatures and a destructive pest-type of oxidation was observed in the lower portions of all specimens. As shown in Figure 65A, a powdery voluminous oxide was formed as a skirt on the base of all test samples. A sharp line of demarcation between pest and protective behavior is evident. With the top surface at 2600°F, the lower half of the specimen was subjected to accelerated attack. The oxidation products were very bulky and occupied a much larger volume than the material being oxidized. The oxidation product was light grey in color and very powdery. Large chunks fell away on handling. The underlying substrate also was very soft and powdery. It appeared to have been subjected to an interparticle attack.

The behavior is a pest-type of oxidation in the classic sense. It is a low temperature form of accelerated oxidation that occurs by an intergranular or interparticle attack. The attack is most severe at temperatures below 2600°F. The hourglass shape of the residual substrate (Figure 66A) indicates a broad temperature range for this type of attack with a sharp well defined temperature for the peak rate. The attack appears to become pronounced at about 2400°F and is most severe at 1800°-2000°F.

An attempt was made to determine this temperature by conducting tests with the top surface at lower temperatures. As shown in Figure 67, a rapid pest attack occurred on the top surface at a temperature of 2000°F. At a temperature of 2200°F, the top still exhibited a non-protective type of behavior but the rate appeared to be lower than that at 2000°F. The maximum rate attack occurs below 2000°F as shown by the accelerated attack at the cooler base of the 2000°F test sample (Figure 67). At 2600°F and above, this material forms a protective oxide. The active to passive transition probably is governed by the softening or flow point of an SiO₂-base glass by oxidation. The behavior is similar in many respects to that found for a SiO₂+60W composite. At temperatures below this range, the oxides formed cannot effectively heal the surface and the graphite phase is selectively attacked.

The severity of this attack is indicated in Figure 66A. After 30 minutes, the substrate has been totally consumed about 1/4-inch above the base. Temperature was estimated to be about 2000°F at this point. The side wall thickness was 125 mil, and the recession rate, therefore, was about 4 mil/min. Furnace tests of JT0992(F-15) gave a recession rate of 2 mil/hr at 3000°F. The maximum rate (at about 2000°F) is indicated to be at least 120 times the rate at 3000°F. No thermal shock failures were encountered in any of the tests with JT0992(F-15). Figures 68 and 69 show typical post exposure photomicrographs of this material.

2. JT0981 (F-16)

The behavior of this material is similar in most respects to that of JT0992. As shown in Figures 65 and 66, a low temperature pest type of accelerated attack was observed. At temperatures of 2800°F and above, a viscous silica or silicate phase was formed and the substrate was protected to a large degree. Below 2800°F, the liquid phase did not form and a rapid degradation occurred. The temperature range for the pest attack is about the same as that observed for JT0992 (1800°-2400°F).

A significant effect of velocity was noted in testing JT0981 above 3200°F. At 2800°F and above, a large bulk of liquid oxide was formed. As shown in Figure 66B, large bubbles and blisters were formed on the surface. The samples appeared to sweat from local regions and the surface was continually active during a test. Increasing the velocity to 150 ft/sec appeared to have little effect on the surface at temperatures to 3200°F. However, at 3400°F the oxide became sufficiently fluid to result in a noticeable washing effect at 150 ft/sec. As shown in Figure 65B, liquid streams of oxide were pushed off the top surface and protruded from the surface. This effect was not observed at a flow rate of 50 ft/sec. Figures 70 and 71 show typical post exposure photomicrographs of this material.

This effect of flow on liquid oxides was not observed with JT0992(F-15). It probably results from the higher silicon content of JT0981 (17% vs. 11% of JT0992), and a low zirconium content (30% Zr vs. 54% Hf for JT0992).

No thermal shock failures were encountered in any of the tests with JT0981(F-16).

I. Oxidation of WSi₂/W (G-18)

The results obtained for WSi₂/W(G-18) are summarized in Table 13. It is significant to note that eutectic melting of the WSi₂ coating on tungsten was observed at 3680°F, Test (30-1) but not at 3600°F, Test (29-1). The phase diagram indicates eutectic melting between WSi₂ and W₅Si₃ at 3650°F. The WSi₂ coating contains W₅Si₃ as an intermediate phase produced by interdiffusion with the substrate. The observation of melting at 3680°F provides a good check on the accuracy of temperature measurement, using the Milletron two-color pyrometer.

Melting in a 3/16 inch wide band on the sidewall about 1/16 inch below the top surface was most pronounced, indicating a slightly higher temperature in this zone. The top surface appeared slightly wrinkled, indicating partial or incipient melting. The observed behavior shows that the indicated top surface temperature may be 50° to 75°F above the true value. This is about a 2 percent error which is considered exceptionally good in this temperature range. The test was aborted at 35 minutes due to a short between turns in the induction coil. A large pit was observed in the tungsten on the sidewall where melting of the coating was observed. No failures were evident on the top surface.

In many of the tests, the top surface temperature was measured with both a two color and a one color pyrometer. The two temperature readings were used to calculate an approximate value of the normal spectral emittance. Results are presented in Table 13.

No failures in 1 hour tests were observed at temperatures to 3600°F with 50 fps flow rate. The samples were covered with a thick clear glassy coating of SiO₂ which is a viscous liquid at temperatures above 3000°F. The liquid glass effectively heals large defects. It completely filled the blackbody (BB) hole in one test where the BB hole was in the top surface. An edge failure did occur at the BB hole due to large defects. Emittance of the coating appears to decrease with increasing temperature from 0.43 at 3400°F to 0.35 at 3680°F. This may be due to increased positive error in true temperature measurement (two color pyrometer) with increased temperature. For example, if the true temperature at an indicated value of 3680°F was 3580°F then, calculated emittance would be 0.46 instead of 0.35. As mentioned, the reading may be 50° to 75°F high based on observed melting behavior. The estimated emittance values are low for a silicide system. Values normally range from 0.6 to 0.7 at 2550° to 3000°F. The reason for this difference is not clear. However, it does not appear to be due to errors in temperature measurement. The calculated values shown in Table 13 were stable throughout a 1 hour test at all temperatures.

Increasing the air flow rate from 50 to 150 fps had no measurable effect on performance at high temperature. The coating is protective for over 1 hour at 3500°F at the two flow rates. Failure in less than 1 hour occurs at 3650°F by eutectic melting of the coating system. However, contact of the coating with ZrO₂ can lead to failure at temperatures as low as 3400°F as indicated by Tests (24-1) and (25-1). These results explain the temperature limit of 3500°F observed in furnace test (3) when WSi₂/W (G-18) is in contact with ZrO₂.

Figures 72 and 73 show post exposure photomicrographs of WSi₂/W(G-18)-40-1. The latter figure illustrates the W₅Si₃ zone mentioned above. In this case, reference to Figure 73 and Table 13 indicates that the W₅Si₃ zone is 3.9 mils wide after exposure at 3500°F for one hour. Zone widths for all of the exposures are given in Table 13 and plotted in Figure 74. The widths observed in exposures which were less than one hour long were corrected by assuming parabolic kinetics due to diffusion control. This behavior has been established by Bartlett and Gage (13) and by Perkins and Packer (14).

Reference to Figure 74 shows that although most of the results generated in the present study (3, 4) are in general agreement with the earlier findings (13, 14), some differences do exist. In particular, the arc plasma tests in the Avco Model 500 facility under HG/CW conditions at surface temperatures below 3000°F resulted in low values of the W_5Si_3 zone width. At higher temperatures, flow rate and oxygen pressure do not appear to affect the growth rate. In addition, the results obtained in furnace air oxidation tests at 1.8 ft/sec and one atmosphere led to the largest zone widths, while exposures in argon resulted in smaller zone widths. It is conceivable that temperature gradients play a role in controlling this behavior. However, the manner in which this factor affects the results is not apparent at present. It should be noted that tests performed at one atmosphere in air and under conditions of reduced oxygen pressure, as well as in a vacuum at Lockheed Missile/Space Company showed no dependence of the Mo_5Si_3 zone width on oxygen pressure (15). Thus, the present results are at variance with earlier findings, and no explanation of the current findings can be offered at present.

J. Oxidation of Sn-Al/Ta-10W(G-19)

The results obtained for Sn-Al/Ta-10W(G-19) are shown in Table 14. Initial tests were inconclusive due to severe reaction with the ZrO_2 support. The samples were stable in contact with water-cooled copper (Test 27-1). A rapid rise in temperature occurs on failure of the coating. A liquid layer of oxide forms over the surface and temperature climbs rapidly. This is believed to be the result of heat liberated by rapid oxidation of the tantalum-tungsten substrate. Tests were terminated at the first sign of failure to prevent complete destruction of the remaining coating material.

Increasing the flow rate from 50 to 150 fps had no measurable effect on coating performance. The coating is protective for over 1 hour at 3000°F for both flow rates. General thinning of the coating on the flow-exposed upper portions of the samples was noted, however, at both flow rates. The coating failed in 15 to 30 minutes at temperatures of 3200°F and higher in air at 50 fps. Performance was not as good as W/ WSi_2 (G-18). Figures 75 and 76 show examples of survival at 3000°F and failure at 3300°F. The results of the tests summarized in Table 14 are in general accord with the furnace tests (3) which indicate a failure temperature of 3200°F. These results at one atmosphere are in general agreement with those obtained by Perkins and Packer (14) at pressures between 10^{-5} and 10^{-1} atm.

K. Oxidation of SiO_2+60w/oW (H-23) Composite

As indicated in Section II-B-4, the SiO_2+60W composite exhibits a pest type oxidation behavior at low temperatures. Six samples of this material were tested in air at 50 ft/sec from 2400° to 2800°F to study the active-to-passive transition in oxidation behavior. As shown in Figure 77, a viscous liquid glass formed on the side wall of the test samples when the top surface temperature was 2600°F or above. The side

wall is always at a higher temperature than the top due to the cooling effect of the air flow. The glassy surface was observed to form on part of the top surface at a temperature of 2800°F. This appears to be a limiting temperature for glass formation and is the temperature at which the transition from passive to active oxidation behavior occurs. As previously concluded, the fusion range of the SiO₂ phase in this composite appears to govern behavior. The rate of attack in the active (pest) range appears to increase with decreasing temperature. Examination of the samples indicates that the maximum rate may occur in the 2000°-2200°F range. Additional tests indicated the temperature for maximum rate to be 2200°F. Behavior in the pest range is characterized by rapid oxidation of the tungsten phase with the formation of large amounts of WO₃ smoke and yellow crystalline deposits of WO₃ on the surface.

The surface recession behavior of SiO₂+60W samples in CG/HW tests is shown in Table 15 and Figure 78. These data are for temperatures below the range of furnace test data in which a pest-type reaction was found (3). The maximum rate of recession was observed at 2750°F with over 60 mil penetration in 30 minutes. This is over 30 times the rate found above 2800°F where a liquid glass formation occurs. Rate also was observed to increase with decreasing temperature below 2600°F as predicted from the appearance of test samples in the preceding discussion. Post exposure photomicrographs of SiO₂+60w/oW(H-23) are shown in Figures 79 and 80.

L. Test Results for Hf-20Ta-2Mo(I-23)

The results obtained for Hf-20Ta-2Mo(I-23) are summarized in Table 16. The earlier discussion of temperature gradients through oxides formed on this material which is presented in Section II-B-2 indicates that the surface temperature exceeded the substrate temperature by 300-500°F. Post exposure photomicrographs were presented in Figures 15-22 and discussed earlier. Comparison of the present results with those obtained in furnace tests (3) is illustrated below.

Sample No.	Temperature		Time (min)	CG/HW Measured Depth of Conversion	
	Substrate °F	Surface °F		High Velocity	Furnace
I-23-L8 (44-1)	Variable	3375	30	14	
		(constant) 3375	30		20-80
I-23-L9 (44-2)	3355 (constant)	3490-3200	60	12	
		(3300 Avg)			
		3355	60		24-60
I-23-L1 (76-1)	3500 (constant)	3300	60		18-50
		3150-3100	60	20	
		(3125 Avg)			
		3500	60		40-100
		3125	60		8-22

Sample No.	Temperature		Time (min)	CG/HW Measured Depth of Conversion	
	Substrate °F	Surface °F		High Velocity	Furnace
I-23-L2 (77-1)	3700 (constant)	3380-3235	60	31	
		(3270 Avg)	60		90-200
		3700	60		18-45
I-23-L3 (77-2)	3900 (constant)	3490-3380	60	60	
		(3450 Avg)	60		150-300
		3900	60		35-90
		3450	60		

Measured depths of conversion based on substrate temperature were 1/2 to 1/3 the measured depth in furnace tests at that temperature. However, conversion depths were in excellent agreement with furnace tests data when surface temperature was used as the basis for comparison. These results clearly show that the temperature of the oxide scale is rate controlling in the oxidation of Hf-Ta-Mo above 3000°F. It is the same as that found for the borides, and again points to transport through the oxide scale (HfO₂) as the rate controlling step.

These tests clearly show that surface temperature control should be used for testing ZrO₂ or HfO₂ scale forming materials.

M. Summary of High Velocity CG/HW Results

High velocity CG/HW exposures at velocities ranging from below 10 ft/sec to 250 ft/sec have been performed for seventeen of the candidate materials. The results of these tests indicate that the behavior of these materials can be divided into two categories. Materials which form condensed oxide scales exhibited no definite dependence on air flow rate. On the other hand, graphites which form volatile oxidation products exclusively, exhibited a strong dependence of oxidation rate on air velocity. Moreover, comparison of the high velocity CG/HW oxidation behavior of materials forming condensed oxidation products with the behavior observed for these materials in furnace tests indicates comparable oxidation rates for equal surface temperatures. Since substantial temperature gradients through the oxide are present in the high velocity CG/HW tests (where the surface is cooler than the substrate) the present results indicate that the rate of oxidation is limited by the minimum temperature in the condensed oxide layer. The importance of these findings is evident with reference to identification of the rate controlling factor in the oxidation process. Since surface temperature is measured and controlled in most tests, oxidation

data will be accurate only if surface temperature is controlling. If substrate or interface temperature controls, the measured rate can be too high or too low depending on the method of heating. Induction or direct resistance heating will cause the substrate to be hotter than the surface. Radiation heating can lead to a cooler substrate. This will be the case in most gas torch or plasma tests. Only furnace tests can result in uniform temperatures through oxide and base material. High velocity CG/HW tests performed for flat faced, hemispherical type and conical samples of graphite, showed that recession rates increased significantly with air flow. A sixfold increase was observed between 1 and 250 ft/sec at 2850°F. This is due to variations of the oxygen pressure at the surface and indicates the need for control in such studies. Recession rates observed in CG/HW tests at 250 ft/sec were comparable with recession rates observed in Mach 0.3 HG/CW arc plasma tests. Recession rates exhibited by conical samples were found to be twice those observed for flat faced cylinders. This is due to a change in oxygen partial pressure at the surface with a change in sample geometry.

High velocity CG/HW tests performed for PT0178(B-9) and Glassy Carbon (B-11) showed that recession rates were also found to increase significantly with air flow. This result is attributed to variations of the oxygen pressure at the surface and indicates the need for control in such studies. Recession rates observed in CG/HW tests at 250 ft/sec were comparable with recession rates observed to Mach 0.3 HG/CW arc plasma tests. The linear recession rates for all of the graphites were found to correlate directly with density. Coating failure temperatures for WSi_2/W (G-18) and Sn-Al-Ta-10W(G-19) were determined as 3650°F and 3200°F in the high velocity CG/HW tests. The former value is higher than that observed in furnace tests and may represent a better evaluation of the temperature limit of WSi_2/W (G-18) in the absence of reactions with ZrO_2 .

The failure temperature for Si/RVC(B-8) observed at 3000°F is in agreement with the results obtained in the CG/HW furnace tests. In addition, the low temperature degradation of JTA(D-13), JT0992(F-15), JT0981(F-16) and SiO_2+60 w/o W(H-23) observed in the furnace tests was also noted in these tests. The temperature gradients observed to exist through a 200 mil wall of $SiO_2 + 60w/oW$ (H-23) were so large that the internal temperature exceeded 4000°F while the surface was only 3150°F. This led to internal melting. The usefulness of this composite was found to be limited by the fact that protective behavior is not observed below the fusion range for silica (2700°-3000°F). However, SiO_2 softens and becomes viscous above this range leading to a loss of strength.

IV. MEASUREMENT OF EMITTANCE AT 0.65 μ FOR CANDIDATE MATERIALS UNDER OXIDIZING CONDITIONS IN HIGH VELOCITY AIR FLOWS

As indicated in Sections II and III, an attempt was made in all tests to obtain data on the normal spectral emittance of the various refractory materials at high temperatures in an oxidizing environment. Simultaneous readings of the top surface temperature were taken at 5-10 minute intervals with a micro-optical pyrometer (0.65 μ) and a two-color pyrometer (Milletron or Pyro Eye). The two-color pyrometers used for measurement of true temperature were calibrated against a standard NBS tungsten filament lamp once a month. Readings of the Milletron Pyrometer were within +2% of true temperature in the range of 2600° to 4200°F (8). Appropriate corrections were used for absorption in prisms or mirrors. Normal spectral emittance was calculated from the two readings by means of Wein's Law. The results are summarized in Table 17 and are discussed for the individual materials.

Reference to Table 3 and the discussion of HfB_{2.1}(A-2) presented in Section III-A a value of 0.50 is shown for HfB_{2.1}(A-2) in Table 17. This value appears applicable under oxidizing conditions between 3000° and 3500°F. Similarly, reference to Table 4 and Section III-B indicate that the emittance of ZrB₂(A-3) is 0.57 for a comparable temperature range. The values obtained for HfB₂+SiC(A-4) and ZrB₂+SiC(A-8) appear to depend strongly upon temperature based upon the results shown in Tables 5 and 6 and the discussion presented in Section III-C. Accordingly, it is expected that these materials exhibit emittance values near 0.60 at temperatures above 3500°F, characteristic of ZrO₂ and HfO₂.

The emittance of Speer 710 graphite was measured from 2550° to 4150°F in the oxidation studies with flat-faced specimens. The results of repetitive measurements over this broad temperature range are given in Figure 81. The data indicate a continuous decrease in emittance from a value of 0.9 at 2550°F to a value of 0.57 at 4150°F in air at 50 fps velocity. The scatter in data existing in the range of 3250° to 3550°F is due largely to a scale change in the two-color pyrometer at 3450°F. Errors appear to be encountered at the high end of the low scale and the low end of the high scale. Unfortunately, the two scales do not overlap. Even with this scatter, the data are in excellent agreement over the entire range of measurement. The variation is less than +10% at all temperatures. The data also are in excellent agreement with published data (16) on the emittance of graphite from 2500° to 3000°F obtained by classical methods of measurement in inert atmosphere or vacuum as shown below:

<u>Temp.</u> <u>°F</u>	<u>Normal Spectral Emittance</u>			<u>Total Normal Emittance</u>			
	<u>This Work</u>	<u>High Purity</u>	<u>Acheson Graphite</u>	<u>CBE Graphite</u>	<u>CBH Graphite</u>	<u>3474D Graphite</u>	<u>7087 Graphite</u>
2500	0.90	0.79	0.89	0.75	0.80	0.81	0.82
3000	0.77	0.79	0.88	0.70	0.76	0.77	0.78

No data in the published literature or available reports for emittance values at temperatures above 3000°F could be found to compare with the results shown in Figure 41. Arc plasma tests (4) yield computed values of total normal emittance for graphites of 0.50 to 0.40 in the range 4500° to 5500°F. An extrapolation of the normal spectral emittance curve of Figure 41 to higher temperatures indicates a value of 0.5 at 5000°F, which is in good agreement with the test data reported in the HG/CW arc plasma tests (4). On this basis the emittance values shown for RVA(B-5) have been assigned.

The emittance data shown in Figure 41 make a significant contribution in a heretofore unexplored temperature range and should be of considerable value in future work on graphites at high temperature. The results also serve to point out the ease with which useful data on emittance under oxidizing conditions can be obtained. By using accurately calibrated pyrometers and careful measurement techniques, data which in many respects are equivalent to those determined by classical measurement techniques can be obtained. Individual measurements of course are not as accurate as those obtained by classical methods. However, by conducting several measurements at each temperature, the data can be averaged and valid results obtained. The advantage of this approach is that the emittance is determined under actual (or simulated) environmental conditions and that the changes in emittance with time can be monitored continuously.

The data shown in Table 7 for Glassy Carbon (B-11) indicate an emittance of 0.55 for this material in the 3000°-3500°F range.

Since the surface of Si/RVC(B-8) and KT-SiC(E-14) are basically the same (silicon carbide) the results shown in Tables 9 and 11 have been averaged in order to arrive at the average value of emittance equal to 0.70 shown in Table 17 for temperatures in the 3000°-3500°F range.

Hypereutectic carbide samples were observed to have very low values of emittance (Table 10). Calculated values ranged from 0.04 to 0.18 at 3000°-3800°F. It is believed that these data are not truly representative of materials behavior and that the true values of emittance are significantly higher. The reason for these anomalously low values is not clear.

As shown in Table 12, the initial values of emittance for JT0992 (F-15) and JT0981(F-16) ranged from 0.38 to 1.0. The values for JT0992 (F-15) averaged 0.88 from 3400° to 3800°F while those for JT0981(F-16) averaged 0.63 from 2800° to 3400°F. No clear trend in change of emittance with temperature was indicated in either case. At the end of 30 minutes, calculated emittance values ranged from 0.77 to 1.0. Average values were 0.97 for JT0992 and 0.93 for JT0981. This apparent increase

probably is due to the high surface roughness of the oxide scales. Brightness temperatures were difficult to measure and readings were not very reliable due to uneven temperature distributions on the top surface. Similarly, the results for JTA(D-13) shown in Table 2 indicate values near 0.70 between 3000° and 4000°F. Accordingly, values of 0.75 were adopted for the emittance of the JT-Composites (D-13), (F-15) and (F-16) between 3000° and 3500°F.

The emittance of $WSi_2/W(G-18)$ as indicated in Table 13 decreases with increasing temperature. Results obtained from measurement by one-color and two-color pyrometers sighted on the top surface are summarized below:

<u>Temperature</u> °F	<u>Flow Rate</u> (fps)	<u>Total Time</u> (min)	<u>Emittance</u>	
			<u>Start</u>	<u>Finish</u>
3400	50	60	0.64	0.57
3500	150	60	0.48	0.55
3600	50	60	0.54	0.54
3680	50	35	0.46	0.46

The emittance values tend to be stable throughout a 1 hour test. The values are in the range expected for silicide-base coatings. Figure 82 compares the present results with those obtained by Allen et al. (17).

The emittance of $Sn-Al-Ta-10W(G-19)$ is higher than that observed for the $WSi_2/W(G-18)$ system. Emittance tends to decrease with increased temperature and with increased time at temperature as shown in Table 14 and below (these values are in the range expected for this coating system):

<u>Temperature</u> °F	<u>Flow Rate</u> (fps)	<u>Total Time</u> (min)	<u>Emittance</u>	
			<u>Start</u>	<u>Finish</u>
3000	50	60	0.79	0.69
3000	150	60	0.76	0.66
3200	50	24	0.74	0.67
3300	50	22	0.65	0.69
3400	50	30	0.67	0.59
3500	50	15	0.62	0.62

Reference to Table 16 indicates an emittance of 0.55 for $Hf-20Ta-2Mo$. This value is in general agreement with the result obtained for $HfB_{2.1}(A-2)$.

REFERENCES

1. Kaufman, L. and Nesor, H., "Stability Characterization of Refractory Materials under High Velocity Atmospheric Flight Conditions," AFML-TR-69-84 Part II Volume I: Facilities and Techniques Employed for Characterization of Candidate Materials, ManLabs, Inc., Cambridge, Mass. (September 1969).
2. Kaufman, L. and Nesor, H., "Stability Characterization of Refractory Materials under High Velocity Atmospheric Flight Conditions," AFML-TR-69-84 Part II Volume II: Facilities and Techniques Employed for Cold Gas/Hot Wall Tests, ManLabs, Inc., Cambridge, Mass. (September 1969).
3. Kaufman, L. and Nesor, H., "Stability Characterization of Refractory Materials under High Velocity Atmospheric Flight Conditions," AFML-TR-69-84 Part III Volume I: Experimental Results of Low Velocity Cold Gas/Hot Wall Tests, ManLabs, Inc., Cambridge, Mass. (September 1969).
4. Kaufman, L. and Nesor, H., "Stability Characterization of Refractory Materials under High Velocity Atmospheric Flight Conditions," AFML-TR-69-84 Part III Volume III: Experimental Results of High Velocity Hot Gas/Cold Wall Tests, ManLabs, Inc., Cambridge, Mass. (September 1969).
5. Kaufman, L. and Nesor, H., "Stability Characterization of Refractory Materials under High Velocity Atmospheric Flight Conditions," AFML-TR-69-84 Part IV Volume I: Theoretical Correlation of Material Performance with Stream Conditions, ManLabs, Inc., Cambridge, Mass. (September 1969).
6. Gulbransen, E. A., Andrew, K. F. and Brassart, F. A., "The Oxidation of Graphite at Temperatures of 600° to 1500°C and at Pressures of 2 to 76 Torr of Oxygen," J. Electro. Chem. Soc. 110, No. 6, 477 (1963).
7. Okada, J. and Ikegawa, T., "Combustion Rate of Artificial Graphite from 700°-2000°C in Air," J. of App. Phys., 24, 1249 (1953).
8. Perkins, R. A., Price, W. L. and Crooks, D. D., "Oxidation of Tungsten at Ultra-High Temperatures," Proceedings of Joint AIME/AFML Symposium on the Oxidation of Tungsten and Other Refractory Metals, AFML-TR-64-162, (April 1965).
9. Jones, M. T., "The Phase Diagram of Carbon," National Carbon Research Laboratories, PRC-3, Parma, Ohio (January 1958).

10. Noda, T. and Inigaki, M., "The Melting of Glassy Carbon," Bull. Chem. Soc., Japan 37, 1709 (1964).
11. Ong, J.N. Jr., "On the Kinetics of Oxidation of Graphite," Carbon, (2), 281-297 (1964).
12. Gulbransen, E.A., Andrew, K.F. and Brassart, F.A., "Oxidation of Pyrolytic Carbon at 1000°-1500°C and Oxygen Pressures of 2 to 38 Torr," J. Electro. Chem. Soc., VIII, No. 5, 626 (1964).
13. Bartlett, R.W. and Gage, P.R., "Investigation of Mechanisms for Oxidation Protection and Failure of Intermetallic Coatings for Refractory Metals," ASD-TDR-63-753, Part II (July 1964).
14. Perkins, R.A. and Packer, C.M., "Coatings for Refractory Metals in Aerospace Environments," AFML-TR-65-351 (September 1965).
15. Perkins, R.A., "Effect of Temperature and Pressure on the Oxidation Behavior of Silicide Coatings on Refractory Metals," Presented at the Gordon Research Conference, New London, N.H., July 1963 (to be published).
16. The Emittance of Ceramics and Graphites, DMIC Memorandum 148, (March 28, 1962).
17. Allen, T.H., Johnson, C.R. and Rusert, E.L., "High Temperature Emittance of Coated Refractory Metals," SAMPE National Symposium, St. Louis, Mo., McDonnell, Co. (April 1967).

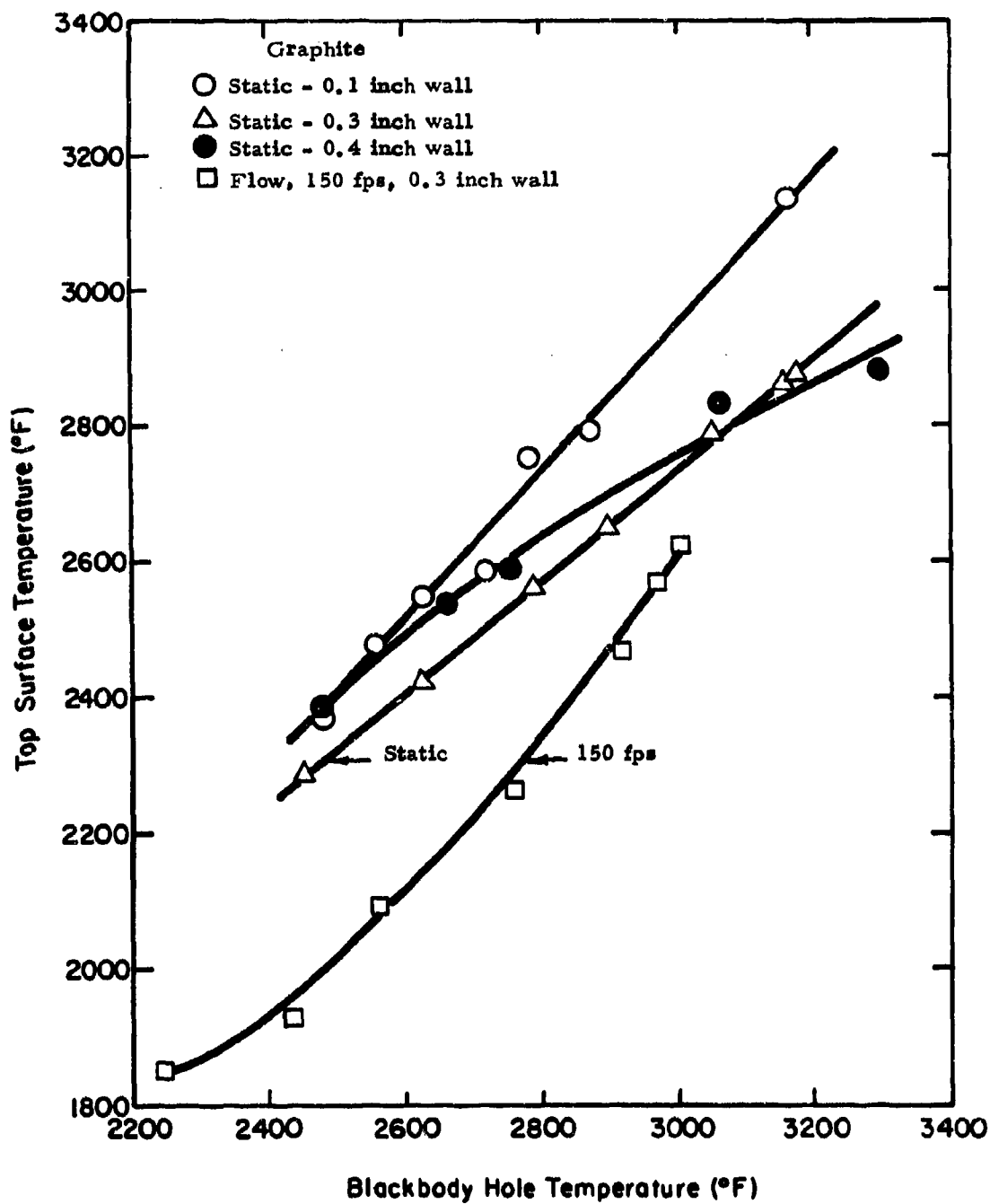


Figure 2. Temperature Relationship in Graphite Test Cylinders.

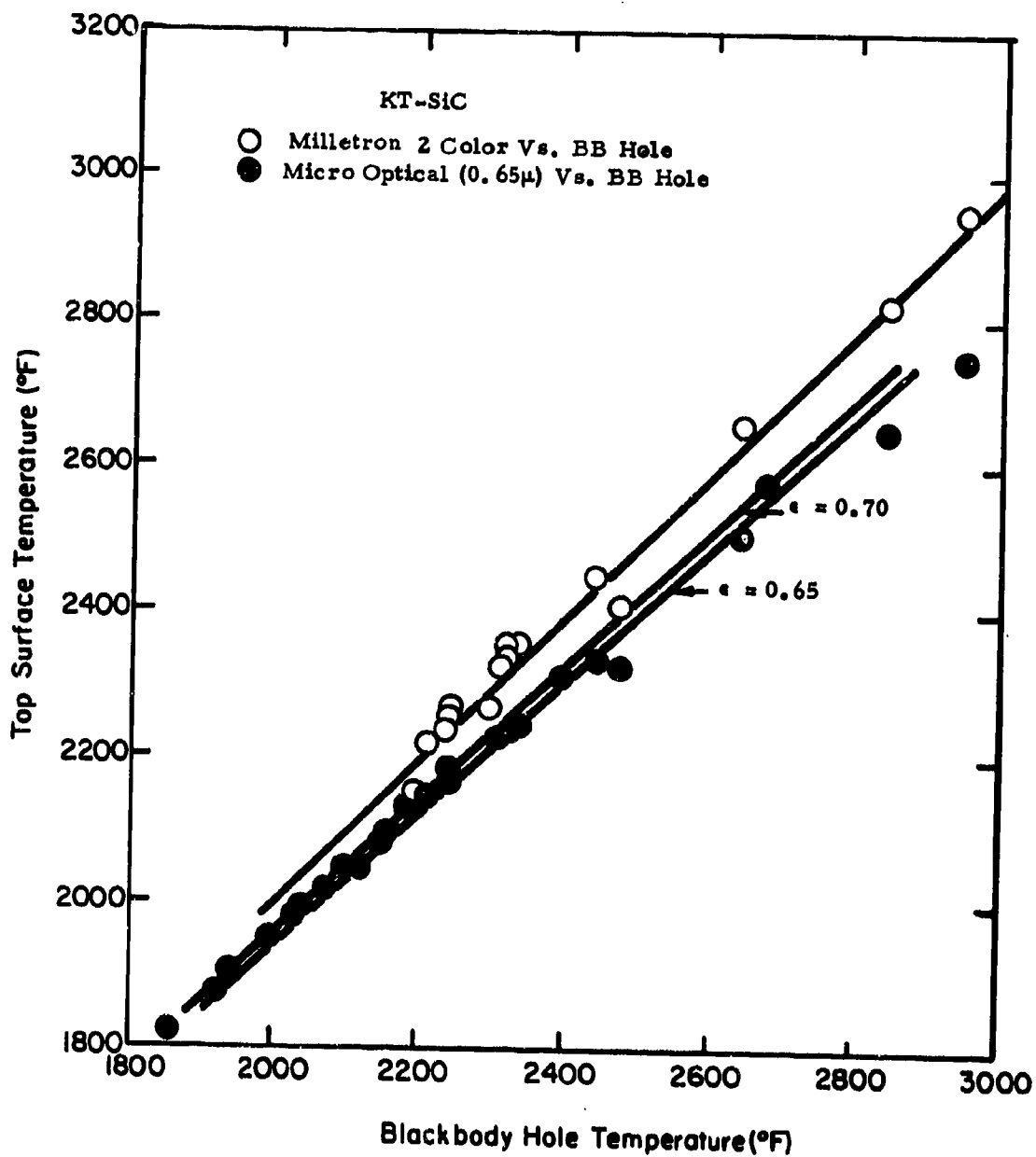


Figure 3. Temperature Gradients and Emittance of SiC in Static Air.

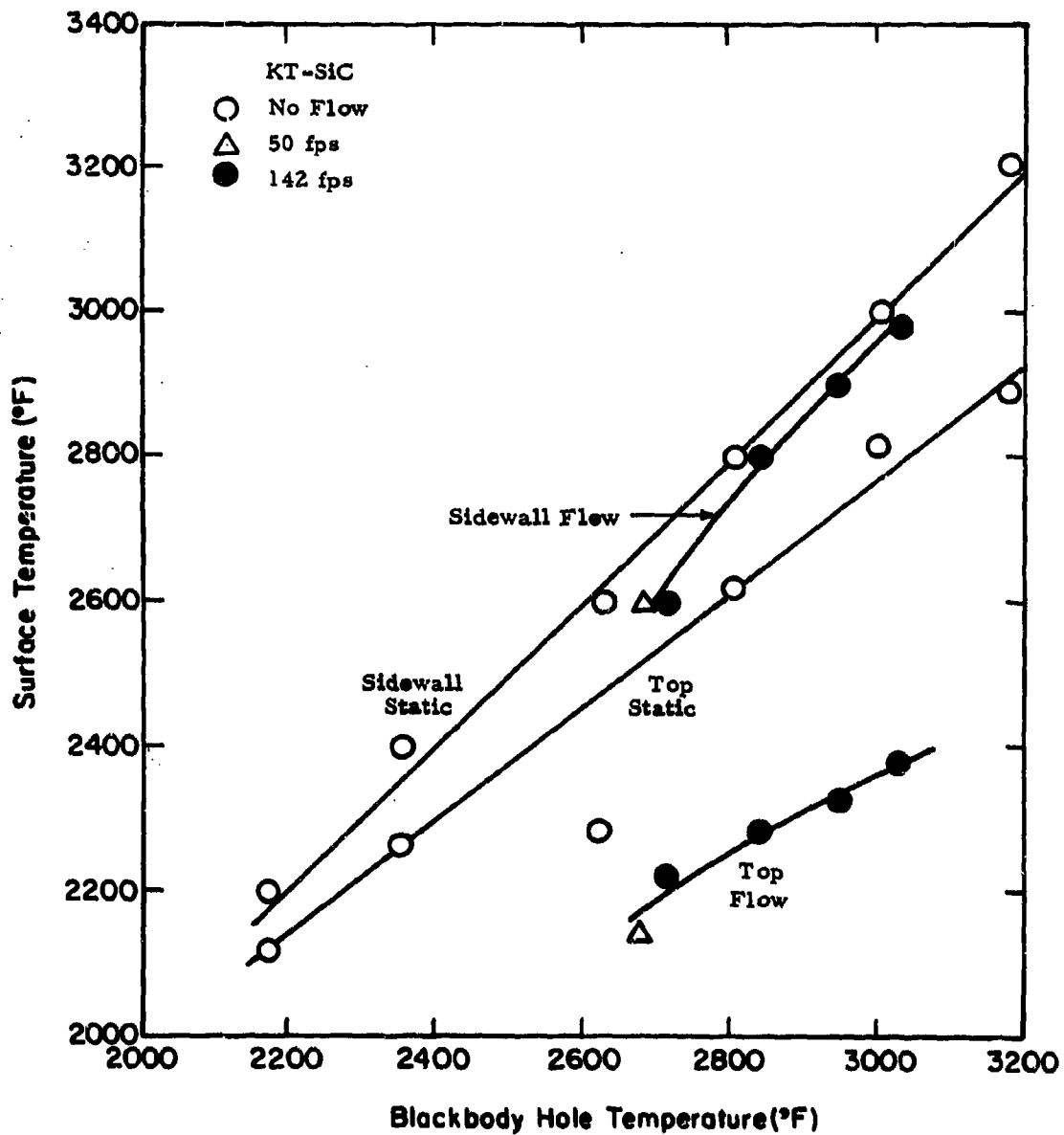


Figure 4. Effect of Flow on Temperature Gradients in SiC Cylinders.

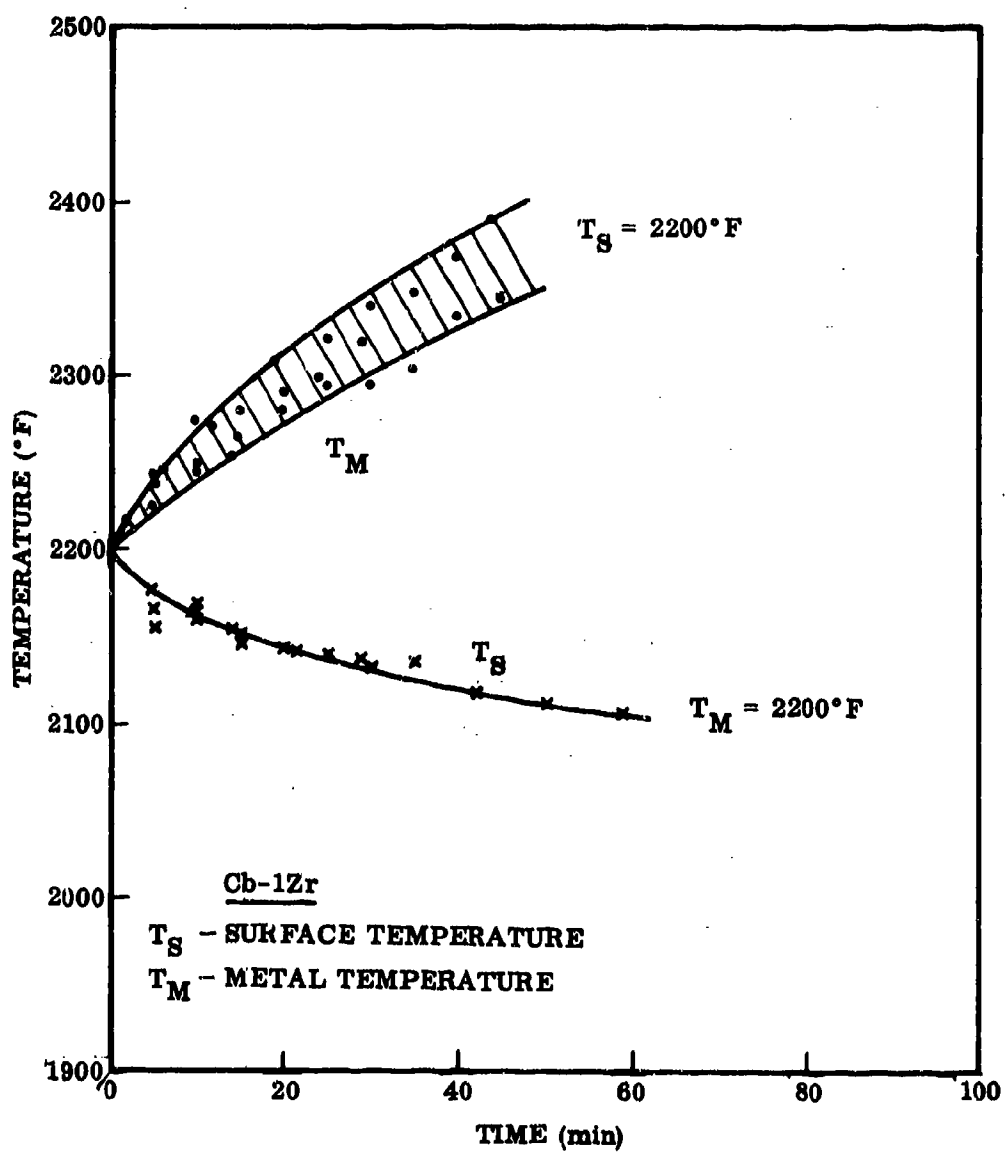


Figure 5. Temperature Drop Through Cb_2O_5 Scale on Cb-12Zr.

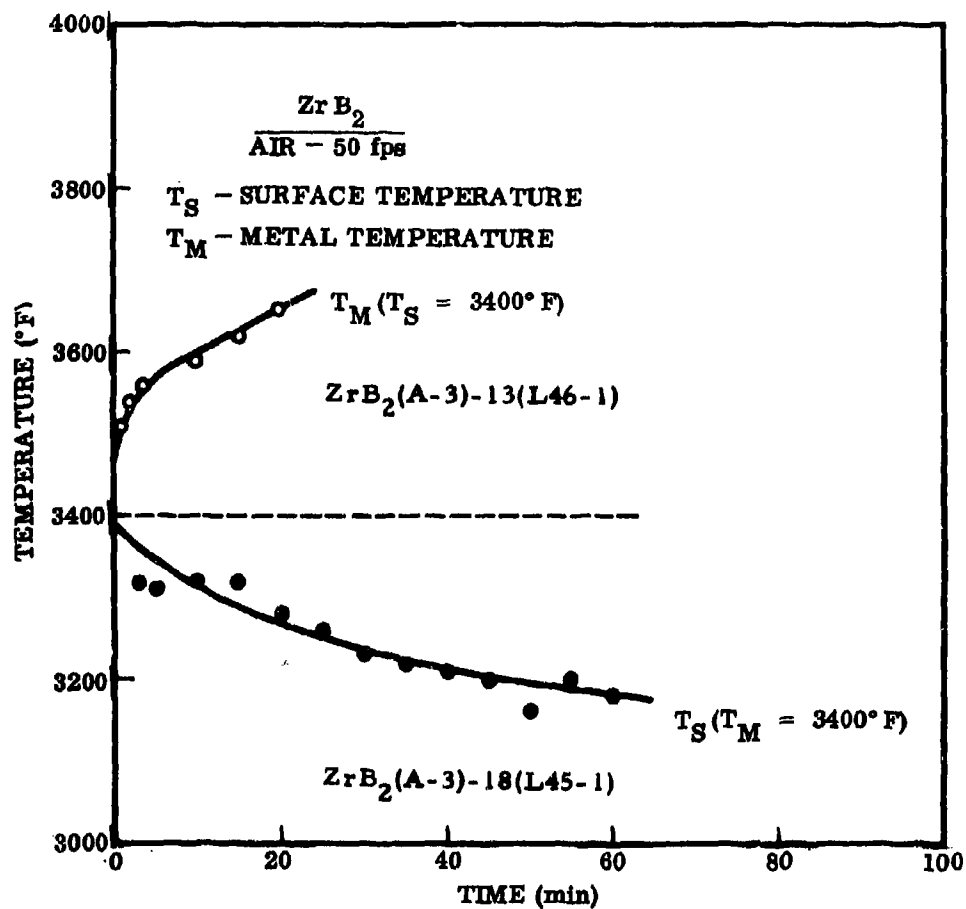


Figure 6. Temperature Drop Through ZrO_2 Scale on ZrB_2 .

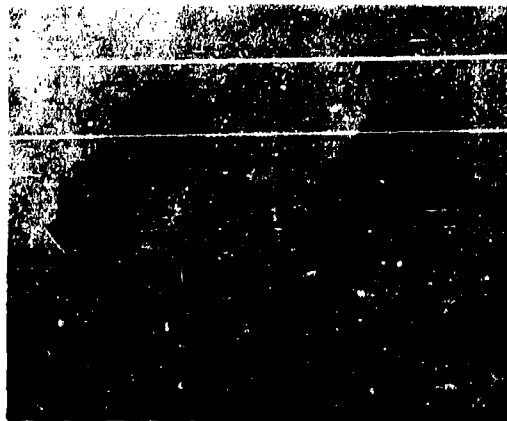


Plate No. 1-7116

Figure 7. Macrophotograph of $\text{ZrB}_2(\text{A-3})$ -18 (Lockheed 45-1) and $\text{ZrB}_2(\text{A-3})$ -13 (L46-1) after High Velocity CG/HW Exposure.



Plate No. 1-7117

As-Polished

X2.75

Figure 8. Section Through $\text{ZrB}_2(\text{A-3})$ -13 (L46-1) after 30 Minute Exposure at 50 ft/sec in Air. Surface Temperature 3400° F. Top Surface at Left.

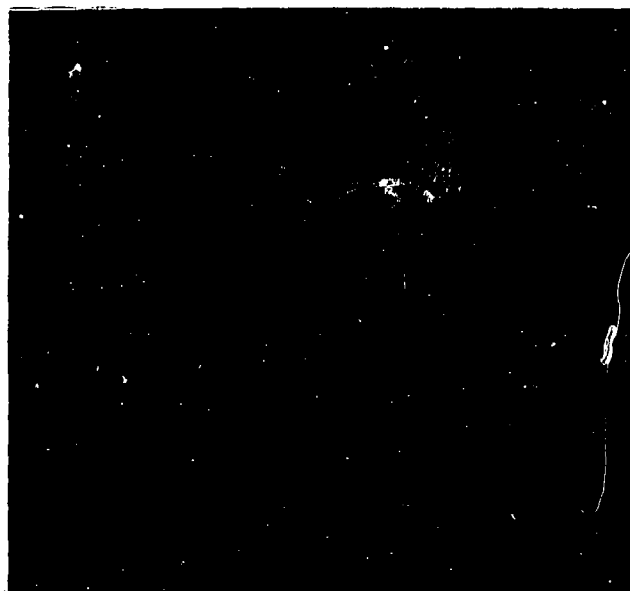
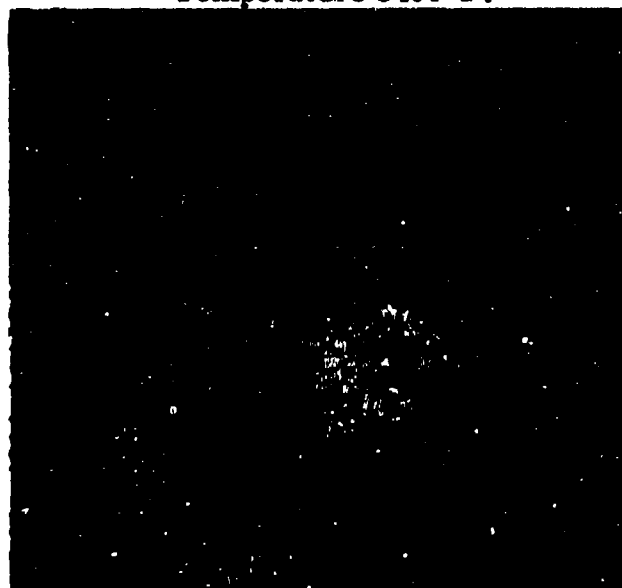


Plate No. 1-7120

As-Polished

X2.63

Figure 9. Section Through $ZrB_2(A-3)-18$ (L45-1) after 60 Minute Exposure at 50 ft/sec in Air. Substrate Temperature 3400°F.



Oxide

Plate No. 1-7123

Matrix

Etched with 10 Glycerine 5HNO₃3HF X250

Figure 10. Oxide-Matrix Interface of $ZrB_2(A-3)-18(L45-1)$ Showing Adherent Oxide.

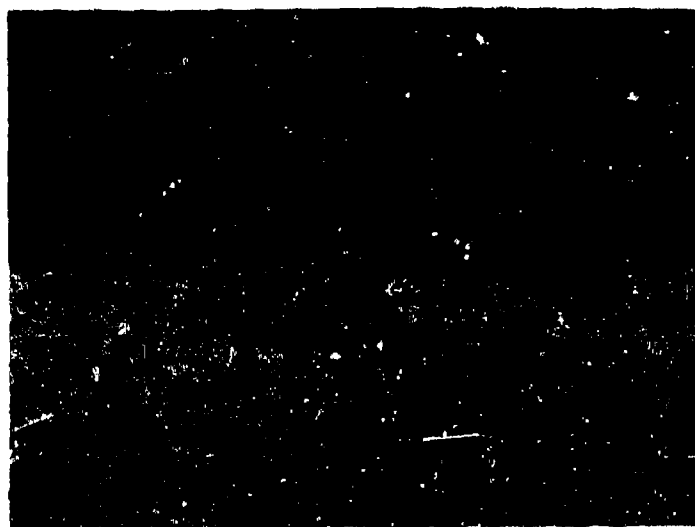


Plate No. 1-4830

As-Polished

X3.5

Figure 11. Section through $\text{HfB}_{2.1}$ (A-2)-13 (L38-1) after 60 Minute Exposure at 50 ft/sec in CG/HW Test. Surface Temperature 3400° F. Oxide Thickness 8 Mils, Conversion Depth 4 Mils. Top Surface at Bottom.



Oxide

Plate No 1-4831

Matrix

Etched with 10 Glycerine 5HNO₃3HF X250

Figure 12. Oxide-Matrix Interface of $\text{HfB}_{2.1}$ (A-2)-13 (L38-1) Showing Adherent Oxide. Oxide at Top.



Plate No. 1-4833

As-Polished

X3.5

Figure 13. Section Through $\text{HfB}_{2.1}$ (A-2)-15(L39-2) after 60 Minute Exposure at 10 ft/sec in CG/HW Test. Surface Temperature 3600°F - 3190°F . Oxide Thickness 25 Mils. Conversion Depth 18 Mils Top Surface at Bottom.



Oxide

Plate No. 1-4834

Matrix

Etched with 10 Glycerine 5HNO_3 3HF X250

Figure 14. Oxide-Matrix Interface of $\text{HfB}_{2.1}$ (A-2)-15(L39-2) Showing Adherent Oxide.

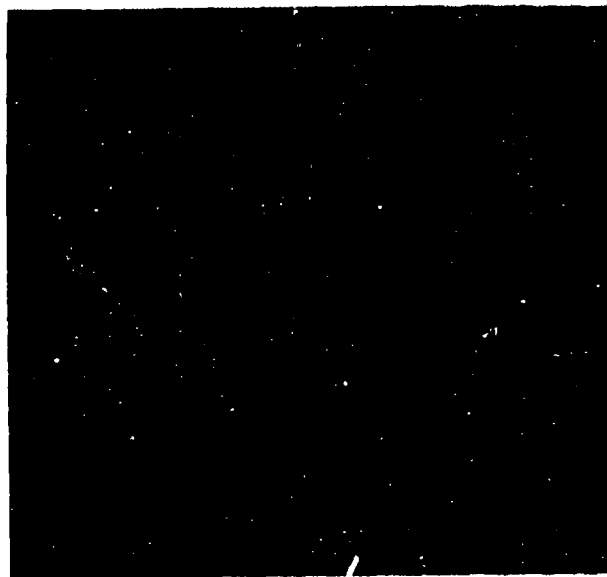


Plate No. 1-7142

As-Polished

X2.69

Figure 15. Section Through Hf-19Ta-2Mo(I-23)(L44-1) after 30 Minutes at 1-10 ft/sec in CG/HW Test. Surface Temperature 3400° F. Sample Cracked after Test. Conversion Depth 14 Mils. Top Surface at Left.



Matrix

Plate No. 1-7599

Subscale

Oxide

Etched with 30 Lactic 10HNO₃ 1HF 0.788 mils/small division

Figure 16. Oxide-Subscale-Matrix Zones in Hf-19Ta-2Mo (I-23)(L44-1). Matrix at Top.



Plate No. 1-7146

As-Polished

X2.62

Figure 17. Section Through Hf-19Ta-2Mo(I-23)(L44-2) after 60 Minutes at 1-10 ft/sec in CG/HW Test. Substrate Temperature 3355° F. Conversion Depth 12 Mils. Top Surface at Right.



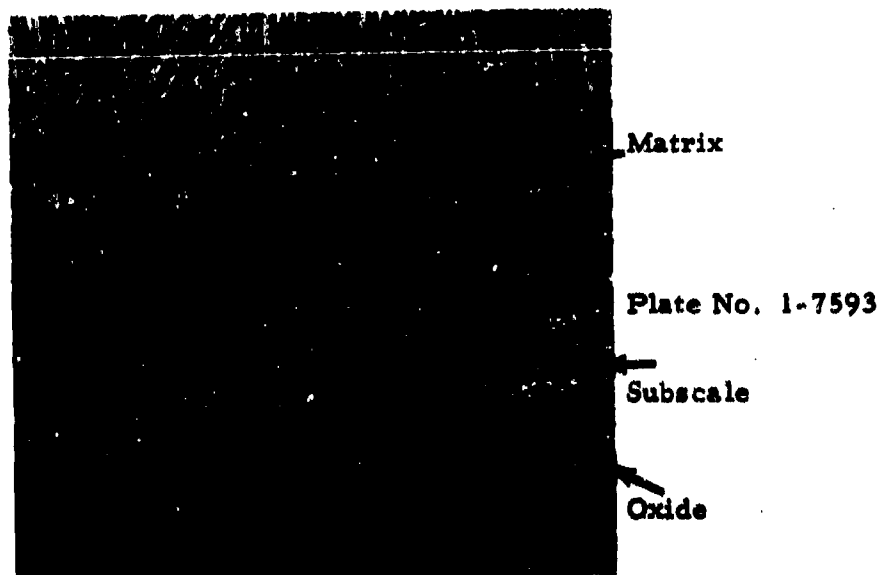
Matrix

Plate No. 1-7600

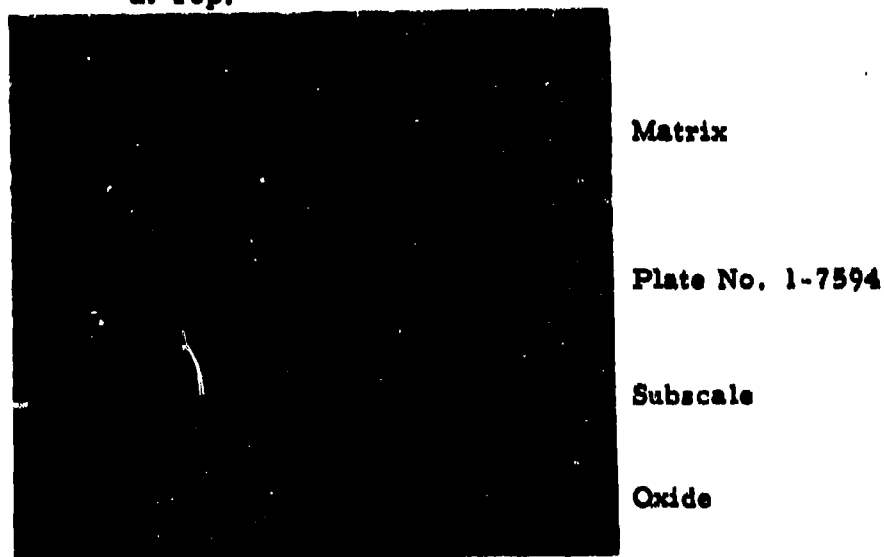
Subscale

Oxide

Etched with 30 Lactic 10HNO₃ 1HF 0.788 mils/small division
Figure 18. Oxide-Subscale-Matrix Zones in Hf-19Ta-2Mo (I-23)(L44-2). Matrix at Top.



Etched with 30 Lactic 10HNO₃1HF 0.788 mils/small division
 Figure 19. Oxide-Subscale-Matrix Interface of Hf-19Ta-2Mo (I-23)(L76-1) after 60 Minute Exposure at 50 ft/sec in CG/HW Test. Substrate Temperature 3500°F. Conversion Depth 20 Mils. Matrix at Top.



Etched with 30 Lactic 10HNO₃1HF 0.788 mils/small division
 Figure 20. Oxide-Subscale-Matrix Interface of Hf-19Ta-2Mo(I-23)(L77-1) after 60 Minute Exposure at 50 ft/sec in CG/HW Test. Substrate Temperature 3700°F. Conversion Depth 31 Mils. Matrix at Top.



Plate No. 1-7137

As-Polished

X2.78

Figure 21. Section Through Hf-19Ta-2Mo(I-23)(L77-2) after 60 Minutes at 50 ft/sec in CG/HW Test. Substrate Temperature 3900° F. Conversion Depth 60 Mils. Top Surface at Top.

Matrix

Subscale



Oxide

Plate No. 1-7595

Etched with 30 Lactic 10HNO₃ 1HF 0.788 mils/small division

Figure 22. Oxide-Subscale-Matrix Zones in Hf-19Ta-2Mo(I-23)(L77-2). Oxide at Right.

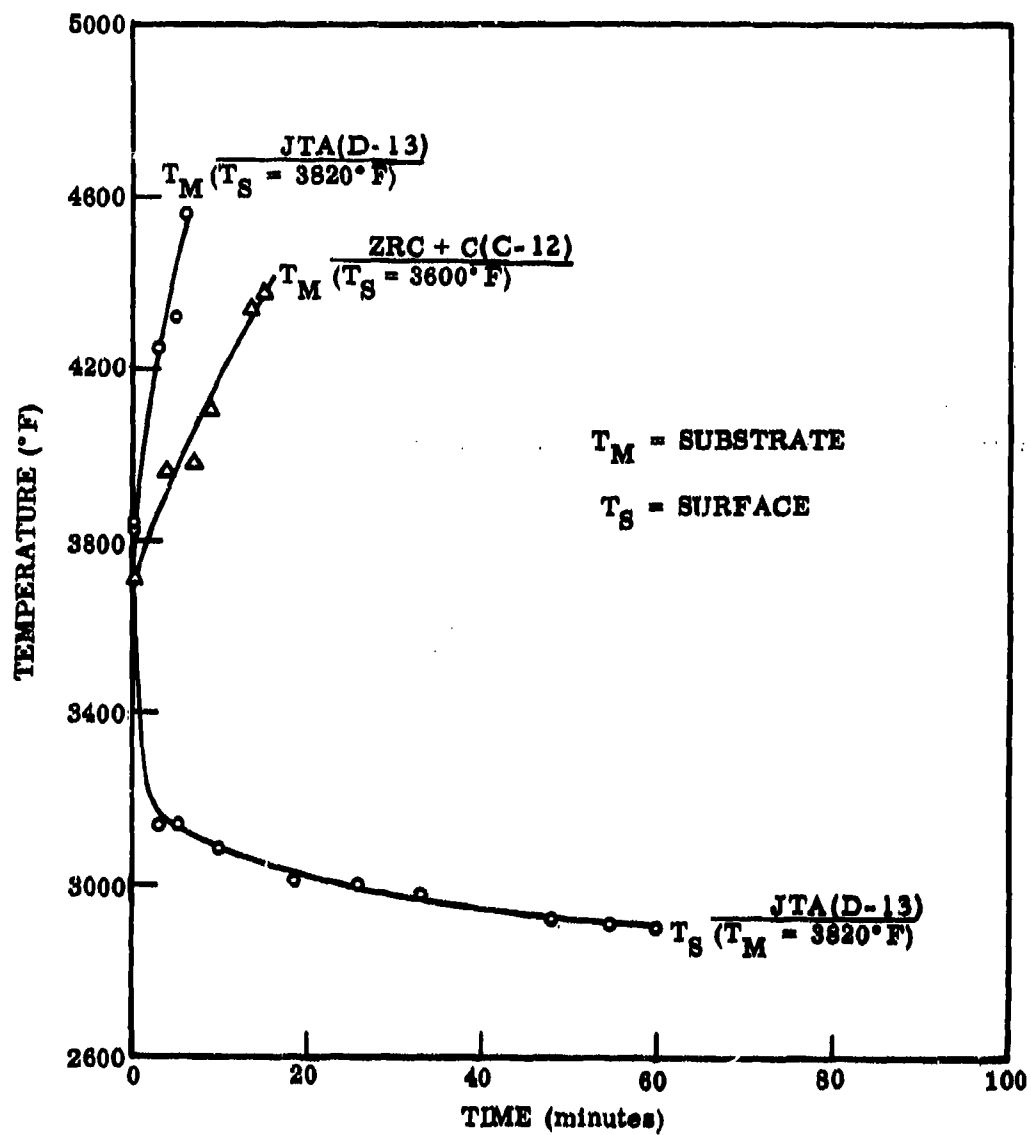


Figure 23. Temperature Gradients in Oxide Scales on Graphites and Carbides



Plate No. 1-7846

X2.70

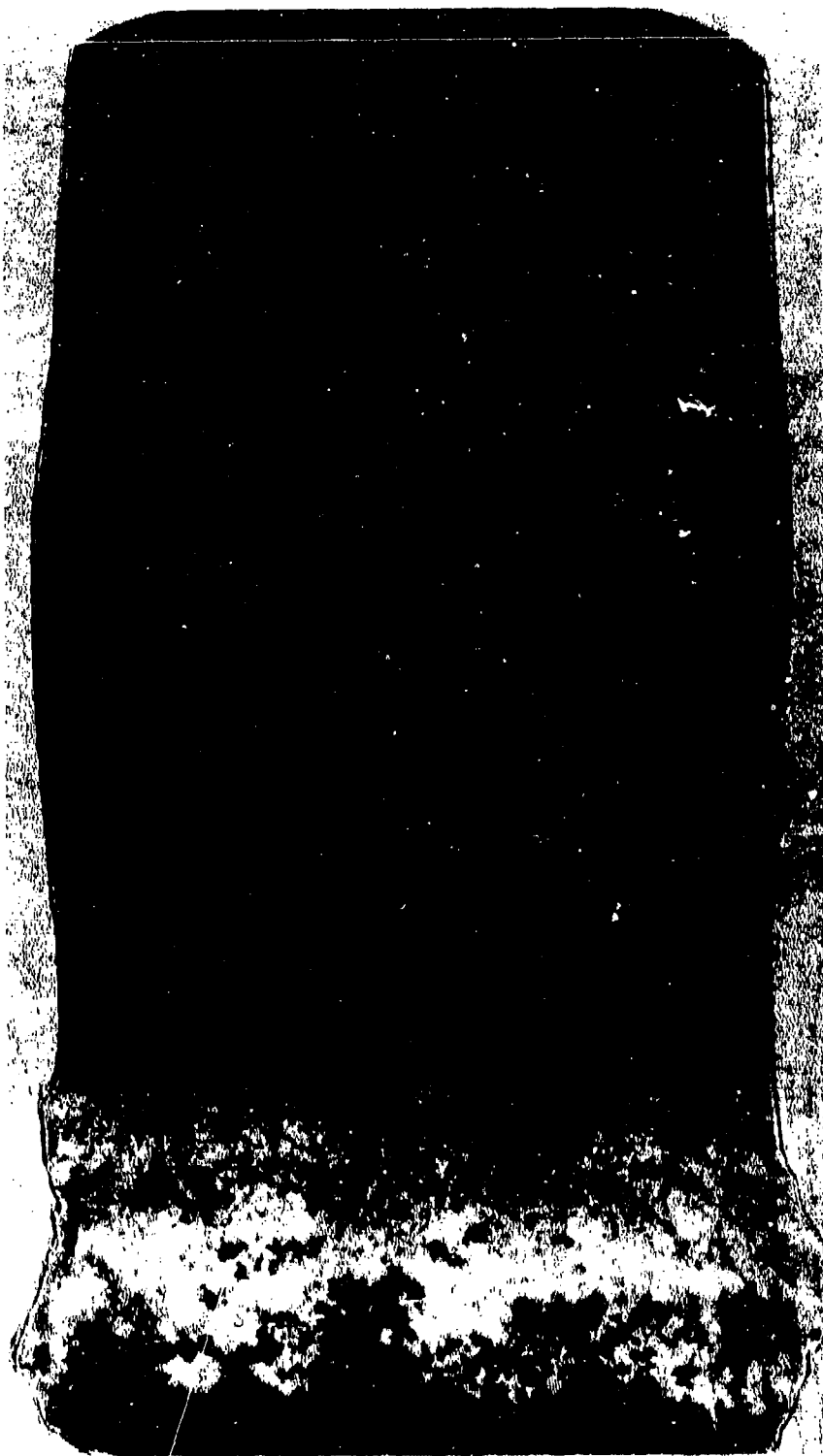
Figure 24. JTA(D-13)-L5, Surface Temperature 3821°F, Air Flow Rate 10 ft/sec. Exposure Time 60 Minutes, Hot Face Up. 33 Mil Recession, One Inch Scale



Plate No. 1-7841

X2.70

Figure 25. JTA(D-13)-L4, Surface Temperature 3921°F, Air Flow Rate 10 ft/sec. Exposure Time 7.5 Minutes, Hot Face Down, 55 Mil Recession, One Inch Scale



TOP
3150°F

SILICA FUSION
LINE
2700-3100°F

BOTTOM
<2000°F

Figure 26. SiO_2 -60% W(H-23-L1), After 15 Min. at 3150°F in Air
at 50 ft/sec (X8)



Plate No. 1-7810

X2.75

Figure 27. SiO_2 -60w/oW(H-23)-L1, Surface Temperature 3150°F , Air Flow Rate 50 ft/sec. Exposure Time 25 minutes, Hot Face Down, Internal Melting, One Inch Scale.

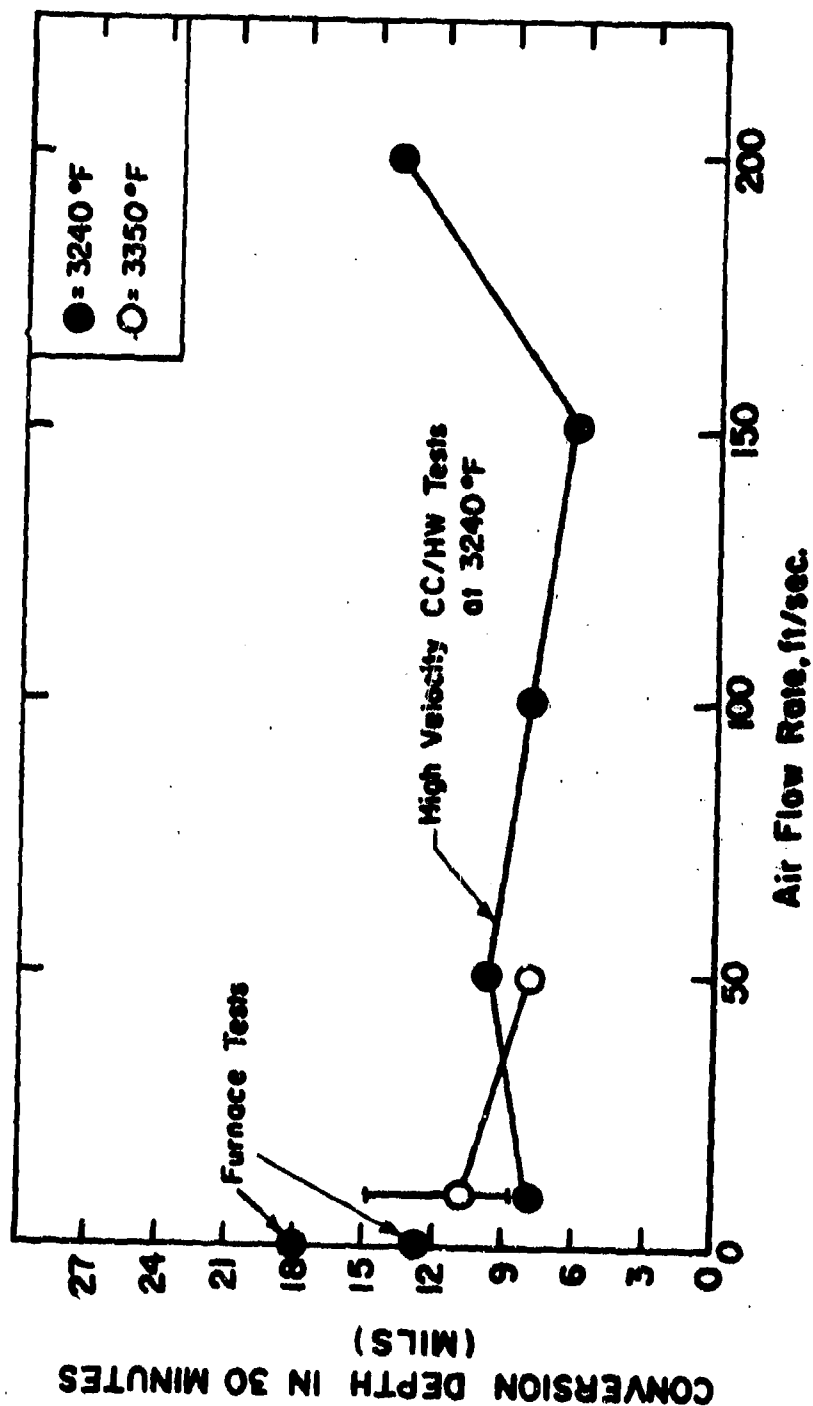


Figure 28. Effect of Air Flow Rate on Oxidation of HFB 2.1(A-2) Near 3300°F.

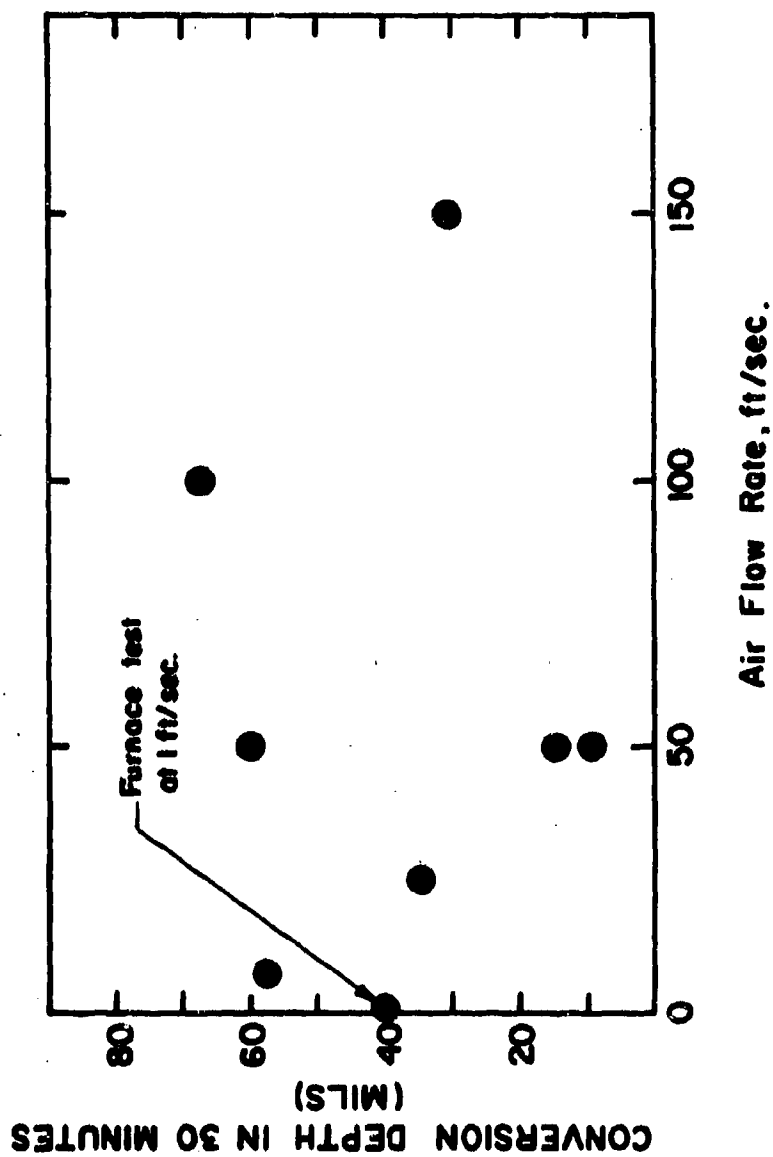


Figure 29. Effect of Air Flow Rate on Oxidation of $ZrB_2(A-3)$ Near $3400^\circ F$.



Plate No. 2-0448

Figure 30. Post Exposure Photomicrographs of $\text{HfB}_2 + \text{SiC(A-4)}$
after Exposure in Air at Flow Rates up to 150 ft/sec
Near 3000°F (See Table 5).

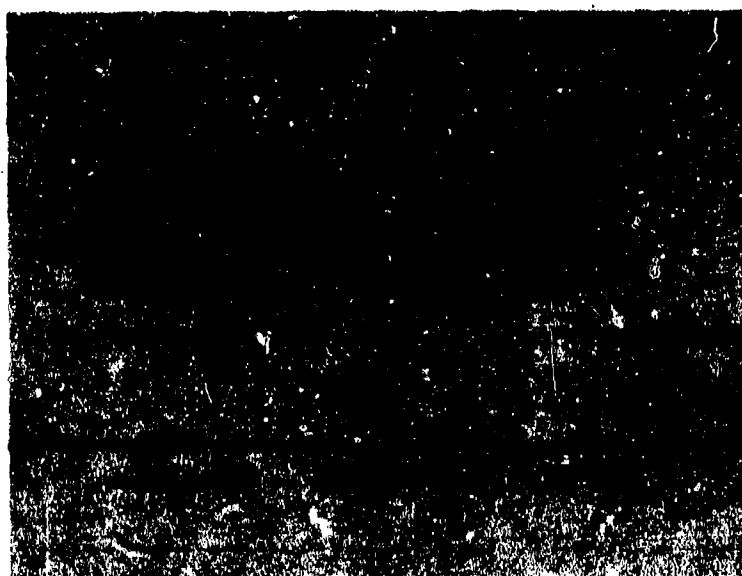


Plate No. 2-0449

Figure 31. Post Exposure Photomicrographs of $\text{ZrB}_2 + \text{SiC(A-8)}$
after Exposure in Air at Flow Rates up to 150 ft/sec
Near 3000°F (See Table 6).

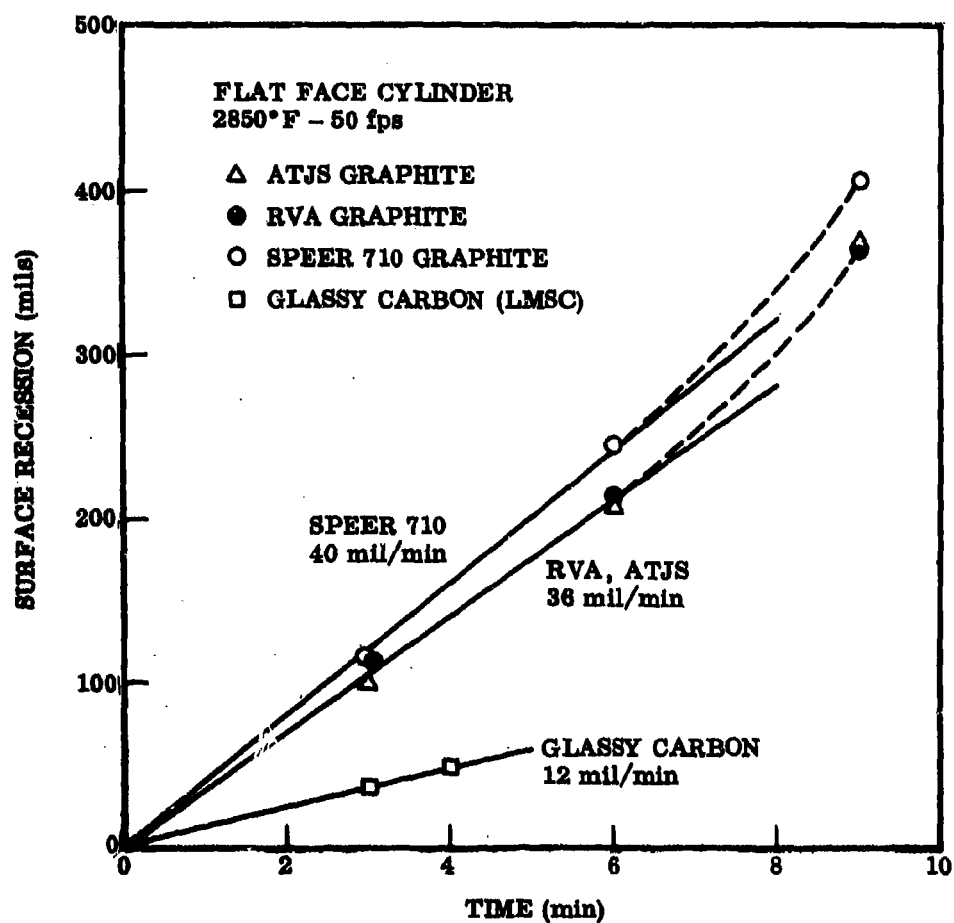


Figure 32. Surface Recession Curves for Four Grades of Graphite in Flowing Air at 2850°F.

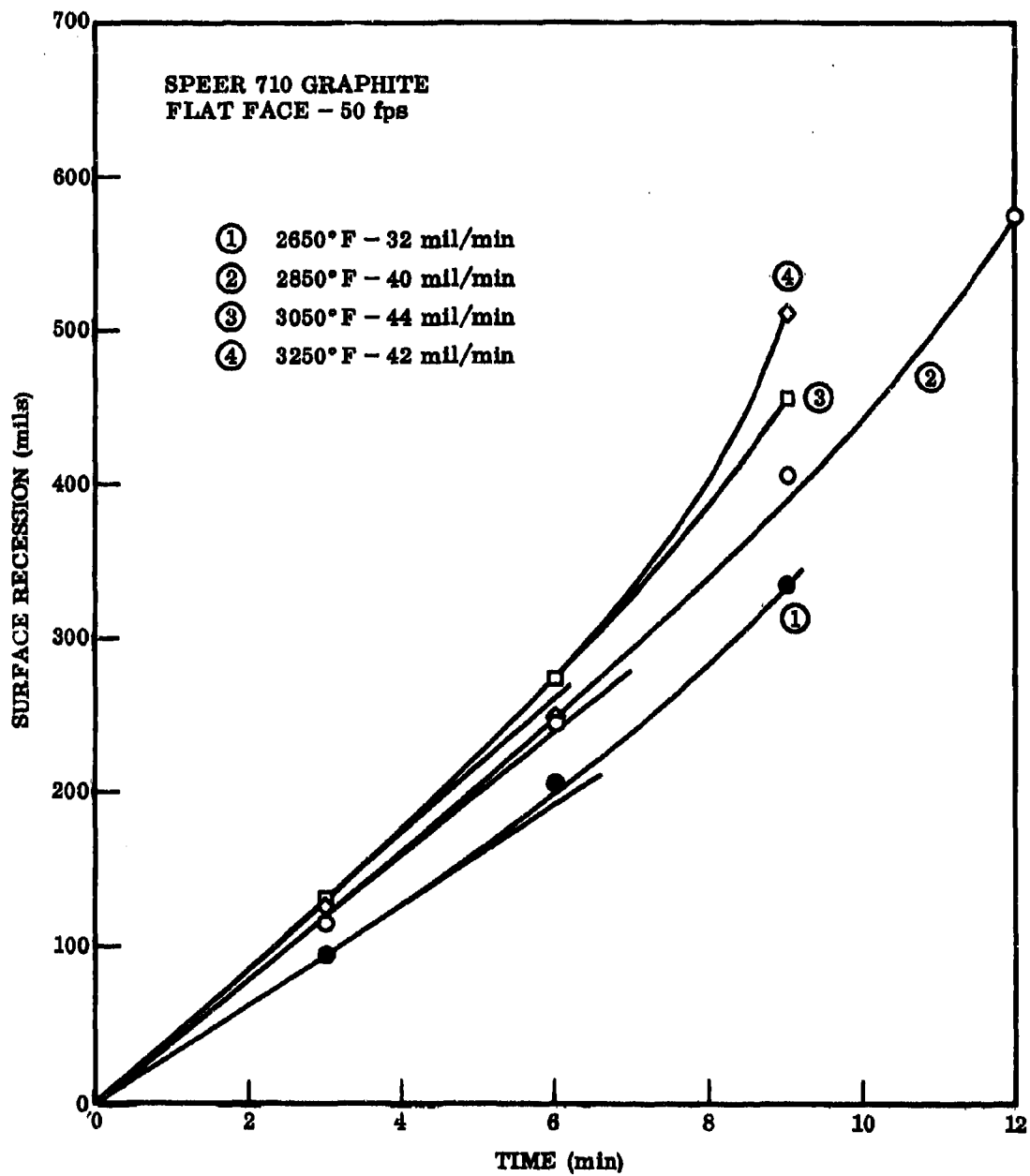


Figure 33. Surface Recession Curves, Speer 710 at 50 fps.

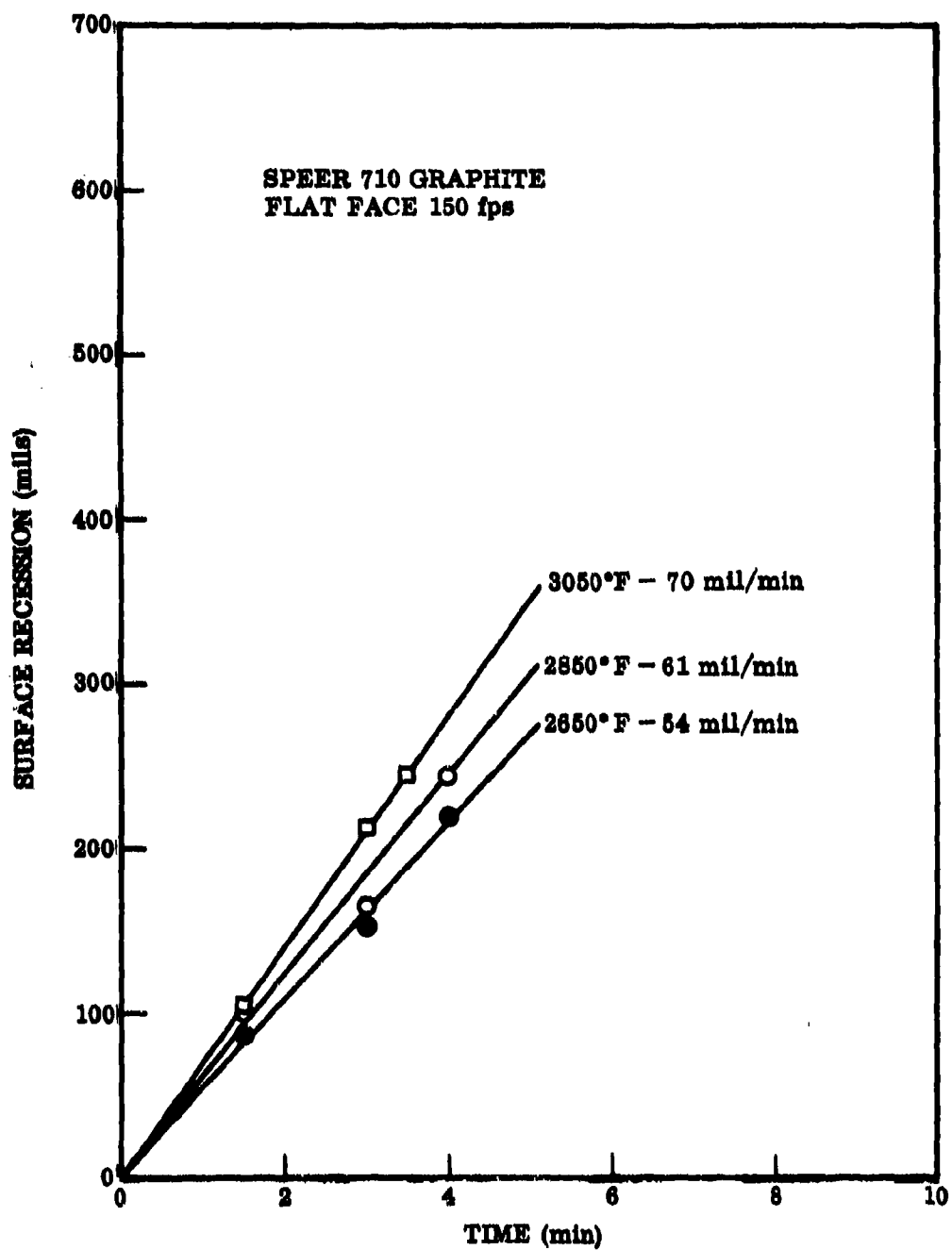


Figure 34. Surface Recession Curves, Speer 710 at 150 fps.

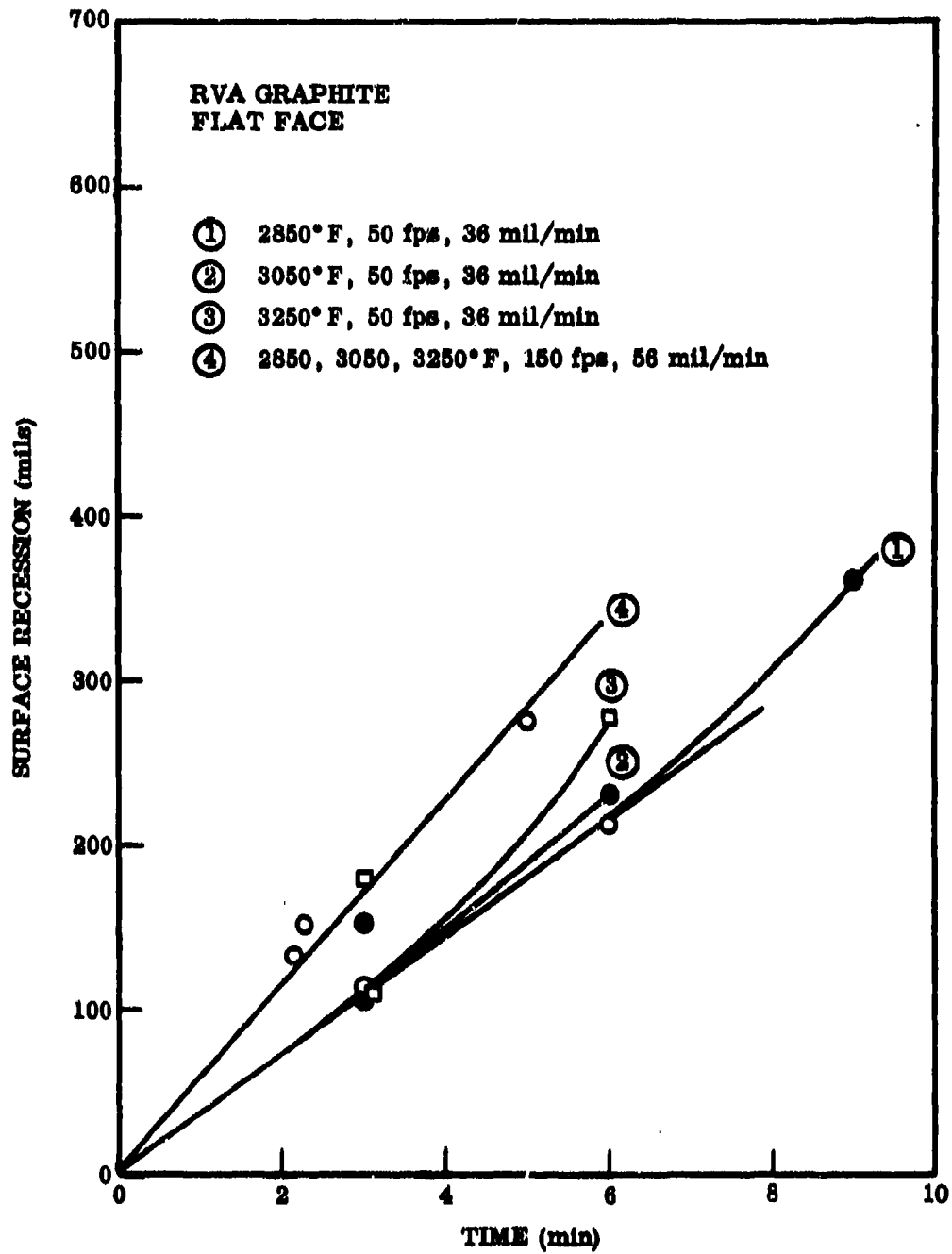


Figure 35. Surface Recession Curves, RVA at 50 and 150 fps.

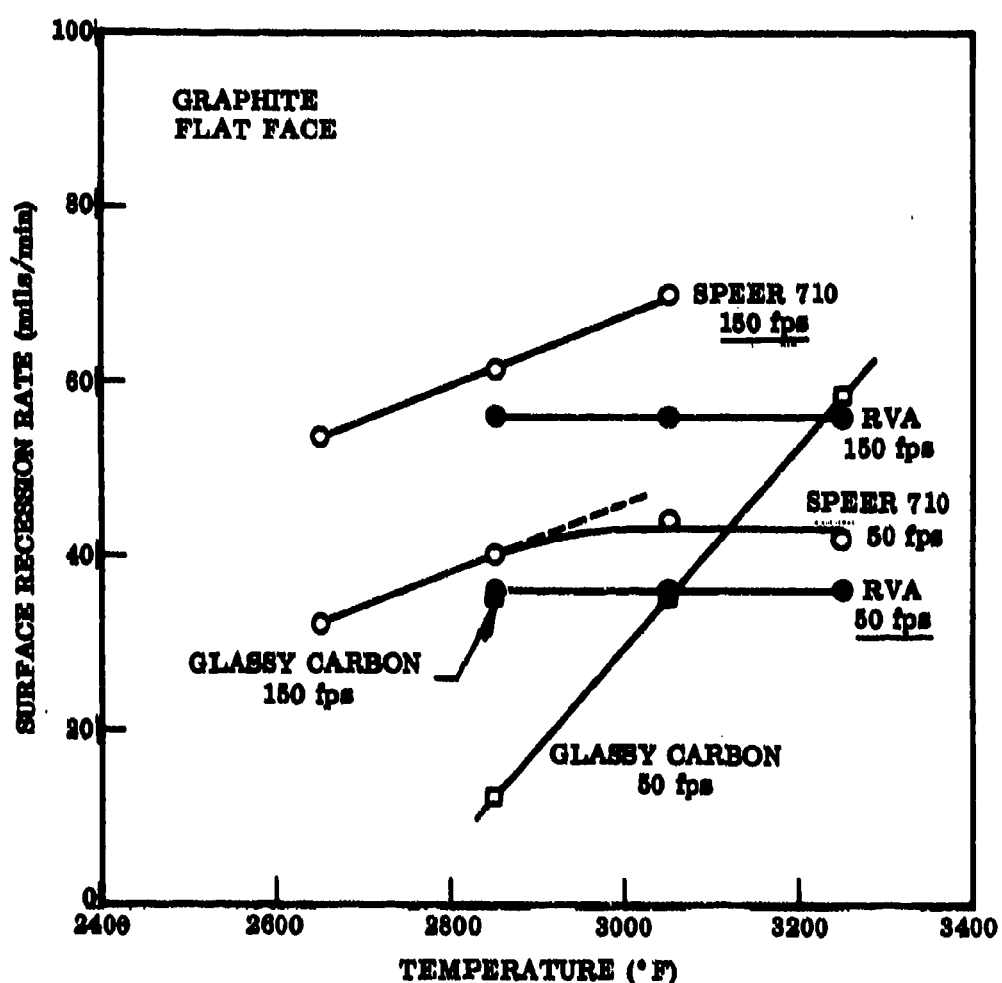


Figure 36. Effect of Temperature and Gas Velocity on the Surface Recession of Two Grades of Graphite.

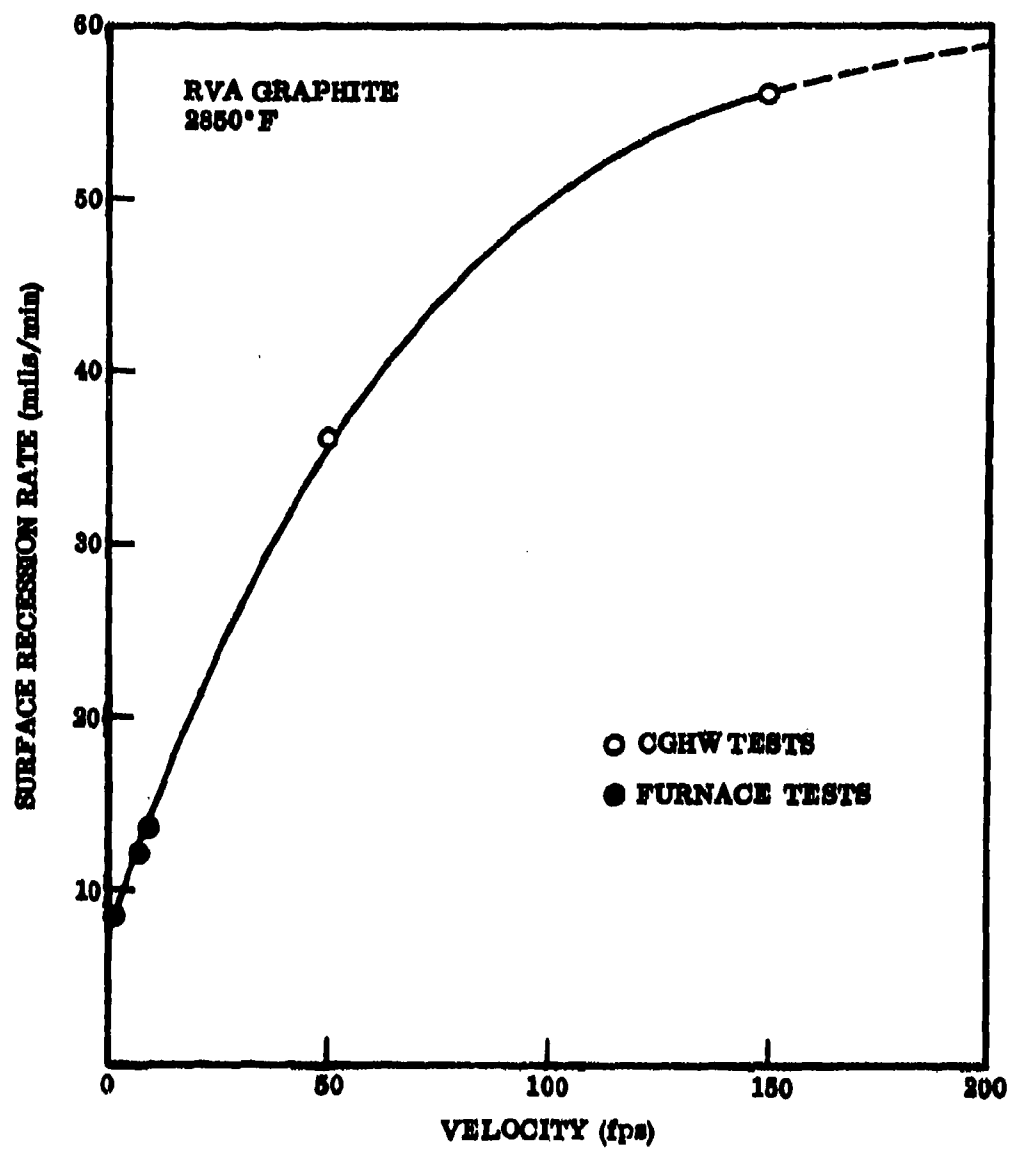


Figure 37. Effect of Velocity on the Surface Recession of RVA Graphite Flat Face Cylinders.

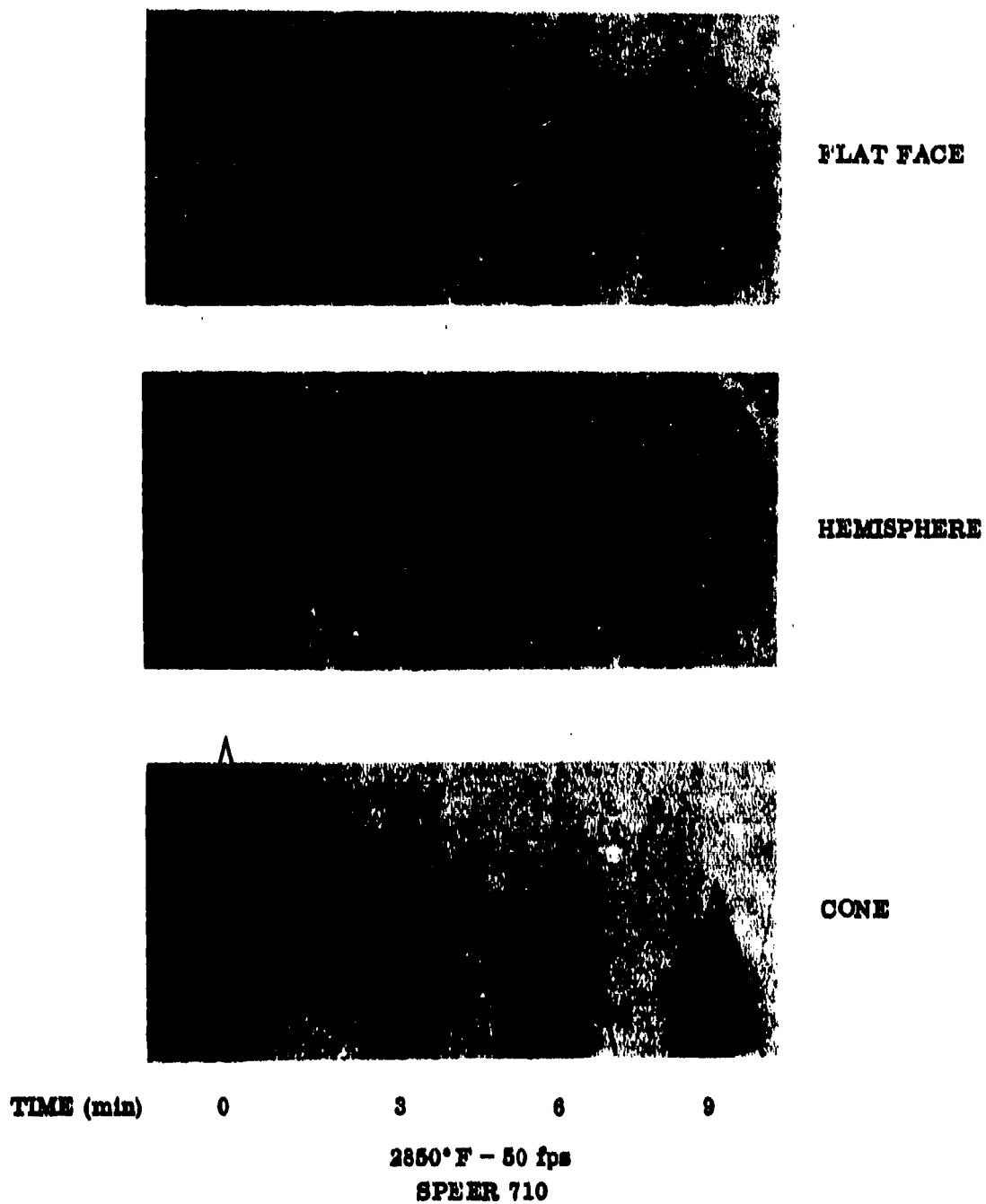


Figure 38. Changes in Specimen Configuration During the Oxidation of Graphite.

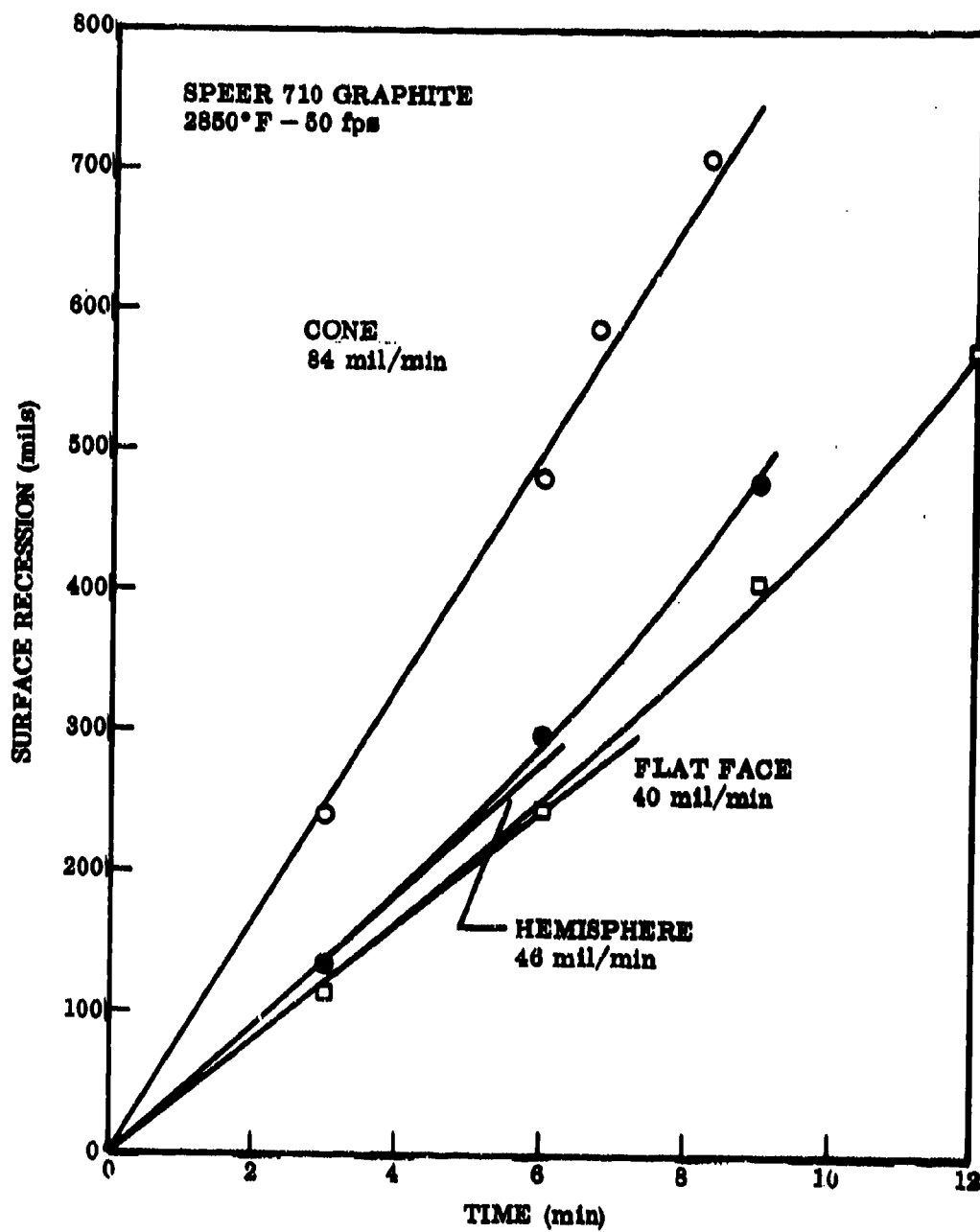


Figure 39. Effect of Specimen Configuration on the Surface Recession of Graphite.

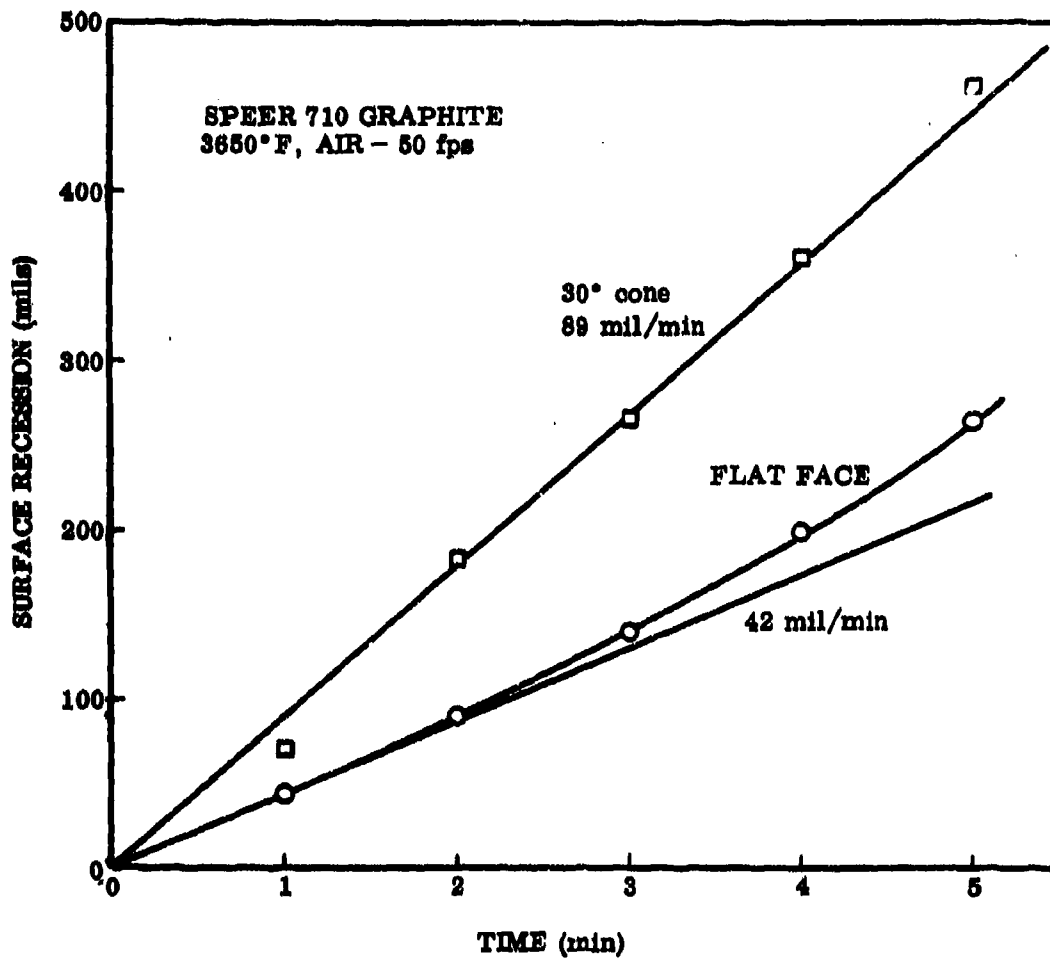


Figure 40. Effect of Specimen Configuration on the Surface Recession of Graphite in CG/HW Tests.

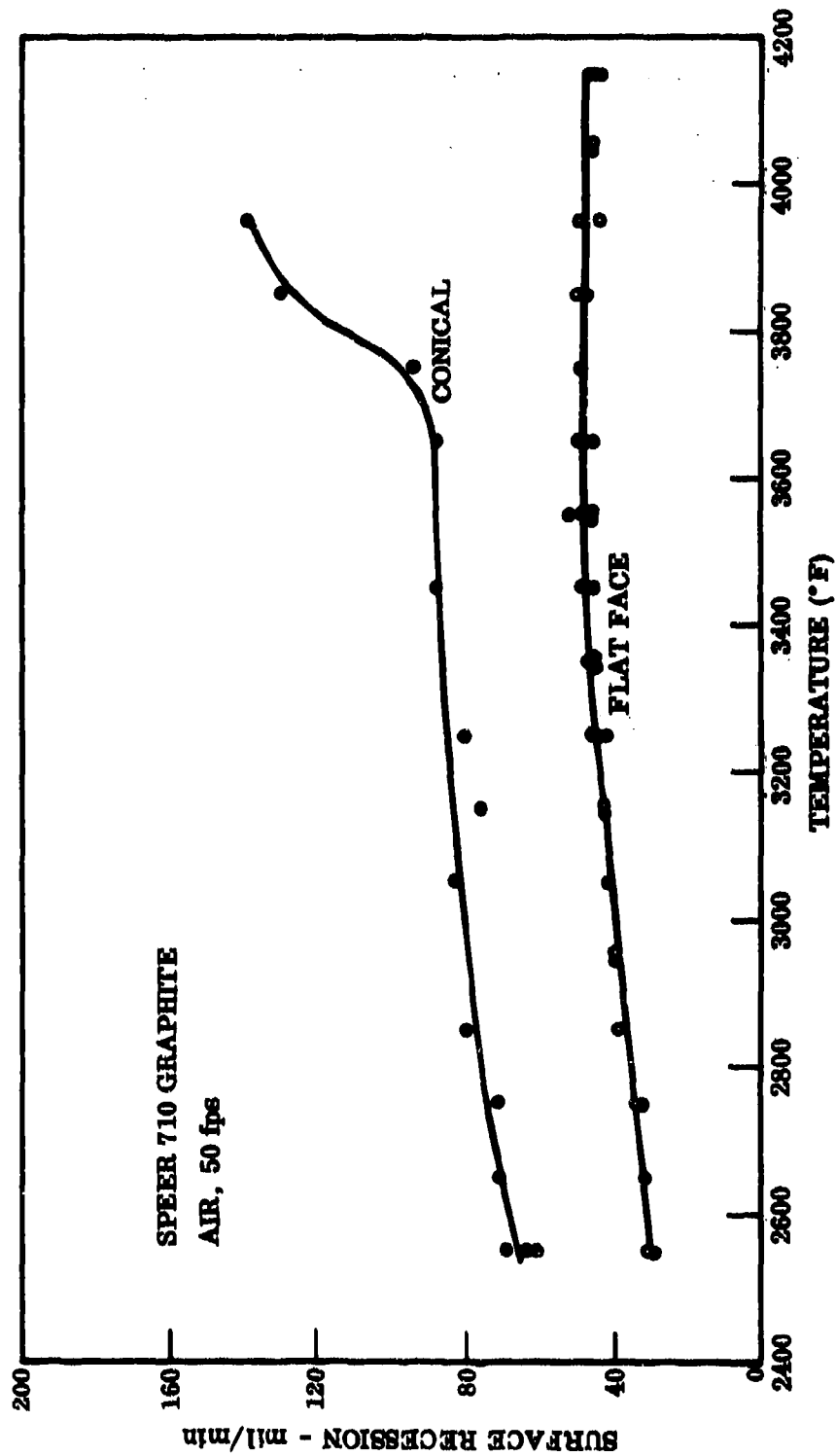


Figure 41. Effect of Specimen Shape on Temperature Dependency of Oxidation Rates for Graphite.



C

B

A

Figure 42. Measurement of Surface Recession on Conical Samples.

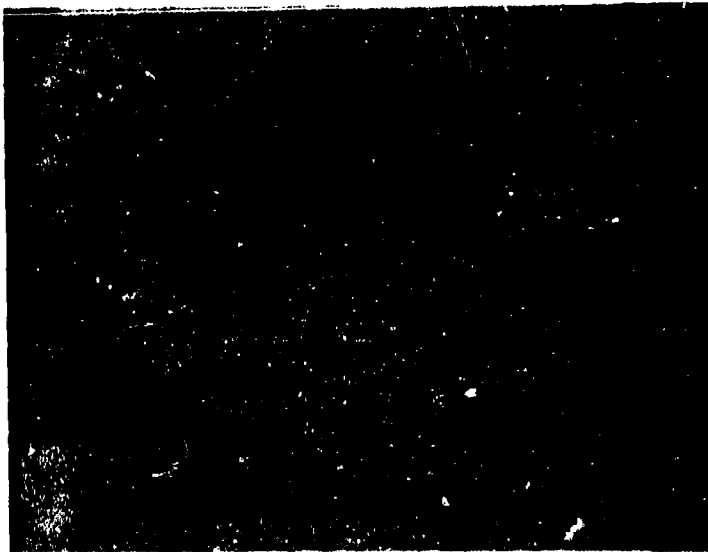


Plate No. 1-7094

As-Polished

X2.65

Figure 43. Section Through RVA(B-5)(L-6)(65-1) after 6 Minutes at 50 ft/sec in CG/HW Test at 3250°F. Initially Flat Face Cylinder 487 Mil Diameter, 1028 Mil Length

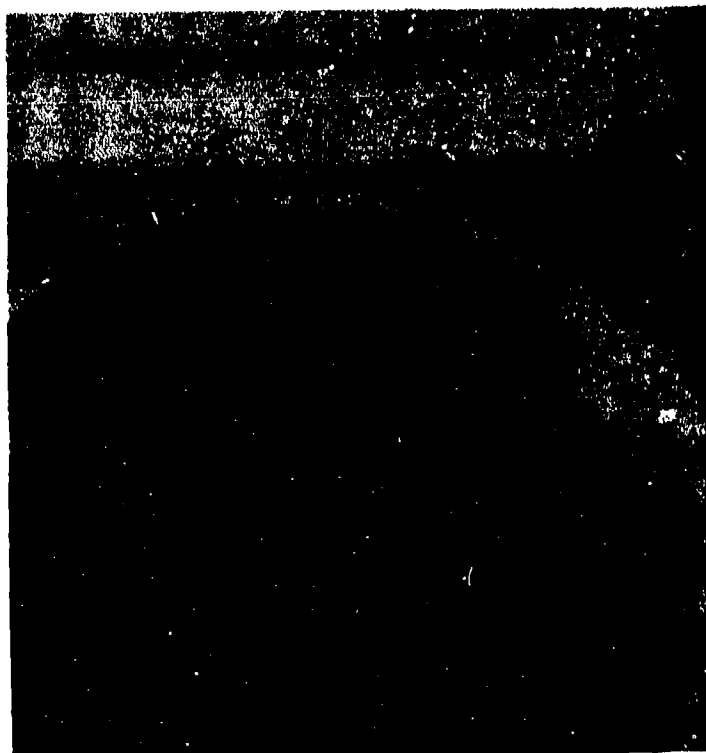


Plate No. 1-7721

As-Polished

X2.94

Figure 44. Section Through RVA(B-5)(L-16)(108-3) after 1.5 Minutes at 50 ft/sec in CG/HW Test at 3850°F. Initially 30° Cone 1486 Mils Long.

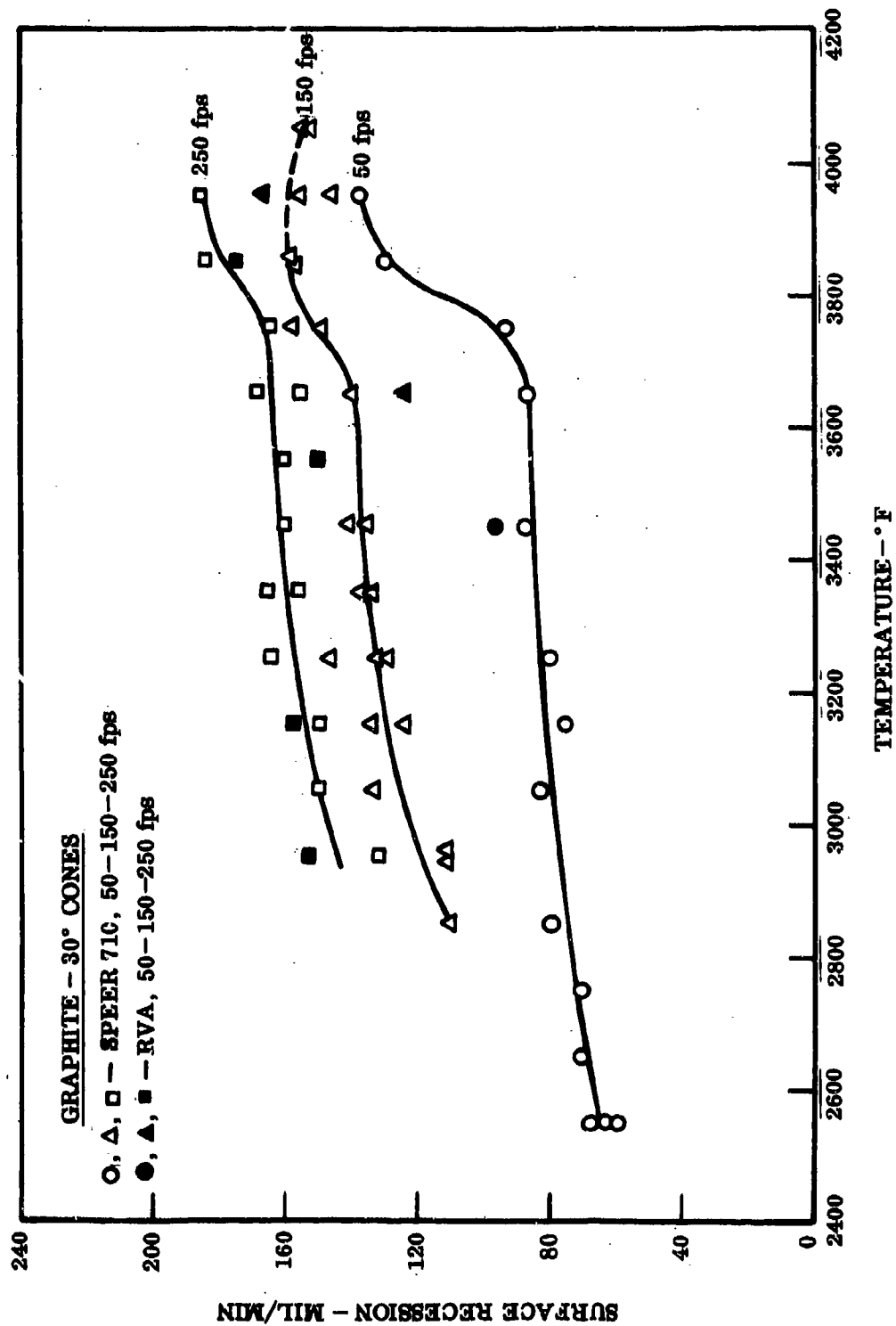


Figure 45. Effect of Temperature and Velocity on the Surface Recession of Graphite.

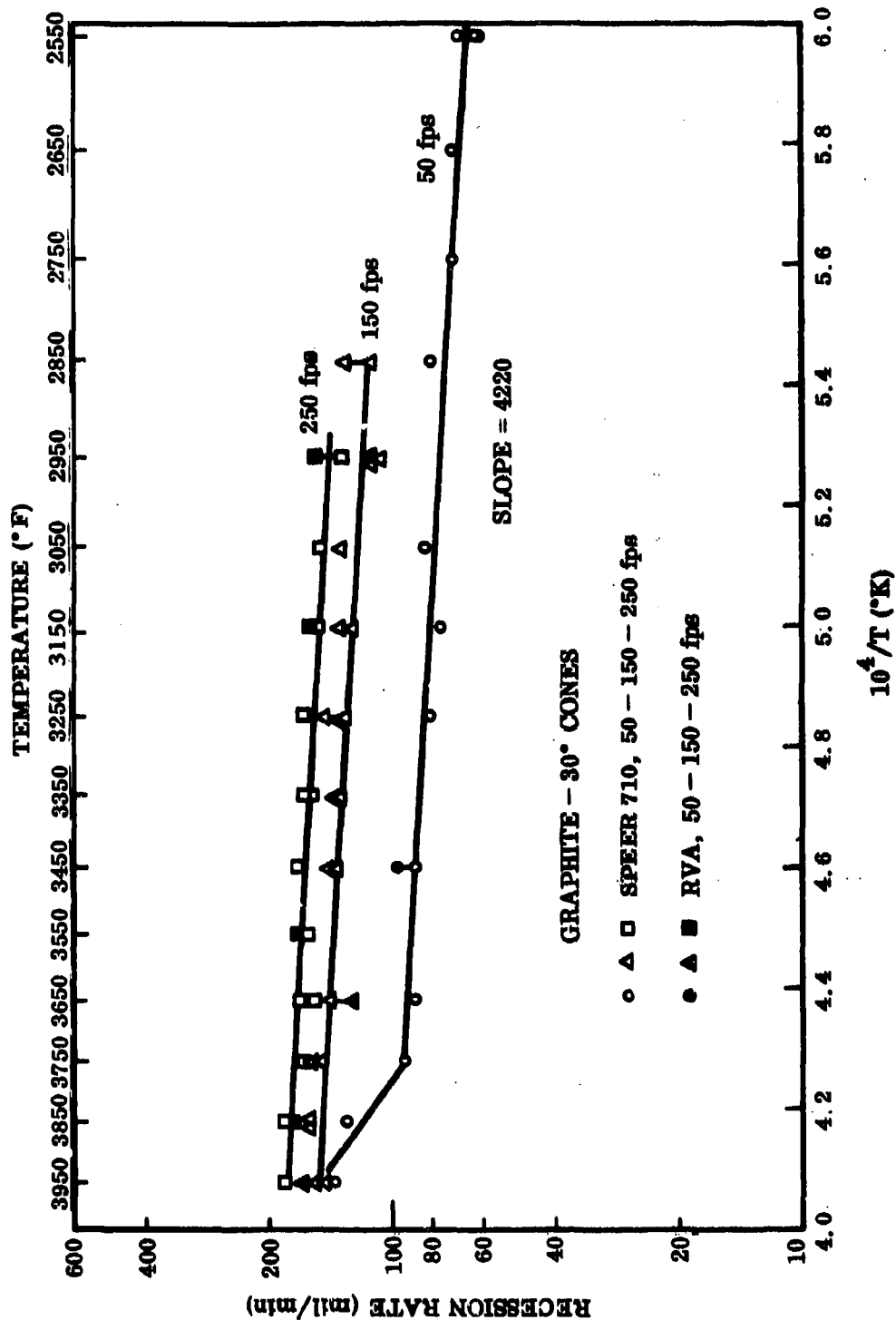


Figure 46. Arrhenius Plot of Surface Recession Data for Graphite in High-Velocity Air.

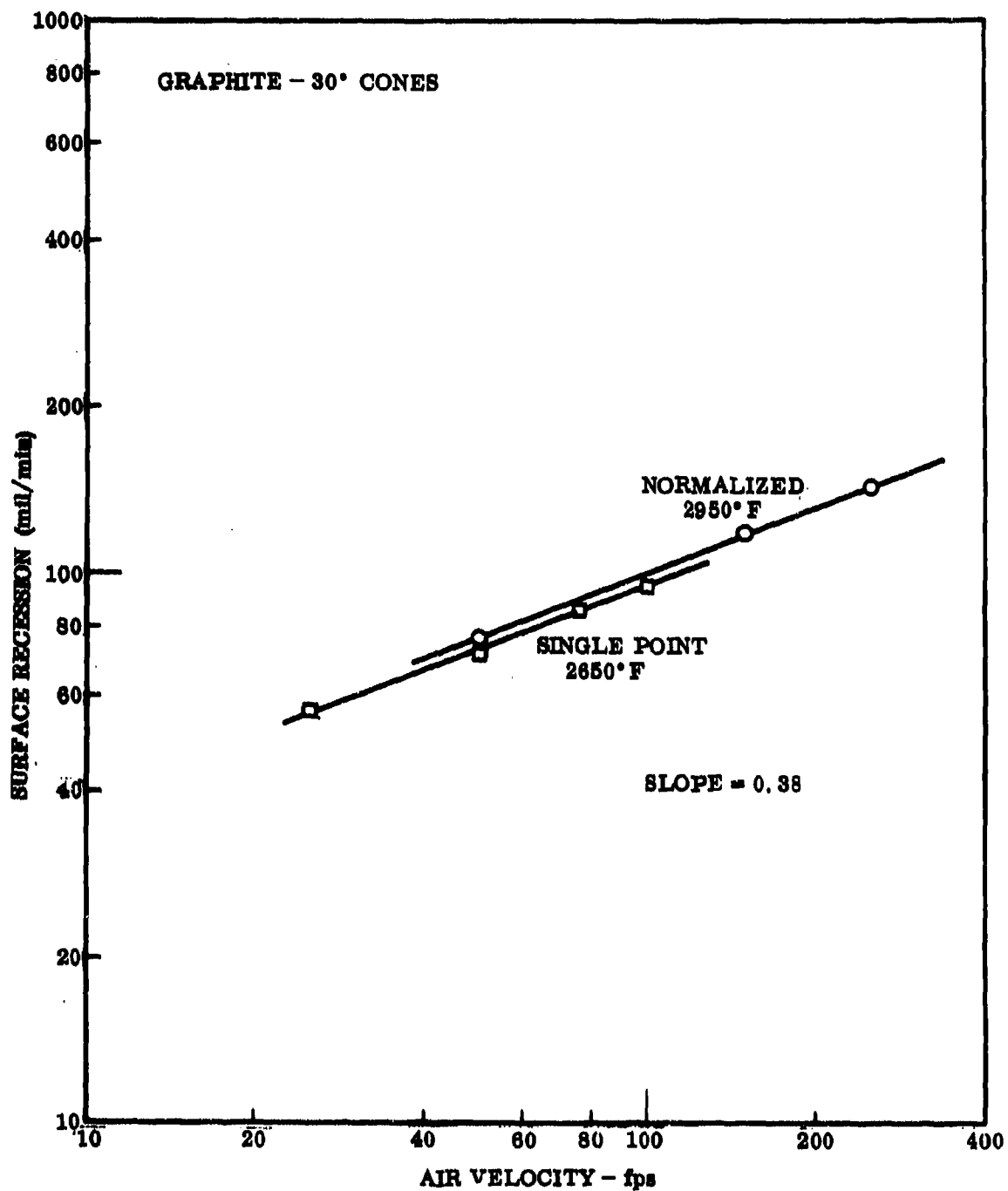


Figure 47. Effect of Velocity on the Surface Recession Rate of Graphite.

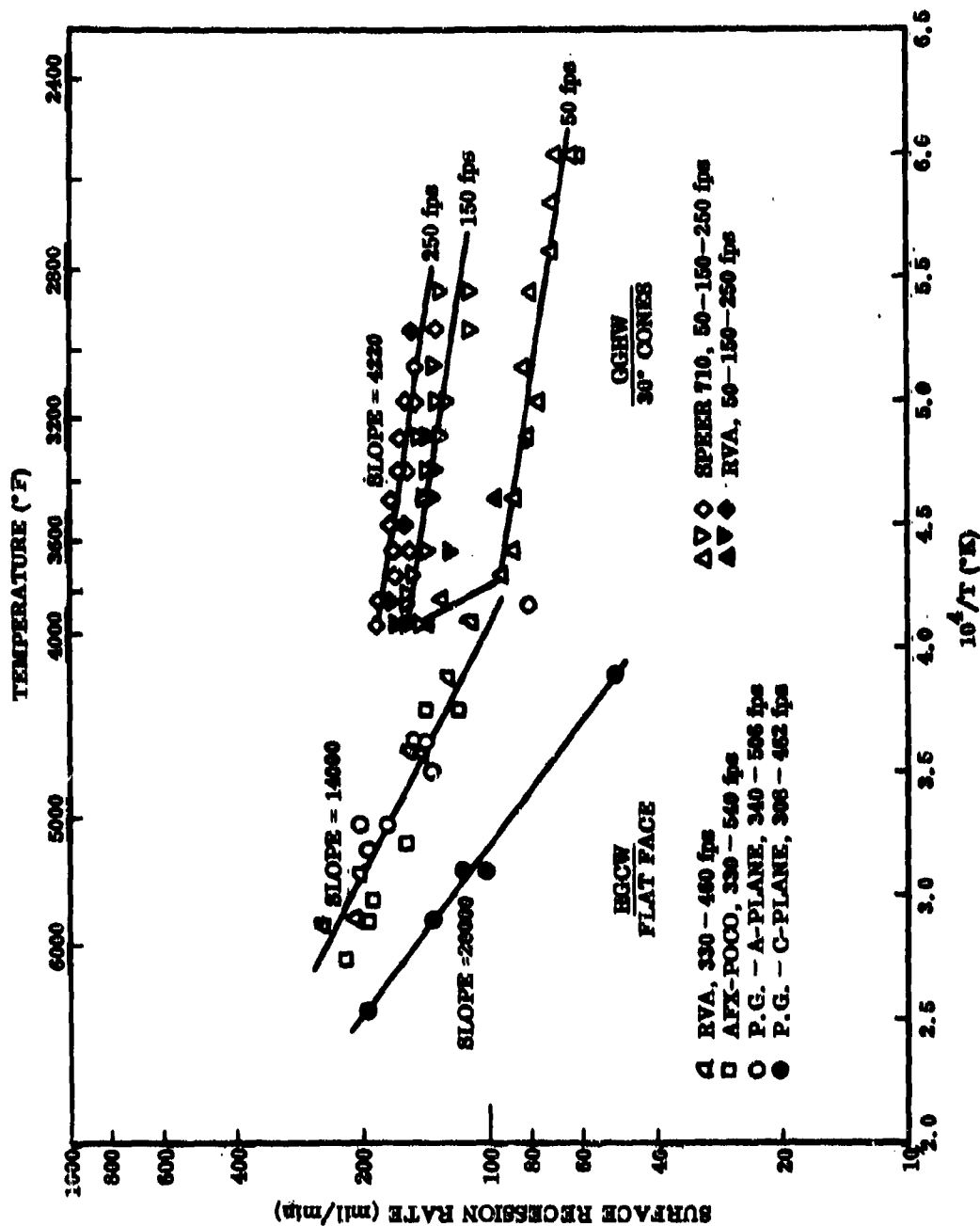


Figure 48. Summary of Graphite Oxidation Data; Subsonic Flow, 2500-6500°F, 1 Atmosphere.

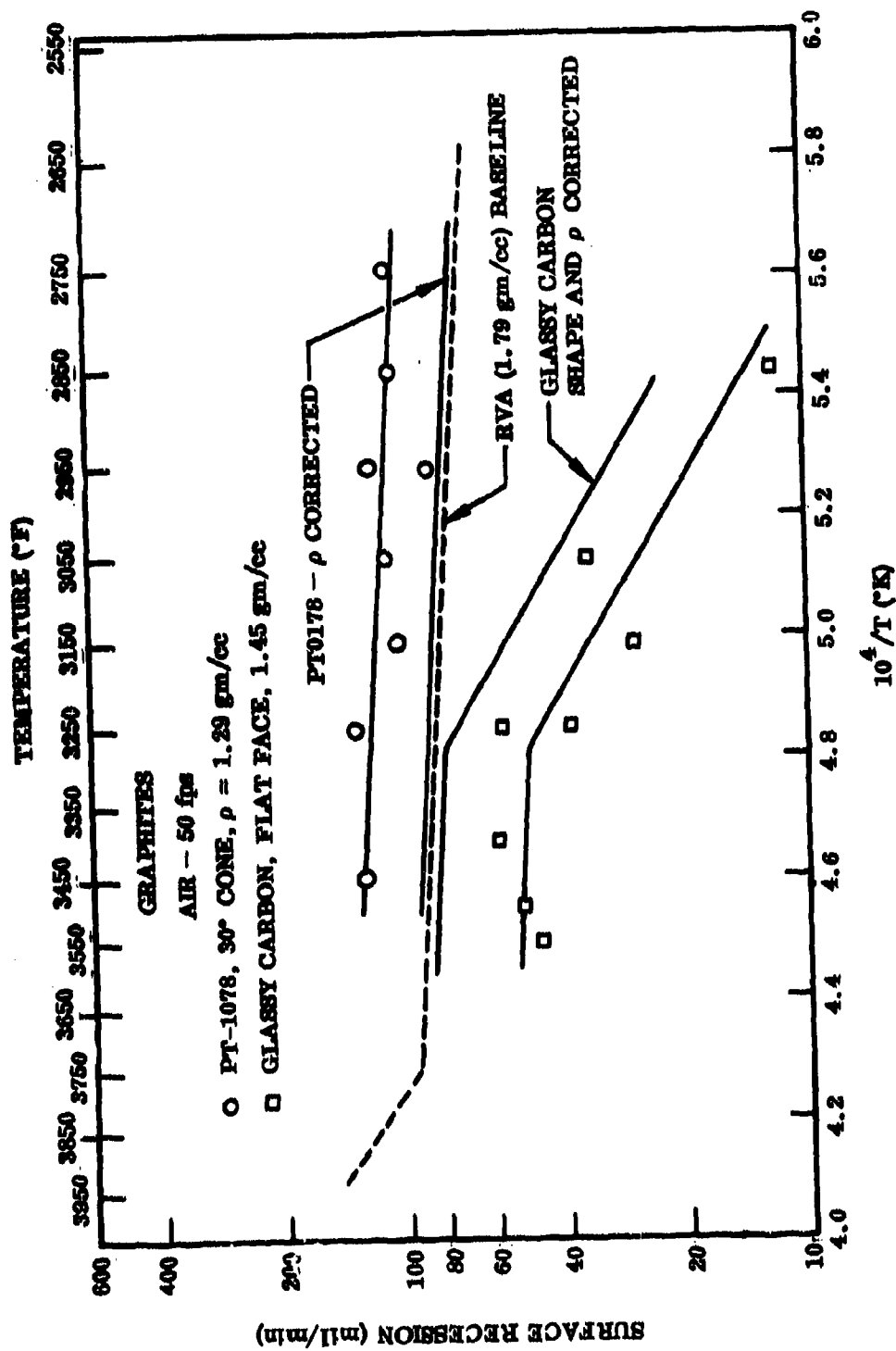


Figure 49. Effect of Structure and Density on the Oxidation of Graphite



Plate No. 1-9411

X2.75

Figure 50. PT 0178(B-9)-L14, Surface Temperature 3050°F, Air Flow Rate 150 ft/sec, Exposure Time 2 minutes, Initial Configuration 30° Cone, 321 Mil Recession, One Inch Scale

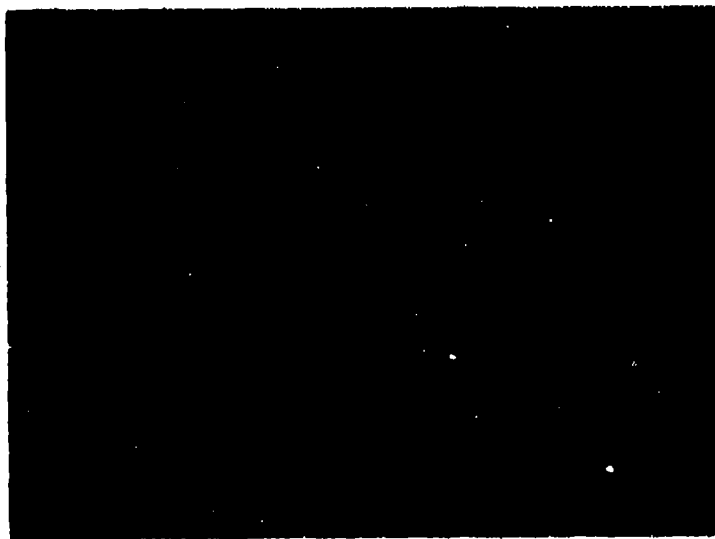


Plate No. 1-9412

X250

Figure 51. PT 0178(B-9)-L14, Hot Surface at Top



Plate No. 1-8492

X2.90

Figure 52. Glassy Carbon (B-11)-2000-3, Surface Temperature 3550°F, Air Flow Rate 50 ft/sec. Exposure Time 1.5 minutes, Initial Configuration Hemispherical Cap, 71 mil Recession, One Inch Scale.



Plate No. 1-8493

Unetched

Small Division = 0.788 mils

Figure 53. Glassy Carbon (B-11)-2000-3, Hot Surface at Left

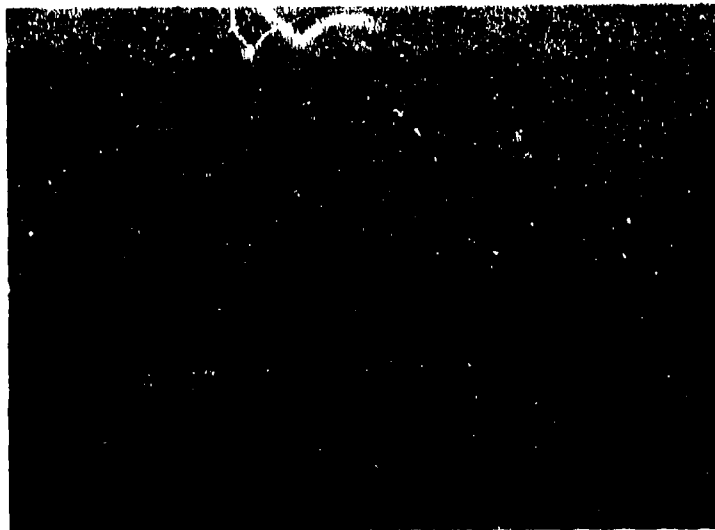


Plate No. 1-9386

X0.90

Figure 54. Si-RVC(B-8)-(L-6) survived 60 minutes at 150 ft/sec and 2900°F; (L-7) coating failed after 15 minutes at 10 ft/sec and 3100°F; (L-8) coating failed after 60 minutes at 10 ft/sec and 3000°F.

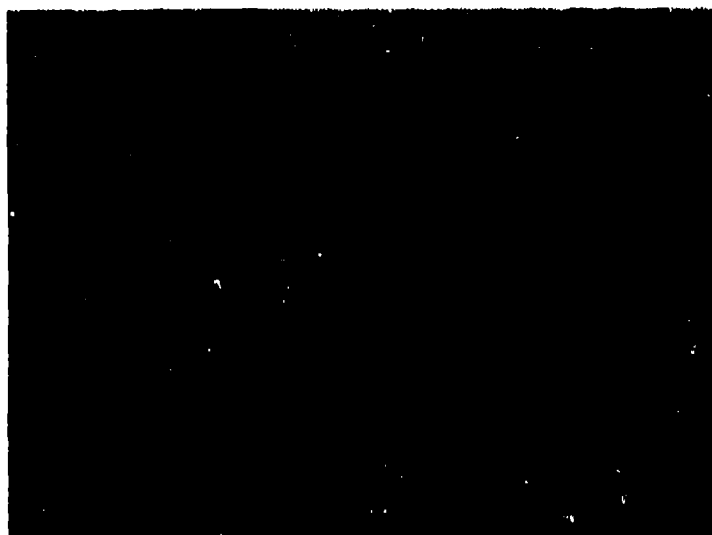


Plate No. 1-9397

X2.90

Figure 55. Si-RVC(B-8)-L-7 High Velocity Cold Gas/Hot Wall Test at 3100°F and Air Flow Rate of 10 ft/sec. Exposure Time 10 minutes. Coating Failed. Hot Face Up.

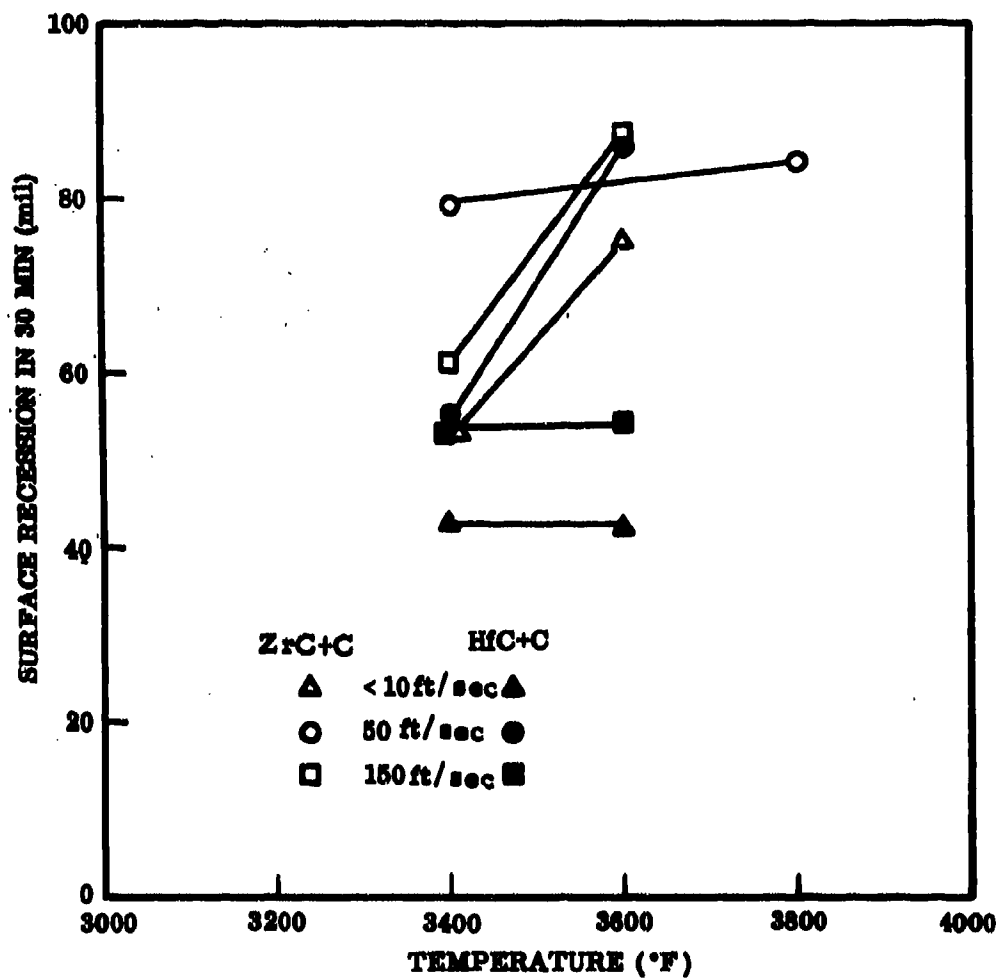


Figure 56. Surface Recession Behavior of HfC + C(C-11) and ZrC + C(C-12) in CG/HW Flow Studies.



TOP

A. Sample C-11-L4, 3600°F, 50 fps, 26 Min. Billet 1416B, 14.25%C.



TOP

B. Sample C-11-L7, 3600°F, <10 fps, 30 Min. Billet 1422A, 13.60%C.

Figure 57. Effect of Carbon Content on Surface Appearance of Oxidized HfC + C Samples.



Plate No. 1-8193

X2.90

Figure 58, ZrC + C(C-12)-L8, Surface Temperature 3800°F,
Air Flow Rate 50 ft/sec. Exposure Time 22 minutes,
Hot Face Up, 72 Mil Recession, One Inch Scale



Plate No. 1-8194

Unetched

X15

Figure 59. ZrC + C(C-12)-L8, Hot Surface. Oxide at Top.

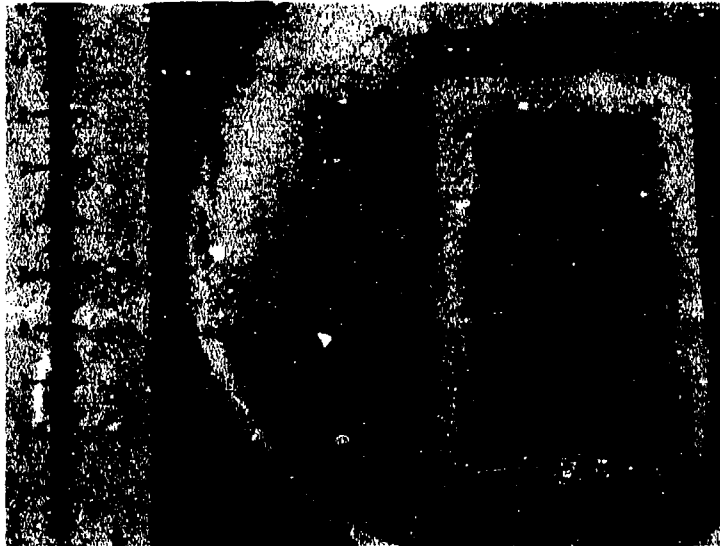


Plate No. 1-8223

X3.00

Figure 60. HfC + C(C-11)-L4, Surface Temperature 3600°F, Air Flow Rate 50 ft/sec. Exposure Time 26 minutes, Hot Face Up, 80 mil Recession, One Inch Scale



Plate No. 1-8224

Unetched

X30

Figure 61. HfC + C(C-11)-L4, Hot Surface, Oxide at Left



Plate No. 1-7162

X2.75

Figure 62. KT-SiC(E-14)-L4, Surface Temperature 3660°F, Air Flow Rate 150 ft/sec. Exposure Time 30 minutes, Hot Face Up. No Length Recession, 15 Mil Diametral Recession. Thermal Stress Failure.



Plate No. 1-7153

X2.60

Figure 63. KT-SiC(E-14)-L1, Surface Temperature 3450°F, Air Flow Rate 50 ft/sec. Exposure Time 27 minutes, Hot Face Up. 15 Mil Length Recession, 115 Mil Diametral Recession, One Inch Scale

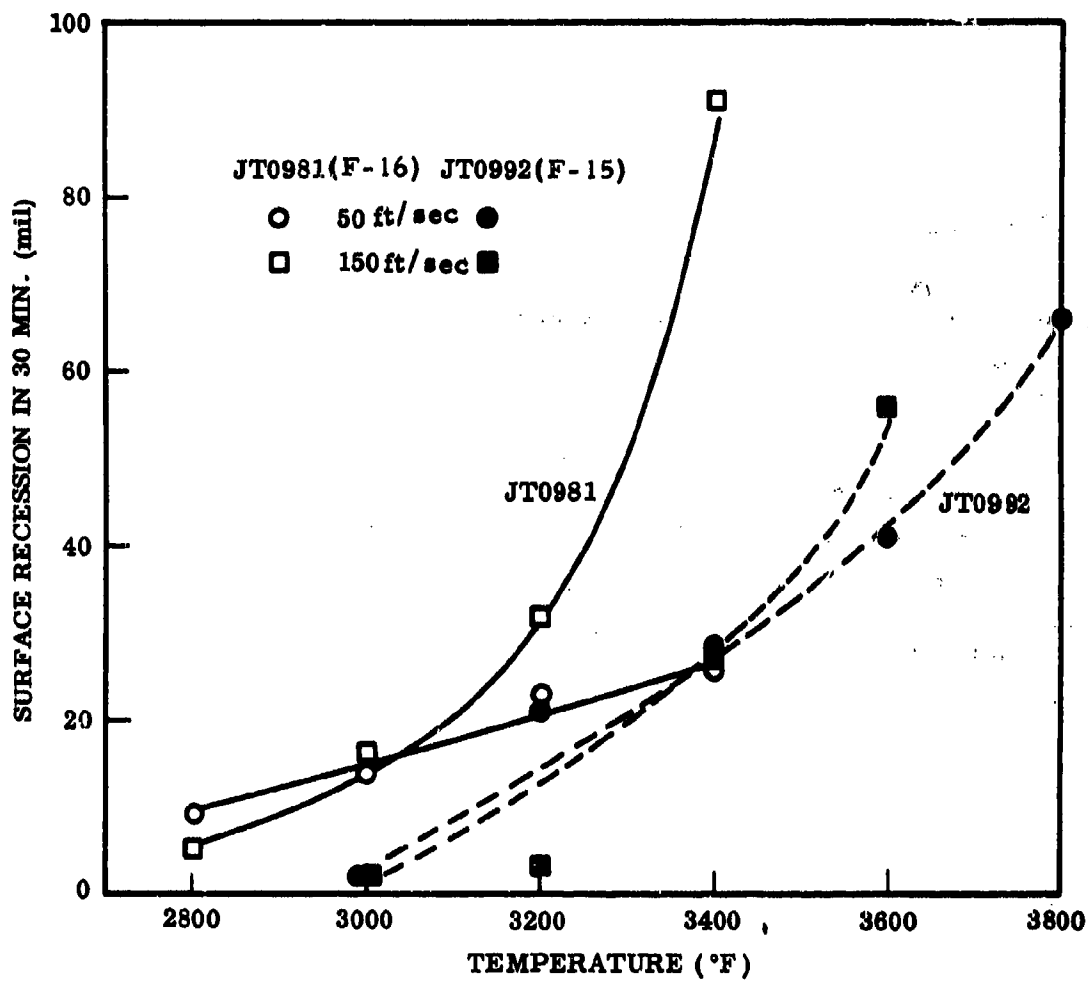
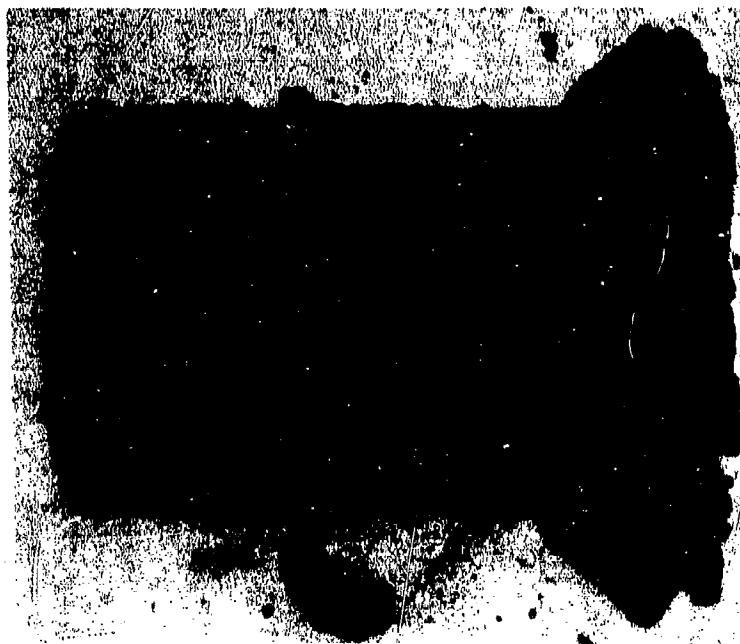
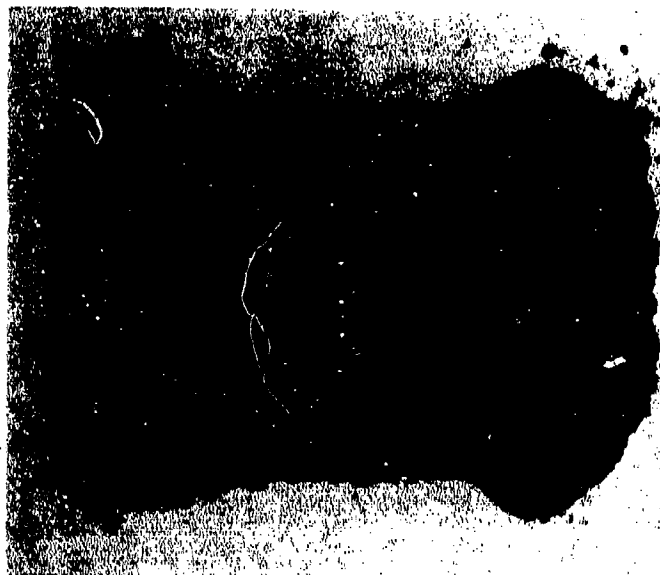


Figure 64. Surface Recession Behavior of JT0981 (F-16) and JT0992 (F-15) in CG/HWFlow Studies



A - JT0992, (F-15)-L4 3400°F - 50 ft/sec -
30 min.

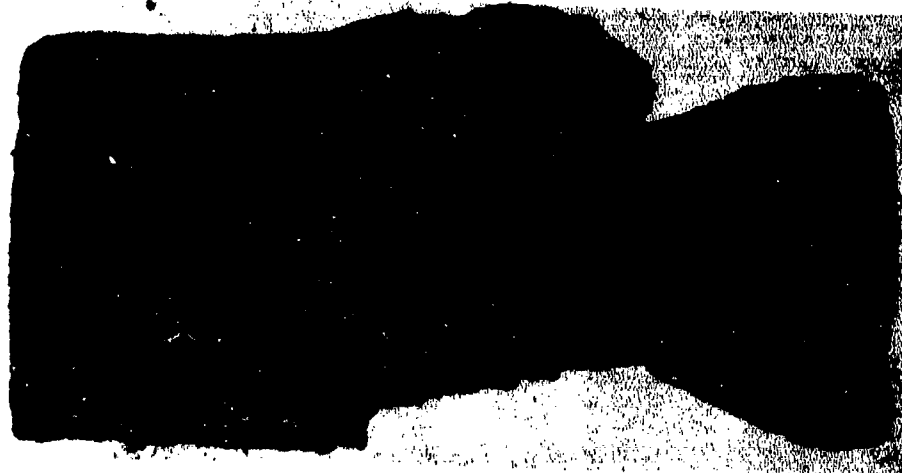


B - JT0981, (F-16)-L5 3400°F - 150 ft/sec -
13 min.

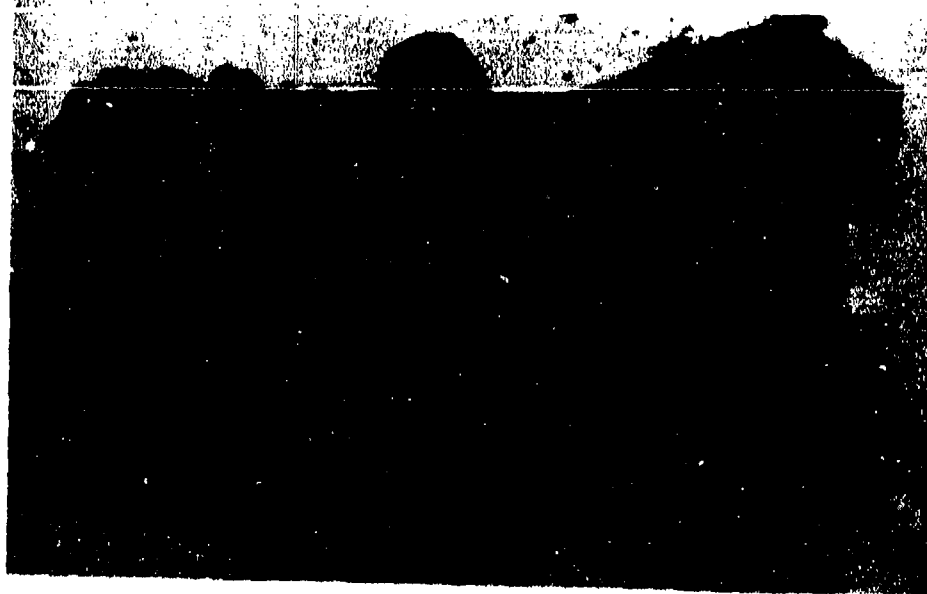
Figure 65 Effect of Velocity on the Oxidation Behavior of JT0992 and JT0981 Graphites. (X4)



As-Tested



Oxide Removed



As-Tested

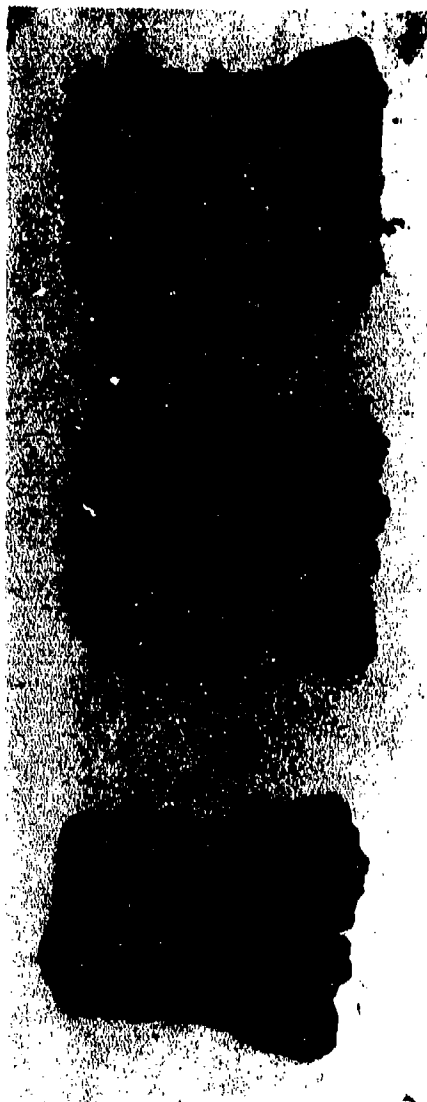
B. - JT0981 (F-16)-L1, 2800°F -
150 ft/sec - 30 min.

A. - JT0992 (F-15)-L9, 2600°F-50 ft/sec -
30 min.

Figure 66 Degradation of JT0992(F-15) and JT0981(F-16) Graphites at Low Temperatures.



2000°F
Test (F-15)-L11



2200°F
Test (F-15) - L15

3000°F
Test (F-15) - L12

Figure 67. Active-Passive Transition in the Oxidation of JT-0992(F-15) Graphite.
(50 ft/sec Air-30 min.)



Plate No. 1-7974

X2.60

Figure 68. JT0992(F-15)-L11, Surface Temperature 3400°F, Air Flow Rate 50 ft/sec. Exposure Time 30 Minutes, Hot Face Up. 6 Mil Recession. One Inch Scale.



Plate No. 1-8197

X2.90

Figure 69. JT0992(F-15)-L4, Surface Temperature 2000°F, Air Flow Rate 50 ft/sec. Exposure Time 30 Minutes, Hot Face Up. 28 Mil Recession. One Inch Scale.



Plate No. 1-8008

X2.60

Figure 70. JT0981(F-16)-L7, Surface Temperature 3200°F, Air Flow Rate 150 ft/sec. Exposure Time 30 Minutes, Hot Face Up. 32 Mil Recession. One Inch Scale.

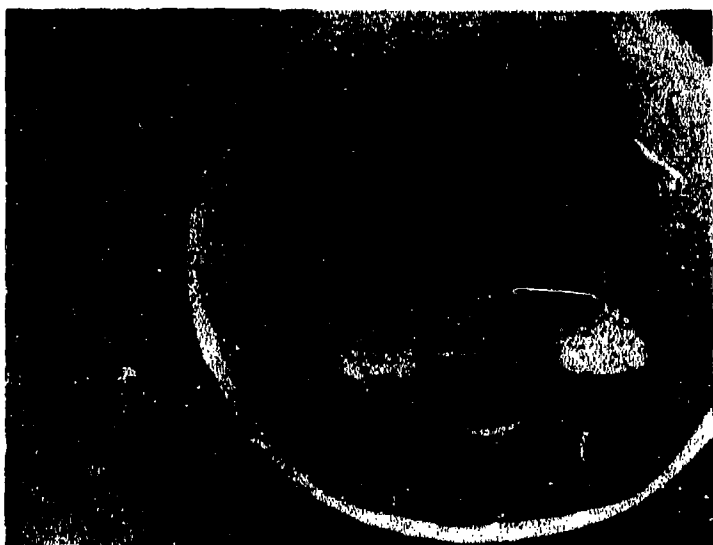


Plate No. 1-8017

X2.60

Figure 71. JT0981(F-16)-L10, Surface Temperature 2800°F, Air Flow Rate 50 ft/sec. Exposure Time 30 Minutes, Hot Face Up. 9 Mil Recession. One Inch Scale.

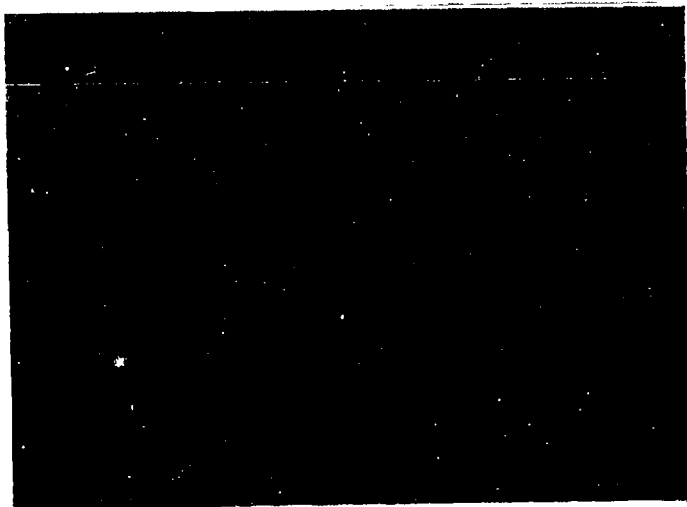


Plate No. 1-5349

X3.50

Figure 72. $WSi_2/W(G-18)-40-1$, Surface Temperature $3500^{\circ}F$, Air Flow Rate 150 ft/sec., Exposure Time 60 minutes, Hot Face Down, No Coating Failure. One Inch Scale.



Plate No. 1-5350

Etched with Murikami's Reagent One Small Division = 0.397 mils

Figure 73. $WSi_2/W(G-18)-40-1$, Hot Surface at Top Showing WSi_2 Layer, Over W_5Si_3 Layer Coating Tungsten Matrix at Bottom

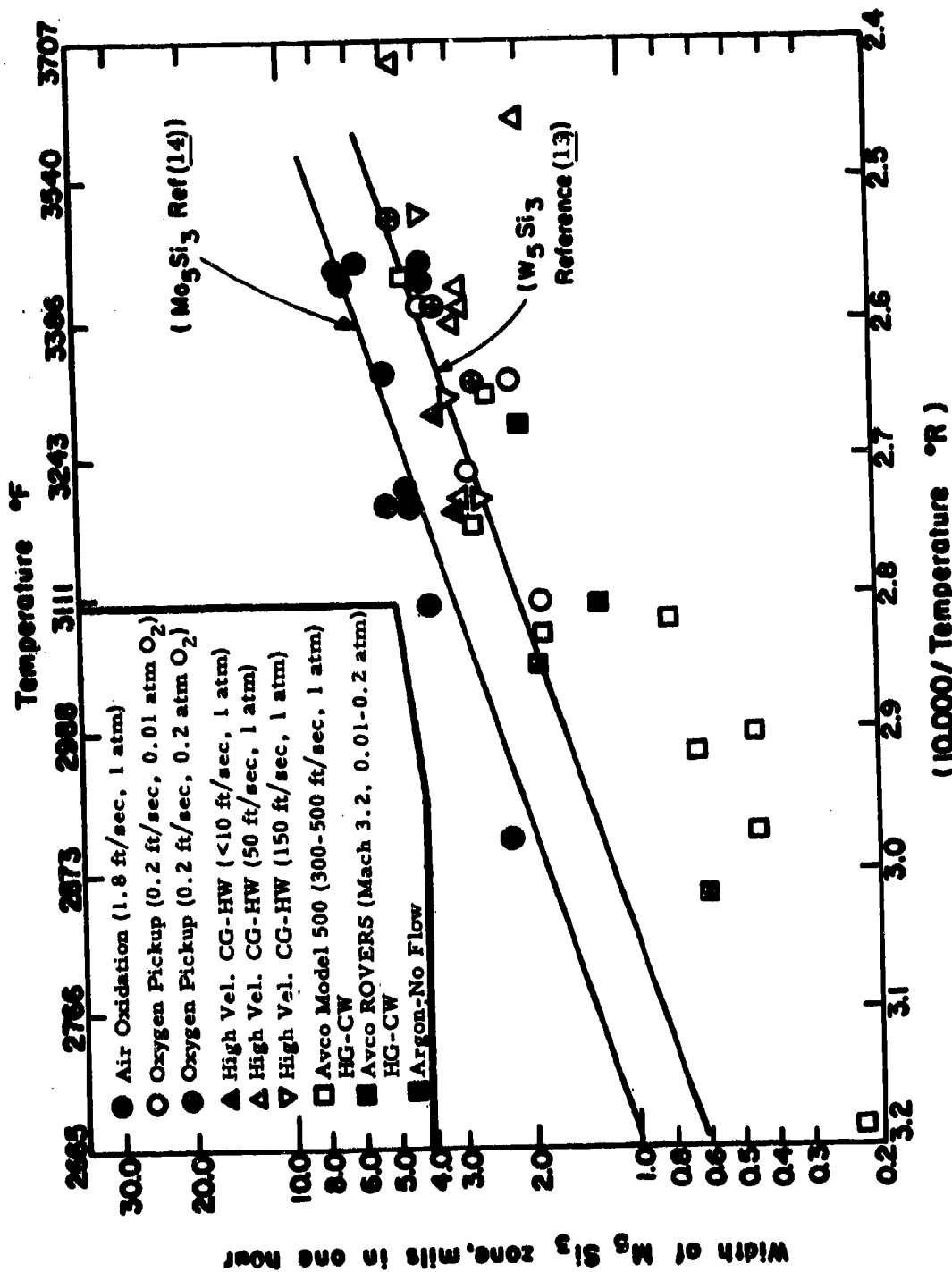


Figure 74. Growth of W_5Si_3 Zone on $WSi_2/W(G-18)$ as a function of Flow Rate and Pressure Compared with the results of Bartlett and Gage (13) for W_5Si_3 and Perkins and Packer for Mo_5Si_3 (14).



Plate No. 1-5061

X250

Figure 75. Sn-Al/Ta-10W(G-19)-41-2, Surface Temperature 3000°F, Air Flow Rate 150 ft/sec, Exposure Time 60 Minutes, No Coating Failure, Coating at Top

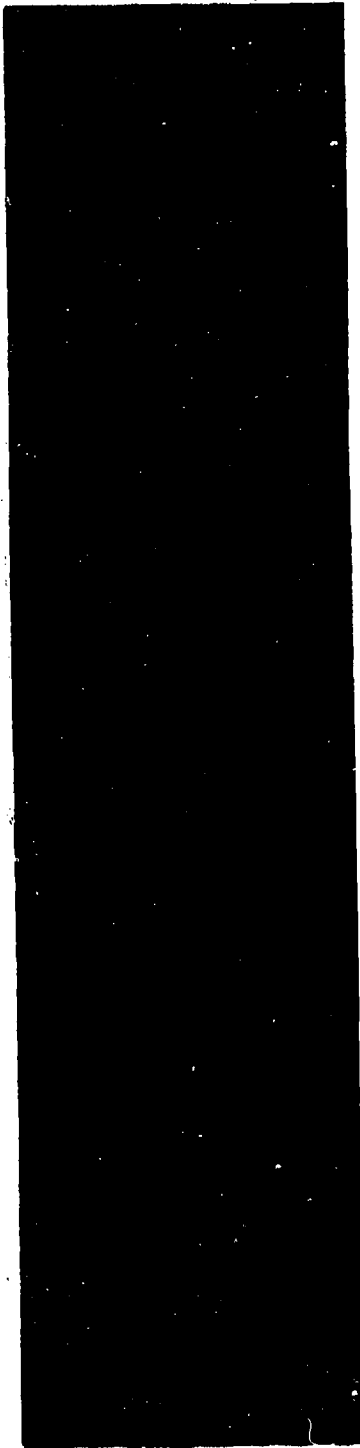


Plate No. 1-5055

Unetched

X250

Figure 76. Sn-Al/Ta-10W(G-19)-37-1, Surface Temperature 3300°F, Air Flow Rate 50 ft/sec, Exposure Time 22 minutes, Coating Failure. Oxidized Tantalum-Tungsten Alloy at Top



2400°F	2500°F	2600°F	2700°F	2750°F	2800°F
(H-23)-L6	(H-23)-L5	(H-23)-L7	(H-23)-L4	(H-23)-L9	(H-23)-L10

Figure 77. Active-Passive Transition in the Oxidation of SiO_2 -60W (H-23)
(50 ft/sec Air - 30 min)

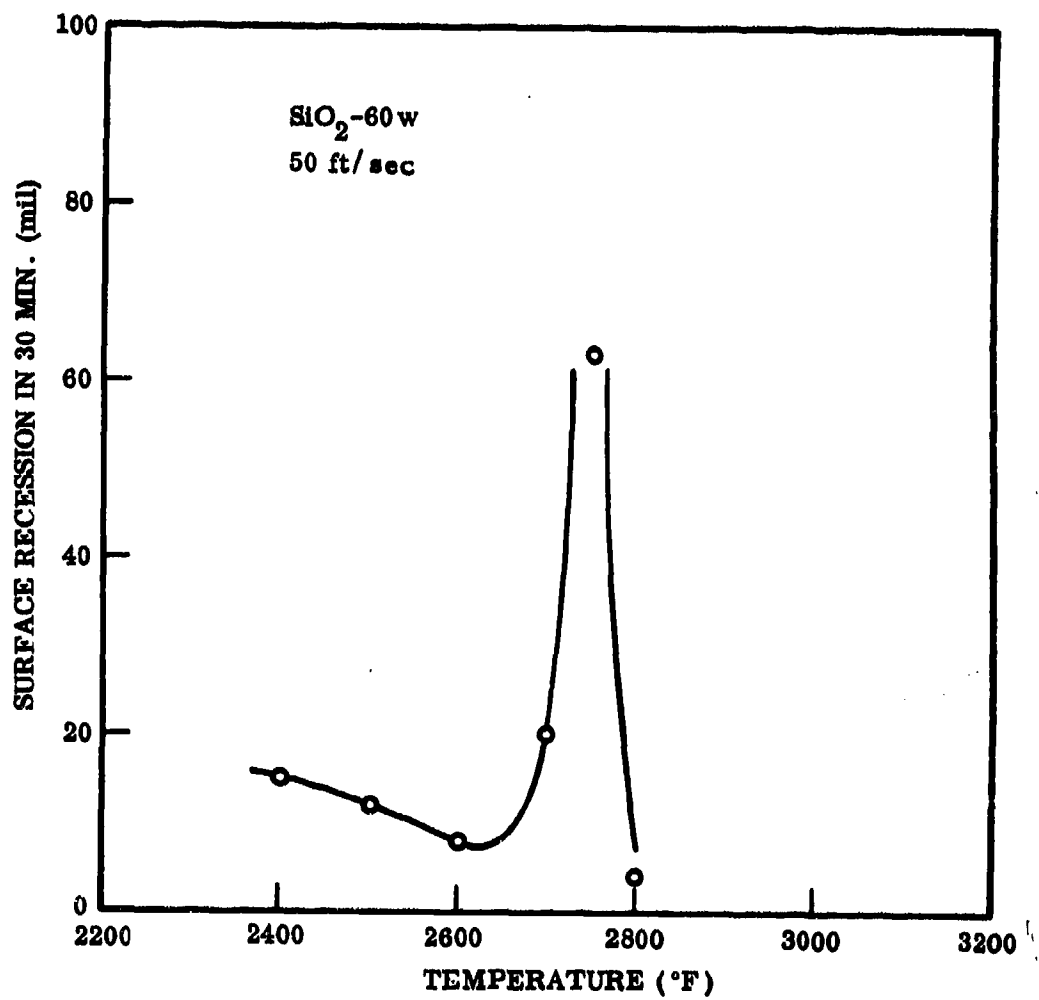


Figure 78. Surface Recession Behavior of SiO₂-60W in CG/HW Flow Studies

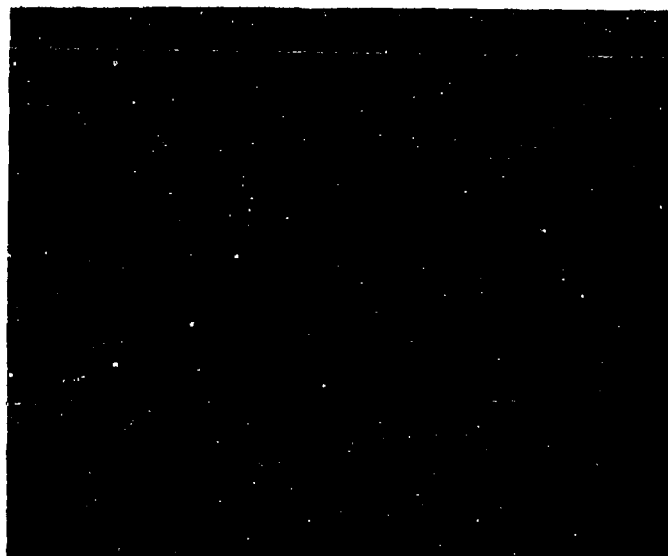


Plate No. 1-8242

X3.05

Figure 79. SiO_2 -60w/oW(H-23)-L5, Surface Temperature 2500°F, Air Flow Rate 50 ft/sec. Exposure Time 30 Minutes, Hot Face Up. 12 Mil Recession, One Inch Scale.



Plate No. 1-8243

X100

Figure 80. SiO_2 -60w/oW(H-23)-L5, Hot Surface at Top Showing Zone Depleted of Tungsten.

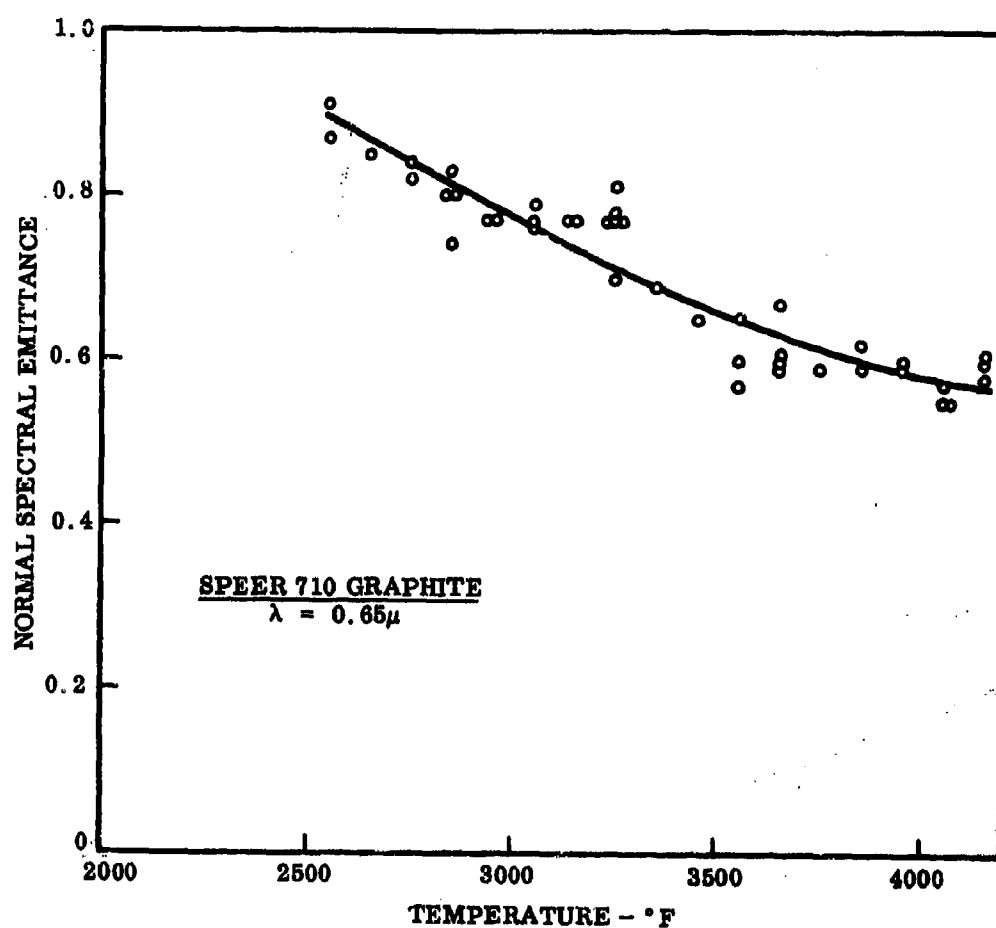


Figure 81. Effect of Temperature on the Emittance of Graphite.

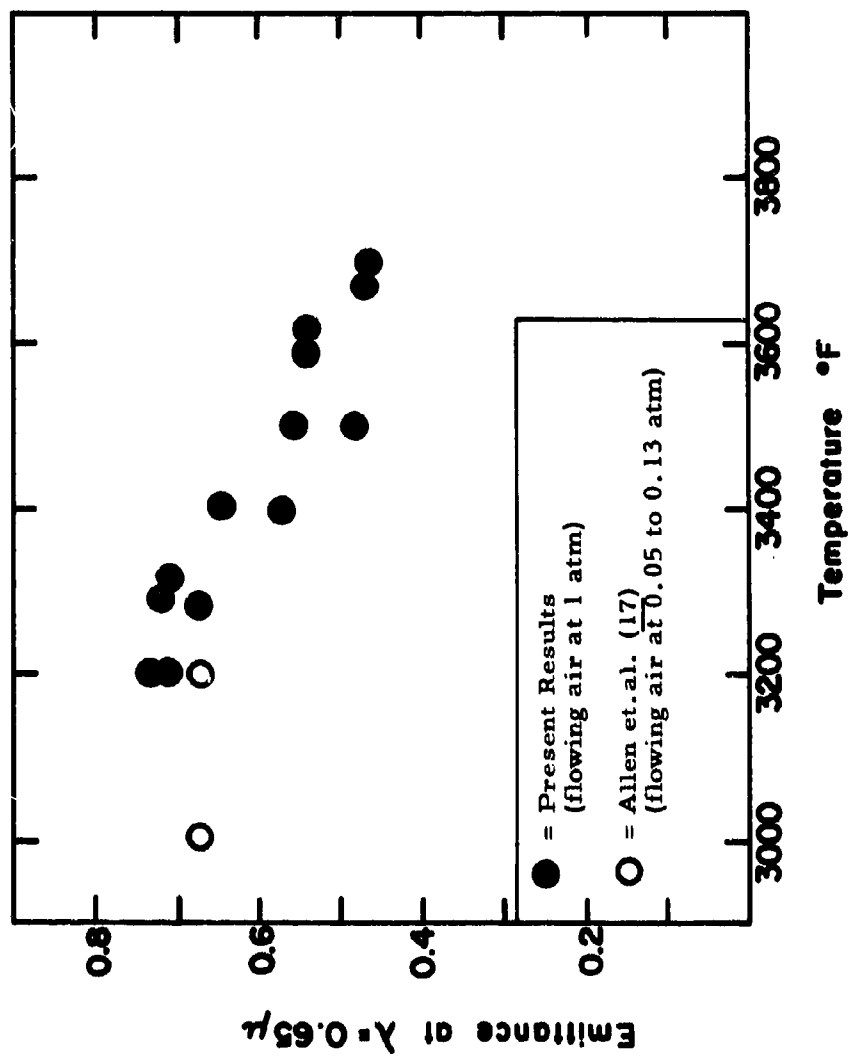


Figure 82. Emissance of $WSi_2/W(G-18)$ in Flowing Air As a Function of Temperature.

TABLE 1

LIST OF CANDIDATE MATERIALS

HfB ₂ .1	Code No. A-2	Carborundum Co., Niagara Falls, New York
ZrB ₂	A-3	Carborundum Co., Niagara Falls, New York
HfB ₂ + 20v/o SiC	A-4	Carborundum Co., Niagara Falls, New York
Boride Z	A-5	Carborundum Co., Niagara Falls, New York
HfB ₂ .1	A-6	ManLabs-Avco AF33(615)-3671
HfB ₂ .1 + 20v/o SiC	A-7	ManLabs-Avco AF33(615)-3671
ZrB ₂ .1 + 20v/o SiC	A-8	ManLabs-Avco AF33(615)-3671
HfB ₂ .1 + 35 v/o SiC	A-9	ManLabs-Avco AF33(615)-3671
ZrB ₂ + 14v/o SiC + 30v/o C	A-10	ManLabs-Avco AF33(615)-3671
RVA	B-5	Union Carbide Corp., New York, New York
PG	B-6	General Electric Co., Detroit, Michigan
BPG	B-7	High Temperature Materials, Lowell, Mass.
Si/RVC	B-8	Union Carbide Corp., New York, New York
PT0178	B-9	Union Carbide Corp., New York, New York
Poco Graphite (AXF-5Q)	B-10	Poco Graphite Inc., Garland, Texas
Glassy Carbon	B-11	Lockheed M & SC, Palo Alto, California
HfC + C	C-11	Battelle Memorial Institute, Columbus, Ohio
ZrC + C	C-12	Battelle Memorial Institute, Columbus, Ohio
JTA (C-ZrB ₂ -SiC)	D-13	Union Carbide Corp., New York, New York
KT-SiC	E-14	Carborundum Co., Niagara Falls, New York
JT0992 (C-HfC-SiC)	F-15	Union Carbide Corp., New York, New York
JT0981 (C-ZrC-SiC)	F-16	Union Carbide Corp., New York, New York
WSi ₂ /W	G-18	General Electric Co., Cleveland, Ohio (type MK-W)
Sn-Al/Ta-W	G-19	TRW, Cleveland, Ohio (WSi ₂ coating)
W-Zr-Cu	G-20	National Research Corp., Newton, Mass. (Ta-10W)
W-Ag	G-21	GT & E, Hicksville, New York (Sn-Al coating)
SiO ₂ + 68.5w/o W	H-22	Rocketdyne, Canoga Park, California
SiO ₂ + 60w/o W	H-23	Wah Chang Corp., Albany, Oregon
SiO ₂ + 35w/o W	H-24	Bjorksten Research Labs, Madison, Wisconsin
Hf-20Ta-2Mo	I-23	General Electric Co., Willoughby, Ohio
Ir/Graphite	I-24	General Electric Co., Willoughby, Ohio
		Wah Chang Corp., Albany, Oregon
		Battelle Memorial Institute, Columbus, Ohio
		General Technologies Corp., Reston, Virginia

TABLE 3
RESULTS OF HIGH VELOCITY COLD GAS/HOT WALL TESTS ON $\text{HeB}_{2.1}(\text{A-2})$
(Surface Temperature Control)

Sample Test	Top Surface Temperature		Initial Dimensions					Top Final Wall (mils)	Conversion Depth (Oxide Thickness) (mils)
	Brightness (0.65 μ)	True (two-color) ($^{\circ}\text{F}$)	Calculated Emittance $\lambda = 0.65\mu$	Flow Rate (ft/sec)	Time (min)	Diam (mils)	Length (mils)		
L15/38-1	3002-3101 Thin, adherent white oxide scale.	3400	0.38-0.42	50	30	500	912	---	4(8)
L15/39-2	3200-2984 Thick, adherent, yellow-white scale.	3600-3190	0.37-0.52	50	60	500	805	---	18(25)
L20/2-25-1*	3038	3240	0.54	<10	30	500	888	---	8(4)
L21/2-32-2*	3047	3240	0.56	50	30	510	934	---	10(6)
L16/2-26-1*o	3065	3240	0.59	100	30	500	910	212	8(8)
L22/2-23-1*	3020	3240	0.51	150	30	500	958	---	6(6)
L17/2-25-2*o	3047	3240	0.56	200	30	510	934	204	14(10)
L18/2-24-1*	3074	3315	0.49	<10	30	500	949	---	8(5)
L14/2-26-2*	3056	3315	0.46	50	30	498	770	---	8(7)
L19/2-24-2*	3227	3350	0.71	<10	30	498	982	---	15(16)

* Light yellow-white coating formed on upper half of sample.
o Radial crack formed at base of internal hole.

TABLE 4
RESULTS OF HIGH VELOCITY COLD GAS/HOT WALL TESTS ON ZrB_2 (A-3)
(Surface Temperature Control)

Sample Test	Top Surface Temperature		Initial Dimensions					Top Final Wall (mils)	Conversion Length (Oxide Thickness) (mils)
	Brightness (0.65 μ)	True (two-color) (°F)	Calculated Emittance $\lambda = 0.65\mu$	Flow Rate (ft/sec)	Time (min)	Diam (mils)	Length (mils)		
L6/38-2	2190-2830	3400-3300	0.55-0.53	50	30	491	1042	---	-----
	Thick, adherent yellow-white scale. Blister on top.								
L18/45-1	-----	3400-3180		50	60	491	1065	110	12(15)
	Thick, white scale - uniform on top and sides.								
L13/46-1	-----	3400		50	30	492	1048	107	14(15)
	Thick, orange-white scale on top and upper 2/3 of side wall. Very thick white scale on lower 1/3.								
L7/2-37-1*	3164-2669	3355-2800	0.57-0.60	100	30	491	1052	203	68(39)
L25/2-27-1*	3092-2714	3350-2675	0.47-1.0	150	30	491	1049	154	30(29)
L21/3-37-2*	3164-2534	3460-2725	0.44-0.45	50	30	492	1053	100	60(38)
L9/2-38-1*	3452-2624	3560-2850	0.74-0.42	<10	30	493	1019	115	59(76)
L12/2-38-2*	3434-2390	3560-2360	0.74-1.0	25	30	493	1073	185	35(53)

* Thick white scale on upper part of sample.

TABLE 5
RESULTS OF HIGH VELOCITY COLD GAS/HOT WALL TESTS ON HfB_2 + SiC(A-4)
(Surface Temperature Control)

Sample Test	Top-Surface Temperature		Calculated Emittance $\lambda = 0.65\mu$	Flow Rate (ft/sec)	Initial Dimensions		Conversion Depth [Depletion Depth] (Oxide Thickness) (mils)
	Brightness (0.65 μ) (°F)	True (two-color) (°F)			Time (mils)	Diam (mils)	
L2-13/39-1	3200	3300	0.75	50	30	488	0[2] (0)
L2-18/2-33-1	2894	2900	0.99	<10	30	488	4
L2-17/2-32-1	2921	2900	1.00	100	30	495	3
L2-14/2-32-2	2885	2900	0.95	50	30	488	4
L2-23/2-29-2	2876	2900	0.92	150	30	478	6
L2-16/2-33-2	2975	2950	1.00	<10	30	478	1 (2)
L2-24/2-28-2	2966	3000	0.89	<10	30	488	3
L2-19/2-28-1	2966	3000	0.89	50	30	474	7
L2-15/2-29-1	2966	3000	0.89	100	30	488	3
L2-21/2-27-2	2952	2980	0.90	150	30	478	4
L2-20/2-30-2	3137	3150	0.96	<10	30	478	4
L2-26/2-31-1	3137	3150	0.96	25	30	478	9
L2-22/2-30-1	3146	3150	0.98	50	30	487	7
L2-25/2-31-2	3191	3200	0.97	<10	30	475	6

Glassy film formed on upper part of all samples.

TABLE 6
RESULTS OF HIGH VELOCITY COLD GAS/HOT WALL TESTS ON $ZrB_2 + SiC(A-8)$
(Surface Temperature Control)

Sample Test	Top-Surface Temperature		Calculated Emittance $\lambda = 0.65\mu$	Flow Rate (ft/sec)	Initial Dimensions			Conversion Depth (Oxide Thickness) (mils)
	Brightness (0.65 μ) ($^{\circ}F$)	True (two-color) ($^{\circ}F$)			Time (mils)	Diam (mils)	Length (mils)	
L2/2-34-2	2678	2675	1.0	<10	30	426	1192	2
L1/2-34-1	2750-2669	2800-2675	0.83-0.98	150	30	426	1172	3
L6/2-36-2	2903	2900	1.0	<10	30	426	1192	3 (4)
L4/2-35-2	2966	3000	0.89	<10	30	426	1200	8 (2)
L5/2-36-1	2966	3000	0.89	50	30	426	1198	10 (2)
L3/2-35-1	3092	3100	0.98	<10	30	426	1157	2

Glassy coating formed on upper half of all samples

SUMMARY OF HIGH VELOCITY COLD GAS/HOT WALL TESTS OF GRAPHITES

111

TABLE 7 (CONT)

SUMMARY OF HIGH VELOCITY COLD GAS/HOT WALL
TESTS OF GRAPHITES

Run No.	Material	Configuration	Top Surface		Emittance (0.65 μ)	Flow Rate (fps)	Time (min)	Length		Surface Recession	
			True (°F)	Brightness (°F)				Initial (in.)	Final (in.)	(mils)	(mils/min)
58-1	Spear Carbon 710	Flat Face	2850	-	0.75	50	3	1.4727	1.3776	95	32
58-2			2850	-			6	1.4981	1.3918	207	35
58-3			2850	-			9	1.5252	1.4088	356	37
48-1			2850	2829			3	1.5216	1.4089	116	39
48-2			2850	2795			6	1.4932	1.3172	340	41
				-2777							
48-3			2850	2804			9	1.5435	1.4378	406	45
				-2786							
50-3			2850	2813			12	1.4766	0.9031	874	48
				2778							
49-1			3050	2777			3	1.4965	1.3697	150	43
49-2			3050	2777			6	1.4644	1.3184	278	45
49-3			3050	2875			9	1.4910	1.0874	487	51
				-2803							
49-4			3250	3110			3	1.4474	1.3817	128	42
50-1			3250	3129			6	1.4855	1.3988	247	43
50-2			3250	3146			9	1.4953	0.9640	811	57
50-3			2050	-		150	1.5	1.4889	1.3466	88	59
50-4			2050	-			3.0	1.4885	1.3538	163	51
50-5			2850	-			4.0	1.4839	1.3033	280	55
50-6			2850	-			1.8	1.5017	1.4019	100	57
50-7			2850	-			3.0	1.3813	1.1687	106	55
50-8			2850	-			4.0	1.4906	1.3488	244	61
51-1			3050	-			1.8	1.4864	1.3806	106	70
51-2			3050	-			3.0	1.4616	1.1691	212	71
51-3			3050	-			3.8	1.5158	1.3715	244	70
52-3			3650	-		150	1.5	1.4776	1.3750	103	69
52-4			3650	-			3	1.4906	1.3624	210	73
52-5			3650	-			1.3	1.4982	1.1774	311	72
52-6			3650	-			1.5	1.4887	1.3787	118	75
52-7			3650	-			3	1.4801	1.2488	248	81
52-8			3650	-			3	1.4897	1.3674	228	77
52-9			3650	-			4	1.4909	1.1686	321	80
52-10			3650	-			4	1.5180	1.3183	203	76
52-11			3050	-			1.5	1.5284	1.3687	138	82
52-12			3050	-			3	1.4739	1.3050	269	90
52-13			3050	-			4	1.5059	1.1487	360	90
53-3		Hemisphere Cap	2850	-		50	3	1.5846	1.3843	130	43
53-4			2850	-			6	1.5288	1.3287	263	44
53-5			2850	-			9	1.4920	1.3019	440	48
53-6			2850	-			3	1.4911	1.3682	156	45
53-7			2850	-			6	1.5033	1.3063	298	50
53-8			2850	-			9	1.5035	1.0781	478	53
53-9			2050	-			3	1.5004	1.3410	166	56
53-10			2050	-			6	1.5056	1.1903	326	54
53-11			2050	-			9	1.4956	0.9787	819	58
54-1		Conical Tip	2850	-		50	3	1.5183	1.2788	240	50
54-2			2850	-			6	1.5189	1.0899	461	50
54-3			2850	-			6.75	1.4983	0.9009	567	57
54-4			2850	-			6.3	1.5437	0.8325	709	55
54-5			2850	-		150	1.8	1.4996	1.3295	169	115
54-6			2850	-			0	1.4874	1.0974	390	130
54-7			2850	-			4	1.5039	0.8680	628	131
54-8	RVA B-3-L1	Flat Face	2850	2828		50	3	0.9883	0.8748	114	38
54-9	B-3-L2		2850	2813/2777			6	1.0018	0.7886	213	35
54-10	B-3-L3		2850	-			9	1.4690	1.1070	368	40
54-11	B-3-L-4		3050	2930			3	1.0143	0.9090	108	30
54-12	B-3-L-5		3050	2897/2850			0	1.0856	0.9381	153	39
54-13	B-3-L-6		3250	3187			3	1.0492	0.9380	113	38
54-14	B-3-L-7		3250	3186			6	1.0376	0.7805	277	48
54-15	B-3-L-8		3250	3282		150	2.25	1.0419	0.8970	160	57
54-16	B-3-L-9		3250	3282			2.15	1.1190	0.8871	232	64
54-17	B-3-L-10		3050	2950			3	1.0144	0.8813	163	51
				-2917							
59-3	B-3-L10		3200	3047			3	1.0200	0.8426	178	59
70-1	B-3-L11		3200	2786			3	1.0814	0.7467	378	56
71-1	Glassy Carbon (LMBC) Grade 3000	Flat Face	2850	-		50	3	Wall	Wall	37	13
								0.123	0.088		
71-2			2850	-		50	4	0.8813	0.6426	49	10
71-3	ATJ6	Flat Face	2850	-		50	3	1.484	1.384	100	33
71-4			2850	-			6	1.391	1.183	209	36
			2850	-			9	1.408	1.048	268	41

TABLE 8
RESULTS OF HIGH VELOCITY COLD GAS/HOT WALL TESTS ON PT0178(B-9) AND GLASSY CARBON(B-11)
(Surface Temperature Control)

Material Sample Test	Surface Temperature °F	Flow Rate (ft/sec)	Time (min)	Initial		Final		Recession Rate(mils/min)
				Tip Geometry	Diam. Length (mils) (mils)	Wall (mils)	Length * Wall (mils) (mils)	
PT0178(B-9)								
L7(135-1)	3150	50	2.2	30 Cone	496	967	760 747 530	230 104
L5(136-2)	2950	50	3.0	30 Cone	496	975	758 717 510	248 83
L4(137-1)	3250	50	1.6	30 Cone	495	980	741 770 537	204 128
L8(137-2)	3450	50	1.0	30 Cone	495	952	729 825 623	106 106
L1(137-3)	2750	50	3.0	30 Cone	497	980	740 656 435	305 102
L3(138-1)	2850	50	2.0	30 Cone	496	957	629 743 435	194 97
L2(138-2)	3050	50	2.0	30 Cone	496	985	699 765 492	207 104
L9(139-1)	2950	50	2.0	30 Cone	497	966	733 726 514	219 110
L10(2-8-1)	3250	150	2.1	30 Cone	496	1430	--- 1061 ---	384 183
L11(2-8-2)	3650	50	0.6	30 Cone	497	905	--- 782 ---	113 188
L12(2-9-2)	3450	150	2.0	30 Cone	455	1360	--- 900 ---	460 230
L14(2-10-1)	3050	150	2.0	30 Cone	498	1497	--- 1176 ---	321 160
L15(2-10-2)	3650	150	1.8	30 Cone	495	1495	--- 1130 ---	365 203
Glassy Carbon(B-11)								
2000-1(132-1)	3150	50	2.4	flat face	510	743	137 677 70	67 27
2000-2(132-2)	3400	50	2.0	flat face	507	708	135 588 15	120 60
2000-3(134-1)	3550	50	1.5	flat face	501	694	130 623 56	74 49
2000-4(134-2)	3500	50	1.5	flat face	514	575	133 497 54	79 52
2000-5(134-3)	3250	50	2.0	flat face	513	599	143 621 63	80 40

***Based on Gross Measurements

***Based on Measurements after sectioning

**Based on Measurements after sectioning

*Based on Gross Measurements

TABLE 9
RESULTS OF HIGH VELOCITY COLD GAS/HOT WALL TESTS ON Si/RVC(B-8) (4 MIL COATING)
(Surface Temperature Control)

Material Sample Test	Surface Temperature °F	Flow Rate (ft/sec)	Time (min)	Initial		Length (mils)	Brightness Temperature °F	Calculate Emittance at λ=0.65μ	Comment
				Tip Geometry	Diam. (mils)				
Si/RVC(B-8)									
L7(2-3-2)	3100	< 10	15	flat	503	700	3100-3290	1.0	Coating Failed
L8(2-4-1)	3000	< 10	60	face	504	703	2960-2980	0.88 - 0.94	Coating Blistered
L3(2-5-1)	2900	< 10	60	"	504	714	2800-2810	0.70 - 0.72	Coating Survived
L5(2-5-2)	2900	50	60	"	500	719	2830-2890	0.79 - 0.94	Coating Survived
L6(2-6-1)	2900	150	60	"	501	716	2860-2860	0.87 - 0.87	Coating Survived
L2(2-6-2)	3000	150	60	"	506	716	3030-3010	1.0	Coating Failed
L4(2-7-1)	3000	50	60	"	504	706	2980-2960	0.94 - 0.87	Coating Failed

TABLE 10
RESULTS OF HIGH VELOCITY COLD GAS/HOT WALL TEST ON ARC CAST HfC+C(C-11) AND ZrC+C(C-12)
(Surface Temperature Control)(FLAT FACED CYLINDERS)

Material Sample Test	Surface Temperature °F	Flow Rate (ft/sec)	Time (min)	Initial Diam. (mils)	Initial Length (mils)	Final Length (mils)	Recession Oxide (mils)	Comments	Brightness Temperature (°F)	Emissance at $\lambda=0.65\mu$
HfC+C(C-11)										
L4(144-1)	3600	50	26	464	714	633	81/100	Large Graphite Flakes, Craze Surface	2600-2980	0.04-0.17
L3(144-2)	3400	50	30	465	711	646	65/75	"	2680-2810	0.08-0.16
L8(145-1)	3600	150	7	460	714	688	26/35	No Graphite Flakes, Smooth Surface	2810-2940	0.09-0.15
L7(145-2)	3600	<10	30	459	715	673	42/55	"	2770-2830	0.08-0.10
L6(2-1-1)	3400	150	16	459	713	674	39/50	"	2780-2820	0.14-0.16
L5(2-1-2)	3400	<10	30	459	714	671	43/55	"	2660-2750	0.09-0.13
L2(143-2)	3850	50	21	463	710	650	60/70	Large Graphite Flakes, Craze Surface	-	-
ZrC+C(C-12)										
L8(141-2)	3800	50	22	464	713	641	72/80	Large Graphite Flakes, Craze Surface	3010-3100	0.12-0.16
L2(142-1)	3400	50	28	463	716	640	76/100	"	2620-2830	0.07-0.17
L3(142-2)	3600	<10	27	463	716	645	71/100	"	2700-2960	0.06-0.16
L4(143-1)	3600	150	12	464	716	661	55/75	"	2920-2990	0.14-0.18
L5(2-2-1)	3400	150	22	464	713	661	52/65	"	2780-2850	0.14-0.13
L6(2-2-2)	3400	<10	30	464	713	660	53/55	"	2610-2660	0.07-0.09
L7(2-11-2)	3000	50	30	462	713	652	61/60	"	2290-2350	0.05-0.07

TABLE 11

RESULTS OF HIGH VELOCITY COLD GAS/HOT WALL TESTS ON KT-SiC(E-14)
(Surface Temperature Control)

Sample Test	Temperature		Calculated Emittance $\lambda = 0.65\mu$	Flow Rate (ft./sec)	Initial Dimensions				Final Wall (mils)	Recession (mils)
	True °F	Brightness ($\lambda = 0.65\mu$) °F			Time (min)	Diam (mils)	Length (mils)	Top Wall (mils)		
L2/59-1	3960-3560	3710	0.60	50	1.9	491	1009	-	-	49 length 25 diam.
Thick puffed scale on top, top surface deeply eroded. Side wall attached.										
L1/59-2	3450	3270-3325	0.60	50	27	488	1007	-	-	15 length 115 diam.
Side wall necked in 1/4 inch below top.										
L3/66-1	3660	-	0.60	50	2	490	1033	-	-	1 length 45 diam.
Heavy attack of side wall, upper 1/2 inch. Could not hold surface temperature.										
L4/67-1	3660	3225-3250	0.60	150	30	490	991	-	-	0 length 15 diam.
Upper one half of side wall blistered and scaled. Thermal shock crack on top surface.										

TABLE 12

RESULTS OF HIGH VELOCITY COLD GAS/HOT WALL TESTS ON JT0981(F-16) AND JT0992(F-15)
(Surface Temperature Control)

Material Sample Test	Temperature		Calculated Emittance $\lambda = 0.65\mu$	Flow Rate (ft/sec)	Initial Dimensions				Recession (mils)
	True O _F	Brightness F			Time Diam. (min)	Length (mils)	Top Wall (mils)	Final Wall (mils)	
JT0981(F-16)-L8 (121-1)	3200	3128	0.81 - 1.0	50	30	490	756	374	351
	3218								23
	- Top and side surface rough yellow and gray with dark glassy beads. Gray powdery skirt starting at the bottom and going up 1/3 the length of sample.								
-L7	3200	3083	0.69 - 0.81	150	30	490	759	381	349
(121-2)	3128								32
	- Top surface and side, yellow and gray with glassy beads. Half way down the side is a band of large glassy beads about 100 mils wide. From the bottom to about 1/4 of the way up the sample is the gray skirt.								
-L4	3000	2732	0.38 - .88	50	30	490	797	429	415
(122-1)	2966								14
	- Top and side yellow and gray glassy beads. Small gray skirt at bottom of sample was less 1/4 of sample.								
-L9	3000	2912	0.74 - 1.0	150	30	490	753	371	355
(124-1)	3092								16
	- Top surface gray, side yellow with large glassy beads. Gray skirt extended 1/3 up from bottom and was very fragile.								
-L10	2800	2660	0.58 - 0.77	50	30	490	775	432	423
(124-2)	2732								9
	- Top and side light gray with a few dark glassy beads. Gray skirt extended almost 1/2 way up sample.								

TABLE 12 (CONT.)

RESULTS OF HIGH VELOCITY COLD GAS/HOT WALL TESTS ON JT0981(F-16) AND JT0992(F-15)
(Surface Temperature Control)

Material Sample Test	Temperature		Calculated Emittance $\lambda=0.65\mu$	Flow Rate (ft/sec)	Initial Dimensions			Recession (mils)
	True T_F	Brightness F			Time Diam. (min)	Length (mils)	Top Wall (mils)	
JT0981(F-16)-L1 (125-1)	2800	2660 2804	0.58 - 1.0	150	30	488	1,098	377
			- Top surface and side, gray with a few large glassy beads. Gray skirt extended 1/3 up from bottom.					
-L5	3400	3254 3452	0.66 - 1.0	50	30	490	790	443
(120-1)			- Yellow surface on top and side with dark gray glassy beads. Bottom 1/4 of sample is a gray powdery skirt.					
-L6	3400	3200 3707	0.57 - 1.0	150	13.0	490	790	485
(120-2)			- Top surface dark rough and glassy with light gray crystals growing over and down from top edge in the direction of flow. The side just under top surface was badly pitted and eroded. There was a gray skirt starting at the bottom and going 1/4 up the sample.					
JT0992(F-15)-L4 (116-1)	3400	3290 3407	0.74 - 1.0	50	30	490	790	390
			- Light gray top and side with dark band on center side Light gray powdery skirt from base, up about one quarter of length.					
-L7	3400	3290 3353	0.74 - 0.87	150	24	490	808	422
(116-2)			- Light gray top and sides with dark band just above the skirt. Light gray powdery skirt 1/4 up length.					
								395
								27
								28
								63
								5

TABLE 12 (CONT.)

RESULTS OF HIGH VELOCITY COLD GAS/HOT WALL TESTS ON JT0981(F-16) AND JT0992(F-15)
(Surface Temperature Control)

Material Sample Test	Temperature		Calculated Emittance $\lambda = 0.65\mu$	Flow Rate (ft/sec)	Initial Dimensions			Final Wall (mils)	Recession (mils)
	True of F	Brightness of F			Time Diam. (min)	Length (mils)	Top Wall (mils)		
JT0992(F-15)-L5 (117-1)	3600	3560 3596	0.91 - 1.0	50	13.5	490	803	428	400
	- Light gray top and sides, with gray powdery skirt from bottom up 1/8 of length.								
-L6	3600	3596 3668	1.0	150	8.0	490	808	420	391
(117-2)	- Light gray top and side with powdery skirt from bottom 1/8 up side.								
-L10	3800	3722	0.84	50	2.0	487	1,032	612	595
(118-1)	- Light gray case about 10 mils thick with small gray skirt.								
-L9	2600	2660 2741	1.0	50	30	488	1,042	632	593
(118-2)	- Top and upper 1/3 of sample brownish gray. Gray skirt started about 1/3 down from top and extended to within 1/4-inch of the bottom. The last 1/4- inch was a dark gray powdery ring.								
-L14	3200	3173 3452	0.91	50	30	491	735	393	372
(127-1)	Substrate Brightness Temperature at 0.65 μ =3844 - 4244°F								
-L13	3200	3173 3193	0.91	150	30	492	763	403	400
(127-2)	Substrate Brightness Temperature at 0.65 μ =3470 - 3965°F								

TABLE 12 (CONT.)

RESULTS OF HIGH VELOCITY COLD GAS/HOT WALL TESTS ON JT0981(F-16) AND JT0992(F-15)
(Surface Temperature Control)

Material Sample Test	Temperature		Calculated Emittance $\lambda=0.65\mu$	Flow Rate (ft/sec)	Initial Dimensions					
	True of F	Brightness of F			Time (min)	Diam. (mils)	Length (mils)	Top Wall (mils)	Final Wall (mils)	Recession (mils)
JT0992(F-15)-L12 (128-1)	3000	2955 2984	0.86	50	30	492	755	393	391	2
-L16 (128-2)	3000	2919 2993	0.76	150	30	492	767	427	425	2
-L15 (129-1)	2200	2200 2237	1.0	50	30	491	766	450	409	41
-L11 (129-2)	2000	2000	1.0	50	30	494	757	392	386	6

TABLE 13

RESULTS OF HIGH VELOCITY COLD GAS/HOT WALL TESTS ON $WSi_2/W(G-18)$
(Top Surface Control, 4 mil coating on 500 mil diameter x 750 mil long cylinders)

Run No.	Support	True (two-color) (°F)	Brightness (0.65μ) (°F)	Calculated Emittance (λ = 0.65μ)	Flow Rate (ft/sec)	Time (min)	Width of W_{Si_3} Zone (mils)
24-1	ZrO ₂ Top surface good. Lower portion failed by reaction with ZrO ₂ .	3400	-	-	50	16.1	1.6
25-1	ZrO ₂ Top surface good. Lower portion failed by reaction with ZrO ₂ . (Helium flow up ZrO ₂ support to shield bottom.)	3400	-	-	50	17.0	1.6
26-1	Cu Top surface good. Bottom edge failed by reaction with Cu.	3400	3110	0.43	50	60.0	2.8
29-1	Cu Edge failure around black body hole, no other failures	3600	3265	0.41	50	60.0	2.0
30-1	Cu Coating melted on sides and top, pit failure on side due to runoff.	3680	3270	0.35	50	35.0	3.6
40-1*	Cu	3500	3225-3280	0.48-0.55	150	60.0	3.9
L13/2-20-1*	Cu	3200	3092	0.72	50	30.0	2.0
L12/2-20-3*	Cu	3200	3092	0.72	150	30.0	1.8
L14/2-19-1*	Cu	3280	3146	0.67	<10	60.0	3.2
L10/2-39-1*	Cu	3300	3182	0.71	150	30.0	2.2
L11/2-20-2*	Cu	3200	3083	0.69	<10	30.0	2.1

* No failure uniform clear glass on surface.

TABLE 14

RESULTS OF HIGH VELOCITY COLD GAS/HOT WALL TESTS ON Sn-Al/Ta-10W(G-19)
(Top Surface Control, 8 mil coating on 500 mil diameter x 1000 mil long cylinders)

Run No.	Support	Top Surface Temperature		Calculated Emittance ($\lambda = 0.65\mu$)	Flow Rate (ft/sec)	Time (min)
		True (two-color) (°F)	Brightness (0.65 μ) (°F)			
23-1	ZrO ₂ Failed at 4.2 min due to reaction with ZrO ₂	3400	-	-	50	5.5
27-1	Cu Coating failed on top and at one side. Slight reaction with copper.	3400	3110	0.43	50	30.0
41-1	Cu No failure, coating thinned on upper part of sample.	2930-2885	3000	0.79-0.69	50	60.0
41-2	Cu No failure, coating thinned on upper part of sample.	2920-2875	3000	0.76-0.66	150	60.0
42-1	Cu Random failure detected at 17 min, total failure at 23.5 min.	3100-3065	3200	0.71-0.67	50	24.0
34-2	Cu Coating failed on side wall and edge.	3315	3500	0.62	50	15.0
37-1	Cu Random failure occurred at 16 min, total failure of top half at 22 min.	3145-3175	3300	0.65-0.69	50	22.0

TABLE 15

RESULTS OF HIGH VELOCITY COLD GAS/HOT WALL TESTS ON $\text{SiO}_2 + 60\text{W}/0\text{W}(\text{H}-23)$
FOR 30 MINUTE EXPOSURES AT A FLOW RATE OF 50 Ft/Sec.

(Top Surface Control)

Material Sample Test	Surface Temperature °F	Initial				Final Wall (mils)	Recession (mils)	Brightness Temperature °F	Emittance at $\lambda=0.65\mu$
		Tip Geometry	Diam. (mils)	Length (mils)	Wall (mils)				
L7(130-1)	2600	Flat	507	1008	710	702	8	2520-2660	0.69 - 1.0
L6(130-2)	2400	face	507	1009	725	710	15	2380-2625	0.91 - 1.0
L5(131-1)	2500	"	507	1008	688	676	12	2480-2570	0.91 - 1.0
L4(131-2)	2700	"	507	1005	758	738	20	2640-2815	0.78 - 1.0
L9(132-2)	2750	"	506	875	641	578	63	2760-2830	1.0
L10(133-1)	2800	"	506	1012	697	693	4	2780-2860	0.93 - 1.0
L8(2-10-3)	2200	"	505	1005	---	1003*	2	---	---
L2(2-11-1)	2000	"	506	1005	---	1004*	1	---	---

*Final Length. Sample Cracked.

RESULTS OF HIGH VELOCITY COLD GAS/HOT WALL TESTS ON HF-20Ta-2Mo(I-23)
(Surface Temperature Control, except# = substrate control)

Sample Test	Substrate Temperature		Top-Surface Temperature		Calculated Emittance $\lambda = 0.65\mu$	Flow Rate (ft/sec)	Initial Dimensions						
	Brightness (0.65 μ) (°F)	True (estimated) (°F)	Brightness (0.65 μ) (°F)	True (two-color) (°F)			Time (min)	Diam (mils)	Length (mils)	Top Wall (mils)	Final Wall (mils)	Conversion Depth (mils)	
28-1	-	-	2730-2660	2950	0.52-0.37	50	60	511	995	-	-	-	
			Tenacious oxide film on top and sides. Flaking scale in band near bottom.										
34-1	-	-	3020-2950	3200-3150	0.57-0.52	50	30	500	1018	-	-	3	
			Light grey oxide film on top. Ring of white scale on side wall.										
L8/44-1	-	-	-	3350-3400	-	1-10	30	499	738	124	110	14	
			Light grey oxide film on top, thick white scale on sides. Sample cracked on cooling.										
L9/44-2*	3145	3355	-	3400-3320	0.55	1-10	60	495	800	140	128	12	
			Light grey oxide on top and side wall.										
L1/76-1*	3275	3500	3050-2860	3150-3100	0.55	50	60	486	966	-	-	20	
			Light grey oxide on top and upper third of wall.										
L2/77-1*	3450	3700	3245-3070	3380-3235	0.55	50	60	499	946	123	92	31	
			Light grey oxide on top and upper two thirds of wall.										
L3/77-2*	3640	3900	3290-3180	3500-3390	0.55	50	60	487	980	151	91	60	
			Light grey oxide on top and upper two thirds of wall.										

TABLE 17
AVERAGE VALUES OF NORMAL SPECTRAL EMITTANCE
UNDER OXIDIZING CONDITIONS

Material	Emittance - ϵ at $\lambda = 0.65\mu$		
	2500°-3000°F	3000°-3500°F	3500°-4000°F
HfB ₂ (A-2)	----	0.50	----
ZrB ₂ (A-3)	----	0.57	----
HfB ₂ +SiC (A-4)	0.90	0.75	0.60*
ZrB ₂ +SiC (A-8)	0.90	----	----
RVA (B-5)	0.85	0.75	0.65
Glassy Carbon (B-11)	----	0.55	----
Si/RVC (B-8)	----	0.70	----
KT-SiC (E-14)	----	0.70	----
JTA (D-13)	----	0.75	----
JT0992 (F-15)	----	0.75	----
JT0981 (F-16)	----	0.75	----
WSi ₂ /W (G-18)	----	0.60	0.55
Sn-Al/Ta-10W (G-19)	----	0.67	----
Hf-20Ta-2Mo (I-23)	----	0.55	----

* Estimated

UNCLASSIFIED

Security Classification

DOCUMENT CONTROL DATA - R & D

(Security classification of title, body of abstract and indexing annotation must be entered when the overall report is classified)

1. ORIGINATING ACTIVITY (Corporate author)		2a. REPORT SECURITY CLASSIFICATION	
ManLabs, Inc. 21 Erie Street Cambridge, Massachusetts 02139		UNCLASSIFIED	
		2b. GROUP	
		N/A	
3. REPORT TITLE			
Stability Characterization of Refractory Materials under High Velocity Atmospheric Flight Conditions, Part III Volume II: Experimental Results of High Velocity Cold Gas/Hot Wall Tests			
4. DESCRIPTIVE NOTES (Type of report and inclusive dates)			
Technical Documentary Report, April 1966 to July 1969			
5. AUTHOR(S) (First name, middle initial, last name)			
Roger Perkins Larry Kaufman Harvey Nesor			
6. REPORT DATE		7a. TOTAL NO. OF PAGES	7b. NO. OF REFS
December 1969		125	17
8a. CONTRACT OR GRANT NO.		8b. ORIGINATOR'S REPORT NUMBER(S)	
AF33(615)-3859		N/A	
a. PROJECT NO.		9a. OTHER REPORT NO(S) (Any other numbers that may be assigned this report)	
7312 Task 731201		AFML-TR-69-84, Part III Volume II	
c. 7350 Tasks 735001 and 735002			
10. DISTRIBUTION STATEMENT			
This document is subject to special export controls and each transmittal to foreign governments or foreign nationals may be made only with prior approval of the Air Force Materials Laboratory (MAMC), Wright-Patterson AFB, Ohio 45433			
11. SUPPLEMENTARY NOTES		12. SPONSORING MILITARY ACTIVITY	
N/A		Air Force Materials Laboratory (MAMC) Air Force Systems Command Wright-Patterson Air Force Base, Ohio	
13. ABSTRACT			
<p>High velocity CG/HW exposures at air velocities ranging from below 10 ft/sec to 250 ft/sec have been performed at temperatures between 2500° and 4000°F for seventeen candidate materials. Materials which form condensed oxide scales exhibited no definite dependence on air flow rate. Significant temperature gradients (200° -1000°F) develop across thin oxide scales formed during oxidation (scale thicknesses ranged between 0.010 and 0.060 inch) due to the insulating oxide scale on the surface. The practical implications of this finding are quite substantial since if thin layers of these solid oxides can result in such large gradients (and if the gradients exist under free flight conditions), the temperature level experienced by the substrate is substantially below that of the HG/CW surface. Thus, the predicted strength and load carrying capacity of the substrate would be much higher than for the case where gradients are ignored. The high velocity CG/HW oxidation behavior of materials forming condensed oxidation products is comparable with the behavior in furnace tests for equal surface temperatures. Thus, the rate of oxidation is limited by the minimum temperature in the condensed oxide layer. The emittance of fourteen of the candidate materials was measured under oxidizing conditions between 2500° and 4000°F.</p> <p>This abstract is subject to special export controls and each transmittal to foreign governments or foreign nationals may be made only with prior approval of the Air Force Materials Laboratory (MAMC), Wright-Patterson Air Force Base, Ohio 45433.</p>			

DD FORM 1473

CLASSIFIED BY FORM 1473, 1 JAN 63, WHICH IS OBSOLETE FOR ARMY USE.

UNCLASSIFIED

Security Classification

UNCLASSIFIED
Security Classification

14.	KEY WORDS	LINK A		LINK B		LINK C	
		ROLE	WT	ROLE	WT	ROLE	WT
	oxidation refractory borides graphites and JT composites silicon carbide hypereutectic metal carbide-graphite composites refractory metals coated refractory metals metal-oxide composites siliconized graphite high velocity temperature gradients oxidation products failure temperatures emittance						

UNCLASSIFIED
Security Classification